Structural design on strengthening multi-bolted connections in pultruded glass fiber reinforced polymer (PGFRP) using multi-directional fiber sheets

（多軸繊維シートを使用した引抜成形ＧＦＲＰのボルト接続部補強の構造設計）

July, 2023

Doctor of Philosophy (Engineering)

Tran Quang Duc
チャン　クァン　ドゥク

Toyohashi University of Technology

ABSTRACT

Date of Submission（month day, year）: July, 3rd, 2023

Department of Department of Architecture and Civil Engineering	Student ID Number	D 209504	Supervisors	Yukihiro Matsumoto
Applicant's name	Tran Quang Duc			

Abstract（Doctor）

Title of Thesis	Structural design on strengthening multi-bolted connections in pultruded glass fiber reinforced polymer (PGFRP) using multi-directional fiber sheets

Infrastructures that have been rapidly expanding in recent years are now reaching a critical age, with widespread signs of deterioration and inadequate functionality. Therefore, designing effective methods for rehabilitating, rebuilding, and maintaining civil infrastructure is essential for sustainable development. Fortunately, glass fiber-reinforced polymer (GFRP) composites have emerged as an excellent material for renewing existing structures. In recent decades, numerous research projects have been conducted to investigate the reinforcement behavior for connections in GFRP structures. However, the main focus of previous studies has been limited to strengthening based on the original material connections in GFRP. This research program aims to investigate a novel and promising method of strengthening bolted connections in GFRP, using multidirectional fiber sheets. The primary advantage of this method is its simplified application, cost-effectiveness, and high effectiveness.

Firstly, a brief introduction to pultruded GFRP (PGFRP) as a material and manufacturing process was presented. The first experiment was conducted a series of experiments to consider the effects of GFS on strengthening PGFRP multi-bolted connections. In this study, three varieties of multi-directional Glass Fiber Sheets (GFS) were employed for enhancing purposes, namely: 0°/90° GFS, ±45° GFS, and chopped strand mat (CSM) GFS, all of which were produced using the Vacuum Transfer Molding technique. The findings of this investigation reveal that all three types of GFS exhibit a marked ability to enhance the maximum failure loads of Pultruded GFRP connections. Furthermore, the impact of all GFS variants on the

reinforcement process was observed to be directly proportional to increases in the ratios of end distances to bolt diameter (*e/d)* or the number of bolts (*n*). In nearly all instances, 0°/90° GFSs outperformed ±45º GFSs and CSM GFSs in terms of the extent of the reinforcement effect achieved.

A subsequent experiment was conducted to evaluate the bonding capability of Pultruded GFRP. This experiment was necessitated by the observation that the specimens with the highest connection strength in the previous experiment had experienced debonding failure. In light of a sequence of material tests, a set of equations were posited to accurately predict the failure modes and ultimate loads of multi-bolted PGFRP connections fortified with multi-directional GFS.

The third experiment investigates the influence of bolt-tightening force on connection strength. A similar series as non-tightening force were designed and tested under applying a 21N.m torque load. The outcomes of the connection testing evince that the employment of GFS for strengthening purposes continues to be efficacious, even when deployed under diverse conditions of bolted PGFRP connection. While there was an increase in the maximum load for all specimen types compared to the untightened state, the system's effectiveness as measured by the ratio of the maximum loads before and after reinforcement with GFSs, exhibited a slight decrement.

The final investigation involved determining failure behavior and strengthening effectiveness in beam-to-column multi-bolted connection. Full scales experiments were implemented to investigate the behavior and effectiveness of beam-to-column connection with and without strengthened by GFS. The experimental findings needed to align with the expected outcomes, owing to unforeseen circumstances in the design of the auxiliary steel components in the beam. Although the adoption of GFS served to enhance the reinforcement of the column, it nevertheless suffered damage before the onset of failure observed in the beam's profile. Consequently, a revision was put forward, which entailed altering the connection of the cleats, to align with the primary objective of the experiment, which was to investigate the behavior of the beam.

To summarize, the all-encompassing research program detailed herein suggests that the use of multi-directional GFS constitutes an effective approach for enhancing the structural

aptitude of civil engineering constructions. Specifically, the incorporation of GFS sheets enhances the load-bearing capacity and overall performance of pultruded PGFRP connections. The findings and formulae proposed in this study possess practical implications for promoting the adoption of cutting-edge materials such as FRPs within the civil engineering industry. Nonetheless, certain pertinent issues remain, which the author has identified as prospective areas for future investigation.

ACKNOWLEDGMENTS

With utmost gratitude and appreciation, I would like to express my heartfelt thanks to the following individuals and institutions for their unwavering support throughout my study and research:

First and foremost, I would like to express my deepest gratitude to my supervisor, Prof. Yukihiro Matsumoto, whose guidance and encouragement were essential to the successful completion of my research work. I am truly grateful for his constant faith in my abilities and his provision of insightful suggestions and directions, which were instrumental in my success.

Furthermore, I would like to express my sincere appreciation to the members of my doctoral thesis committee, Prof. Shoji Nakazawa, Prof. Taiki Saito, and Assoc. Prof. Tomoya Matsui, for their valuable feedback and constructive comments that have greatly contributed to the quality of my research work.

I am deeply thankful to Toyohashi University of Technology for their support and for generously providing me with the opportunity to pursue my studies through the JICA (Asia Innovation program) and Ministry of Education, Culture, Sports, Science, and Technology (MEXT) scholarship.

My lab mate, Phan Viet Nhut, your assistance and suggestions in the research process are wonderful and I would like to express my appreciation to you.

I am grateful for my late mother, and I believe that she watches over me from heaven, providing guidance and inspiration whenever I need it.

My deepest gratitude goes to my wife, Xoan Nguyen, for her unwavering support and patience throughout my academic journey. I would like to thank my papa, parents-in-law, and my brother, Trung for your support. This work would never have been completed without support from my family.

Finally, thanks to my sons, who brought happiness into my life. Their presence has been my greatest motivation, and I am tremendously proud to be their father. In honor of them, I dedicate this doctoral thesis.

CONTENT

LIST OF TABLES

LIST OF FIGURES

CHAPTER 1
INTRODUCTION

1.1. Background

The exceptional properties of glass fiber reinforced polymers (GFRPs), such as their high strength, chemical resistance, and flexibility, have resulted in their widespread use across various fields of civil engineering industry. GFRPs can be composed of different forms of glass fiber reinforcements, including glass roving, chopped strands, fabrics, and mats. The pultrusion method is currently a widely utilized technique for producing GFRP products with various cross-sectional areas. The PGFRP profiles are a sought-after material and have captured the attention of designers owing to their remarkable characteristics such as low density, high weight-to-strength ratio, excellent corrosion resistance, low heat transmission, and versatility in terms of shapes. The adoption of pultrusion methods for manufacturing GFRP profiles has facilitated the cost-effective production of glass FRP materials, thereby promoting their extensive utilization.

Many authors have demonstrated the performance advantages of PGFRP in previous studies. However, there are several drawbacks to its application in buildings and other structural utilities. In addition to its inherent weaknesses such as sensitivity to elevated temperatures and fire, PGFRP must also contend with connection structure behavior during its performance period. The main issues such as bolted connections and mechanical properties have been addressed in numerous publications. In PGFRP members utilizing steel bolted connections, joint strength is commonly considered the criterion rather than the strength of the profile members. Conversely, the capacity of connections is determined by the shear or bearing strength of the material due to the significantly higher mechanical properties of steel bolts.

This work proposes the use of Glass Fiber Sheets (GFS) as a method to strengthen bolted connections in PGFRP. This strengthening approach offers a range of benefits, including but not limited to 1) highly effective improvement of the ultimate load in the PGFRP connection by bolts; 2) convenience and cost-effectiveness in creating the strengthening solution; and 3) applicability to existing structures.

1.2. Research objective

The principal objective of this investigation is to examine a novel and promising approach for augmenting the durability of multi-bolted connections in pultruded glass fiber reinforced polymer (PGFRP) utilizing glass fiber sheets (GFS). This technique's simplicity and ease of application are particularly attractive, as it does not necessitate the use of intricate or complicated methodologies, rendering it convenient for implementation in existing or new constructions. The study aims to evaluate the efficacy of the GFS sheet strengthening method on multi-bolted connections in PGFRP via a combination of experimental and analytical approaches. Furthermore, the research aims to create analytical models to determine the strength of the reinforced members in design. An additional goal of this research is to contribute to the scientific advancement of the civil and structural engineering fields by presenting innovative discoveries.

1.3. Thesis organization

This thesis comprises seven chapters, each with a concise overview as follows:

Chapter 1*: Introduction*. The first chapter of this dissertation is the Introduction, which offers a context for the research program. It also outlines the goals of the current study and provides an overview of the other chapters included in this dissertation. The final section of this chapter presents a brief preview of the subsequent chapters.

Chapter 2: *Literature Review*. Chapter two of this dissertation is dedicated to a literature review of methods for enhancing the strength of multi-bolted connections in PGFRP using GFSs. The review is structured into four segments: PGFRP materials, member connections, techniques for strengthening bolted connections, and beam-to-column connections. Furthermore, this chapter addresses research gaps in previous studies and current solutions in the field.

Chapter 3: *Multi-bolted connection of PGFRP under strengthening by GFS*. This chapter presents experimental and analytical investigations related to the proposed method of using GFSs to enhance the strength of bolted connections in PGFRP. The chapter provides details regarding the serial specimens, GFS preparation using the VaRTM process, materials used, test setups, instrumentation, test results, and failure modes. Additionally, this chapter proposes design equations to estimate the maximum failure loads (ultimate loads) of multi-bolted PGFRP connections reinforced by GFSs based on various connection failure modes.

Chapter 4: *Influence of bonding strength in PGFRP on the bolted connection under strengthening by GFSs.* In Chapter 3, as the result of the experiment, the debonding failure was observed in failure specimens. The failure mode observed indicates that the bond strength in PGFRP impacts the connection capacity, emphasizing the need for further examination of the bond strength. Therefore, this chapter discusses experimental work and presents a formula for determining bonding strength between laminates of PGFRP and its effect on connection strength.

Chapter 5: *Influence of tightening force on bolted connection under strengthening by GFSs.* In addition to the parameters and material properties discussed in Chapter 3 and Chapter 4, the tightening force plays a significant role in influencing the bolted connection in PGFRP. This chapter presents the experimental work to enhance the strength of multi-bolted connections in PGFRP using GFSs under the tightening force applied in bolted connections. The chapter provides a detailed discussion on the influence of tightening force on the failure modes and ultimate loads of the connection after performance testing.

Chapter 6: *Strengthening by GFS in a beam-to-column connection for pultruded GRP square profiles*. Upon investigating PGFRP bolted connections under various conditions, it is imperative to proceeding with a full-scale experiment is imperative to obtain a more comprehensive assessment of the effectiveness of using GFS to strengthen connection. This chapter describes the steel parts, strengthening GFS materials, and serial of full-scale specimens used in the experiment. The cyclic behavior of the connection is also presented in the chapter. Based on the results of the cyclic tests, the behavior of the beam-to-column connection is discussed in several aspects, including moment and relative rotation behavior, failure modes, stiffness variation, strength, and dissipated energy under the specimens.

Chapter 7: *Summary and Conclusions*. The final chapter of this dissertation summarizes the research program and the key findings presented in the previous chapters. The conclusions drawn from the research are also discussed in this chapter, highlighting the effectiveness of using GFSs to strengthen bolted connections in PGFRP. Additionally, recommendations for future research in this field are provided, to enhance further the knowledge and understanding of strengthening PGFRP bolted connections using GFSs.

CHAPTER 2
LITERATURE REVIEW

2.1. Introduction

This chapter describes an up-to-date outline of research about pultruded glass fiber reinforced polymer (PGFRP) focusing on strengthening bolted connection. In the first part, the general properties of PGFRP and its related studies are presented, and a summary of studies for member connection investigations follows it. The next section also summarizes studies that investigated strengthening connection members using GFS. Afterward, research programs available for beam-to-column connection strengthening using GFS are examined in one combined section. The last section of this chapter focuses on research gaps in previous studies and addresses current solutions.

2.2. Pultruded GFRP

2.2.1. Material introduction

Pultruded glass fiber material has a relatively short history, developed only in the mid-twentieth century. However, in the decades since its creation, this material has revolutionized the construction industry and become a critical component in many products. The pultrusion process was first developed in the 1950s to manufacture fiberglass-reinforced polymer products. Initially, pultruded fiberglass was used primarily in the marine industry to manufacture boat hulls and other parts. However, as technology improved and new applications were discovered, pultruded fiberglass began to be used in various industries. Today, it is commonly used in construction, transportation, infrastructure, and other industries [1,2].

There are four (4) types of layers as shown in Figure 1.1 in a typical pultruded section as following Davalos et al., 1996 [3]

a) A resin-rich layer of randomly oriented chopped fibers (nexus veil). This thin layer is noticeable on the surface of the composite.

b) Different weights of continuous strand mats (CSM). It consists of continuous randomly oriented fibers

c) Stitched fabrics (SF) with different angle orientations

d) Continuous unidirectional fiber bundles or known as a roving layer.

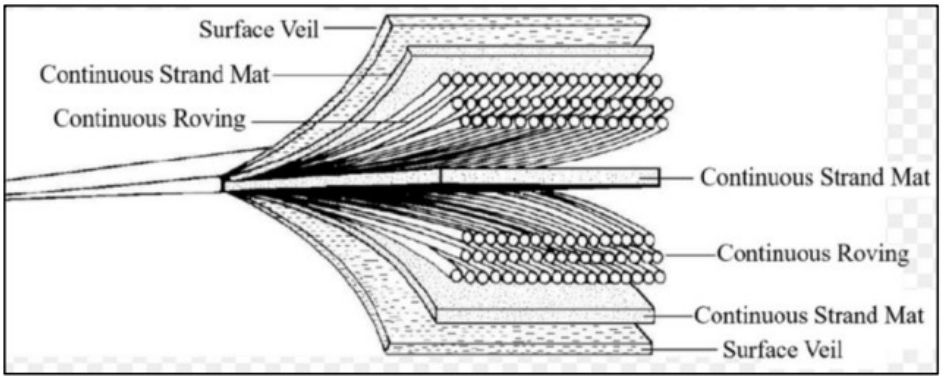

Figure 1.1 Typical pultruded layer *(www.creativepultrusions.com)*

The advancement of pultrusion technology resulted in the manufacturing of structural profiles composed of unidirectional and ±45o fiber becoming a viable construction material in civil infrastructure. The pultruded material has extraordinary mechanical and important in-service properties that look promising for civil applications if employed innovatively. However, some limitations restrain the growth of this material which requires further investigation.

2.2.2. Manufacturing procedure

The production procedure of pultruded glass fiber reinforcement polymers (PGFRP) was presented in the work of Bank [4]. Figure 1.2 shows the manufacturing progress to mass production of PGFRP. The manufacturing procedure of pultruded glass fiber reinforced polymer (GFRP) involves the following steps:

a) Fiber Selection: The first step in the pultrusion process is selecting the appropriate type and grade of glass fibers. These fibers are typically made from E-glass or S-glass and come in different diameters, lengths, and strengths.

b) Impregnation: Once the fibers have been selected, they are coated with a thermosetting resin, typically epoxy or polyester, in a liquid state. This impregnation process ensures that the resin is distributed evenly along the length of the fibers.

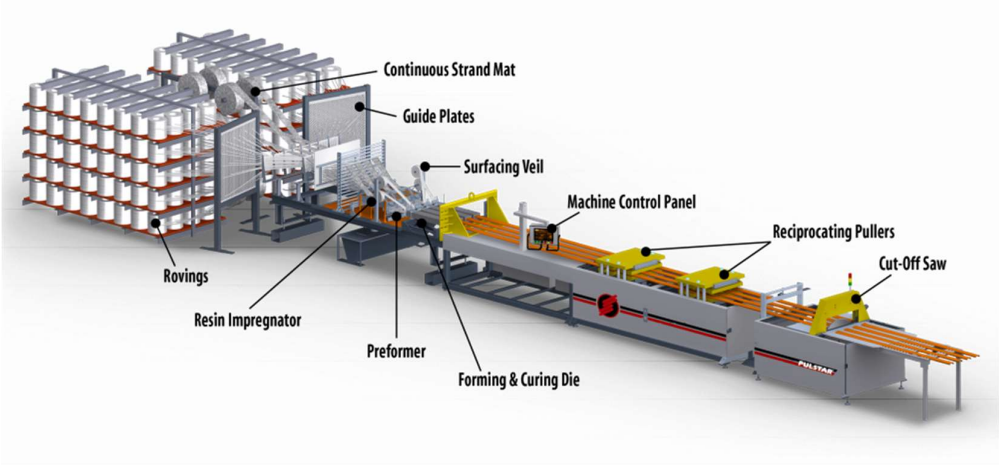

Figure 1.2 Manufacturing progress for Pultruded glass fiber reinforcement polymer *(Strong well, strongwell.com)*

c) Pre-forming: The next step is pre-forming the impregnated fibers into a desired shape, which can be done manually or using automated equipment. Pre-forming helps to ensure that the fibers are aligned in the correct orientation and that the resin is evenly distributed.

d) Curing: The pre-formed fibers are pulled through a heated die, which cures the resin and solidifies the composite material into its final shape. The temperature and speed of the pull can be adjusted to achieve the desired mechanical properties.

e) Post-curing: Once the composite material has been formed, it is often subjected to a post-curing process to strengthen further and stabilize the material. This involves heating the material in an oven or autoclave at a higher temperature for a specific period.

f) Cutting: After post-curing, the composite material is cut to the desired length using saws or other cutting tools.

g) Finishing: Finally, the finished GFRP products are subjected to finishing processes such as sanding, painting, or coating to enhance their appearance and durability.

Throughout the manufacturing process, quality control measures such as visual inspection, dimensional checks, and mechanical testing are used to ensure that the final product meets the desired specifications and quality standards. Commercial products were provided in many shapes and sizes as shown in Figure 1.3.

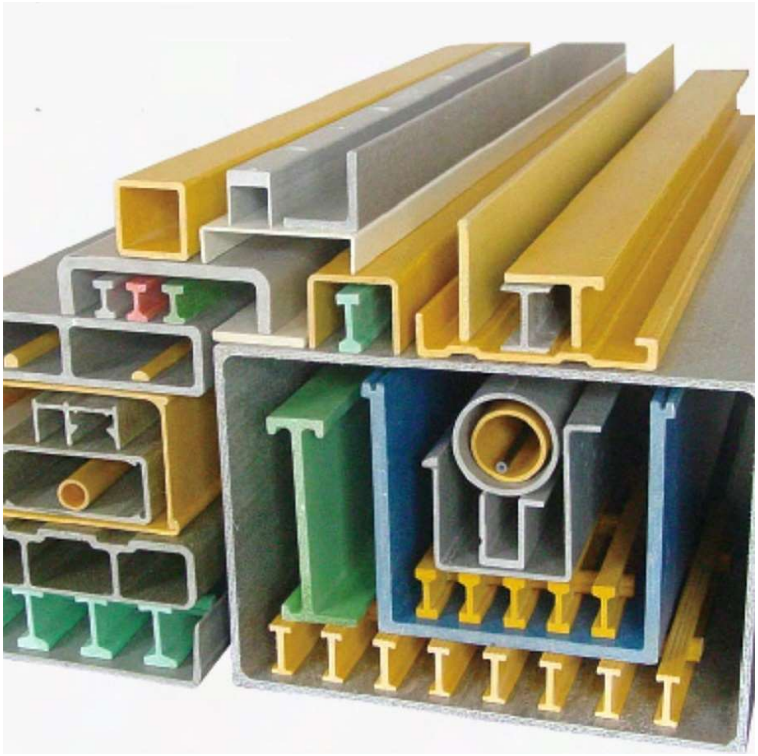

Figure 1.3 Common product of PGFRP product *(Hebei Huawei FRP Co., LTD)*

2.2.3. Development in civil engineering applications

PGFRP has emerged as a promising material for various applications in civil engineering due to its advantageous properties. The potential applications of PGFRP in civil engineering are diverse and have been extensively researched.

Bridge construction is one of the primary application areas for PGFRP in civil engineering. PGFRP has been used as reinforcement for concrete decks, girders, and piers in various types of bridges as Saleem Muhammad Azhar et al, 2021 [5] presented. The use of PGFRP in bridge construction can result in significant weight savings, reduced maintenance, and improved durability. PGFRP bridges offer the advantage of quick replacements for deteriorated structures while also providing a longer life cycle and lower maintenance costs compared to conventional steel or concrete bridges, particularly in environments with high levels of corrosion [6]. These benefits arise from the unique properties of PGFRP materials, which include high strength, low weight, and corrosion resistance. Compared to traditional steel or concrete bridges, PGFRP bridges can be manufactured offsite and assembled on-site, significantly reducing the construction time and costs. The modular design of FRP bridges also

allows for easy customization and modifications to fit different site requirements. In addition to their ease of installation, FRP bridges require minimal maintenance due to their inherent resistance to corrosion and other forms of degradation. [7]

Figure 1.4 Pedestrian and bicycle FRP bridge

In addition, PGFRP has been utilized in to construct various building components such as cladding, beams, and columns. PGFRP has demonstrated the ability to improve the strength and stiffness of these elements, leading to improved performance in earthquake or seismic events. PGFRP is a lightweight material with high tensile strength, making it ideal for seismic applications. The high strength-to-weight ratio of PGFRP means that it can provide equivalent or greater strength to traditional construction materials such as steel or concrete while weighing much less. [8]

Furthermore, PGFRP has been used as a strengthening material for the rehabilitation of existing concrete and masonry structures. The use of PGFRP in rehabilitation applications can extend the service life of structures and reduce the need for costly and disruptive replacement. [9,10].

Despite the numerous advantages of PGFRP materials for building applications, concerns still exist regarding their performance in elevated temperatures and fires. Studies have shown that PGFRP materials experience a significant reduction in strength at temperatures of 220°C, with reductions of 46%, 89%, and 95% in tensile, shear, and compressive strength,

respectively [11]. Moreover, it has been observed that glass fiber sheets (GFS) used in PGFRP materials are susceptible to thermal degradation, as confirmed by comprehensive experimental studies [12]. Therefore, it is crucial to consider these limitations when designing structures incorporating PGFRP materials. The lack of design guidelines, limited knowledge of material behavior under long-term loading, and high initial cost are also challenges in PGFRP applications. Although there are some challenges to using PGFRP materials in civil engineering, the increasing research in this area has demonstrated its potential as a viable alternative to conventional construction materials.

2.3. PGFRP member connection

2.3.1. Mechanically parameters of bolted connection

According to Bank et al. [13], the design of connections is the most critical aspect of the PGFRP design process. Similarly, Shin, Y.H [10] addressed that the joining system for pultruded FRP structures presents an intriguing area of study, particularly since steel is commonly used as the material for bolts while the web cleats, splice plates, and gussets are made of FRP material. Three types of FRP connections are widely used: mechanical, bonded, and combined. Mechanical or bolted connections are preferred in the construction aspect because they are not sensitive to temperature, humidity, surface preparation, convenience in replacement, or inspection [14]. In fact, bolted connections are commonly used in existing structures such as short-span road bridges, roofs and building frame structures. Turvey [15] pointed out that most composite structures made from custom and standard structural PGFRP are designed to utilize bolted connections only in specific situations. The design of the connection structure was also identified as a significant factor that affects the structural integrity and load-carrying capacity of the entire structure [14]. Bolted connections can use high-strength metallic bolts or FRP bolts with a smooth shaft. Therefore, the use of bolted connections in PGFRP members is an important research topic in many studies [16, 17]. There are two main ways to study the behavior of connections or joints: experimental and finite element analysis. Coelho et al. [18] presented experimental and analytical methodologies used in the bolted connection in PGFRP. Li et al. [19] also developed a simplified two-dimensional model to study the shear stress distribution in composite bolted joints. Balc et al. [20] employed ABAQUS to conduct a finite element analysis on the bolted connection between a beam and column end plate in their studies. To simplify the model, they utilized a finer mesh in regions likely to experience higher stress levels, specifically the support regions and contact areas.

However, due to gaps in design standards that limit the input of accurate material properties, theoretical models in finite element method (FEM) software may not fully capture all structural behaviors of PGFRP materials. Thus, the experimental method is advantageous for investigating pultruded FRP materials. It provides accurate and reliable data on their mechanical and physical properties, validates models and simulations, identifies material properties, and optimizes manufacturing processes. Previous studies have conducted experiments to investigate many aspects such as the influence of geometry, pultrusion direction, and fastener parameters. Feo.L et al. [21] concluded that in multi-bolt joints, the load distribution is not consistent due to differences in bolt position, clearance around the bolt holes, the tightness of the bolts, friction between the member plates, and at the interface between the washer and the plate. S. Russo [22] carried out an experimental investigation that focused on multi-bolted connections in FRP plates. The study in [22] incorporated recent experimental data to evaluate the structural performance of these connections, while also comparing the experimental results against anticipated ultimate strengths and existing design formulas. The researchers in [21,22] highlighted that the current structural design formulas used for joints comprising multi-bolted FRP plates must be more suitable and reliable.

2.3.2. Bolt torque tightening effects on static testing

The pre-tightening of bolts has been found to have a positive impact on both static strength and fatigue life of bolted joints in Fiber-Reinforced Polymer (FRP) laminates. Although different composite material systems respond differently to bearing fatigue loading, previous studies have consistently shown that bolt pre-torque tightening enhances the strength and life of FRP laminates under static loading conditions. Several aspects of the effects of pre-tightened bolts on FRP laminate strength under static loading have been explored [23-25]. Crews [26] performed static bearing tests using graphite/epoxy (T300/5208) laminate specimens and observed a significant increase in ultimate bearing strength due to the clamp-up effect. It was also observed that the maximum hole elongation prior to failure occurred in the case of zero bolt preload, and that the failure mode of specimens with torqued bolts occurred beyond the washer, as opposed to non-preload cases where bearing failure in the vicinity of the contact area was exhibited. Khashaba et al. [27] noted complementary results, with increased clamp-up torque leading to an increase in ultimate bearing strength for glass fiber-reinforced epoxy specimens. The effect of washer size on ultimate bearing strength was found to be limited but had a significant impact on hole elongation prior to failure. Sen et al. [28]

investigated the effect of various layup combinations using single lap joint configurations, achieving results similar to previous authors with a noticeable increase in ultimate bearing strength with increasing clamp-up torque. Ramkumar and Tossavainen [29] conducted an extensive static and fatigue testing program on both single and double-lap configurations. They found that increasing the torque from finger tight to 22.6 Nm achieved a 30% increase in bearing strength under static loading conditions. Poon and Gould [30] conducted a series of static and fatigue tests on several IM6/5245C composite material specimens in a double lap configuration, with clamp-up torques of 0 Nm, 5.6 Nm, and 16.9 Nm applied to the bolts. The results indicated that significant improvement in ultimate bearing strength was achieved with increased clamp-up torque. However, previous studies have conducted limited investigations into the influence of bolt fastening force on the efficacy of PGFRP connection structures when incorporated with strengthening materials such as carbon fiber (CF) or glass fiber sheet (GFS). This lack of research can be attributed to the relatively novel nature of strengthening using CF or GFS applications, making it challenging to obtain comprehensive and sufficient data on this topic.

2.4. Strengthening of multi-bolted connection in PGFRP

Various research studies have investigated specific aspects of bolted connections to improve their mechanical performance, including plate-to-plate connections, multi-bolted connections, and beam-to-column joints [31-34]. Ascione [31] examined the ultimate load that a pin-bearing could support and found that it decreased linearly as the bolt diameter decreased. The study suggested a formula for designing pin-bearings based on experimental results. Cooper and Turvey [32] conducted a statistical analysis to determine the ultimate load and the strength of single bolt joints to withstand damage at various levels. Wang [33] investigated the relationship between the size of a hole and the compressive bearing strength under load and found a strong correlation between the test results and predictions. Hassan et al. [34] reported on an experimental study of 105 multi-bolted double-shear lap connections, analyzing the impact of various factors including component width, distance from the edge, number and pattern of bolts, distance between bolts, component thickness, and fiber direction. The study [34] also examined failure behavior influenced by these factors. In general, the main parameters considered in PGFRP bolted connection are illustrated in Figure 1.5.

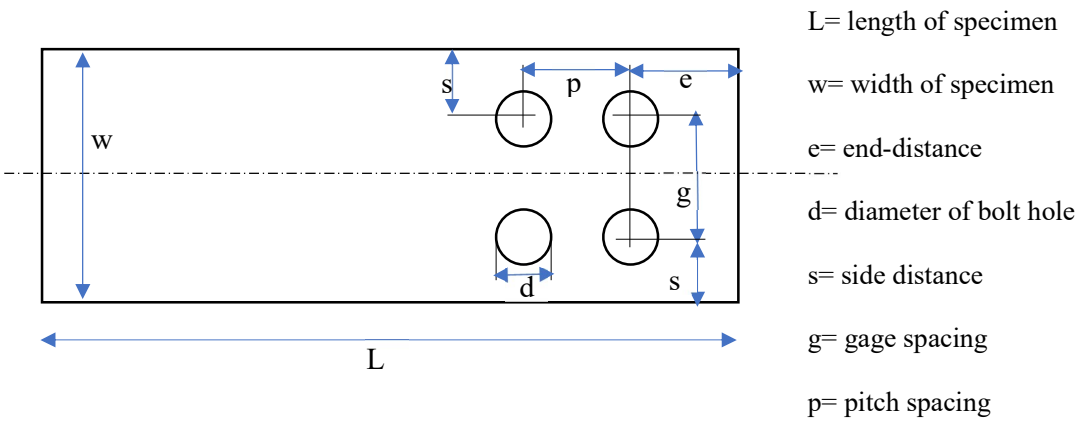

Figure 1.5 Geometric parameters for the multi-bolt joint connection

The complexity of failure modes associated with bolted connections of PGFRP profiles necessitates further research efforts to develop design guidelines and codes of practice. Among the factors affecting the connection strength of PGFRP structures, geometric parameters such as the end-distance-to-bolt-diameter ratio (*e/d*) and width-distance-to-bolt-diameter ratio (*w/d*) are particularly important. The significance of proper design parameters and guidelines for joining composite materials, specifically bolted and adhesive bonded joints, has been recognized in recent design guidelines such as the "Pre-Standard for Load Resistance Factor Design (LRFD) of Pultruded FRP structures" [35] and EUROCOMP [36]. These guidelines provide detailed parameters and requirements for designing FRP connections, including joint geometry, material thickness, clamping pressure, bolt hole tolerance, and loading conditions. It is recommended that these parameters be carefully considered in designing FRP bolted connections, as they significantly impact failure modes, such as bearing, shear-out, net tension, and combinations of these. Research studies by Kumar et al. [37], Machado et al. [38] and Nerilli and Vairo [39] have further explored and expanded on improving FRP connection design parameters, which have the potential to be included in future design guidelines and codes of practices. These parameters dictate failure modes and ultimately determine the strength of the joint connection. Shear-out failure typically results from a small *e/d* ratio, while a small *w/d* ratio leads to net-tension failure. Cleave failure, a combination of net-tension and shear-out failure, can also occur, and large values of e/d and w/d often lead to bearing failure.

To improve the performance of bolt connections in composite structures, various approaches have been proposed by different authors, such as increasing the bolt number or end-distance or utilizing strengthening layers made of materials like carbon nanotubes, nano clay,

or metal inserts [40-42]. Uddin, N. (2004) calculated that the Glass Fiber Sheet (GFS), which is composed of glass fiber and epoxy resin, can be an economical material for enhancing the strength of PGFRP [43].

Nhut et al. [44-46] have investigated the effects of GFSs on the single-bolted connections considering different parameters of bolt diameter, end distance of PGFRP plate to bolt diameter (*e/d*), and ratio values of width of PGFRP plate to bolt diameter (*w/d*). The authors suggested equations for estimating the ultimate strength of connections and predicting the potential modes of failure that may occur in various conditions of materials and parameters for single-bolted cases. However, almost no previous research was conducted on strengthening the multi-bolted PGFRP connection using GFS. In previous studies, the research objectives are limited to a single bolted connection under strengthening by GFS.

In this thesis, the preliminary experiments involved using non-tightening forces for bolts, with specimens divided into two-, four-, and five-bolt groups and categorized into three kinds of GFS material. Moreover, a supplemental bonding test was conducted to evaluate bond strength. The main objective of this investigation was to introduce an integration method that employs GFS to enhance the strength of PGFRP multi-bolted connections. The results of the conducted and the derived equation for predicting joint strength provide valuable insights for designing PGFRP structures with strengthened multi-bolted connections.

2.5. Strengthening for beam-to-column connection in PGFRP

The PGFRP commercial product can adopt various cross-sectional shapes, whereas the latter often imitate structural steel profiles, such as I, tubular, and angle sections. Numerous studies have been conducted about frame connections for beams-to-columns since the late 1980s. In the design of structures made of glass fiber reinforced polymer (GFRP), the connections between beams and columns play an important role. Additionally, these connections can help in reducing the deflections of GFRP flexural members [47]. Hence, the examination of PGFRP frame connections is of utmost importance for several reasons. The joints usually govern the design of PGFRP structures and are susceptible to brittle failure modes, e.g., Bank [48], which can significantly affect their robustness. Secondly, when analyzing the deflections of beams designed based on serviceability requirements [49,50], it is crucial to consider the actual stiffness of the joints.

When designing steel frames, it is common practice to assume that beam-to-column

connections are either fully rigid or pinned, referred to as Qureshi and Mottram [51]. However, the actual stiffness of these connections lies between these two phases, resulting in a "semirigid" behavior [52]. This behavior is characterized by a moment-rotation curve that exhibits properties such as stiffness, ultimate moment, and rotation capacity. To obtain the values for these connection properties, it is necessary to determine the complete moment-rotation curve through testing

The review was based on fifty-nine moment-rotation tests conducted by J. Turvey and C. Cooper [53] on bolted beam-to-column joints between pultruded GFRP profiles. Despite the potentially greater efficiency of adhesive bonding, most of these frames employ bolted joints to connect beams and columns. This is due to various reasons such as the simplicity of site connection, ease of dismantling, and simpler inspection.

Initially, all-composite connection systems were proposed for investigation, which showed improvements in stiffness and strength compared to previous steel-like connection systems. However, these systems had proprietary and complex auxiliary parts, which made them impractical for the construction industry. Mottram and Zheng have proposed connection systems with additional metallic parts [54,55]. Papers by Bank et al. (1990) [48], Bass and Mottram (1994) [56], and Turvey and Cooper (1996b) [57] contain moment-rotation characteristics for different connections, which could be classified as semirigid. These investigations used conventional steel parts for connection, such as cleats at the web and flange. However, these researchers soon discovered that replicating common steel practices was an unsuccessful approach. Therefore, they proposed several novel approaches, such as using different types of connection steel parts or combining bolted and bonding connection methods.

Bank et al. (1994) [58] modified the joint layout to achieve improved initial rotational stiffness and ultimate moments using gusset plates and multicellular elements. In an effort to improve joint performance in bolted joints between pultruded GRP profiles, researchers carried out finite element [59,60], parametric analysis [61] or combined analytical (CM) and numerical (FE) analysis [62] to determine the optimal shape of an element that would fulfill the function of the previous joint tests. The results of the analysis were used to develop the optimized component. To compare the effectiveness of different connections for PGFRP frames, Smith et al. conducted testing on various connection types including standard connections made by cleat, gusset, and cuff connection in both PGFRP and steel materials [63]. The results showed

that connection and frame stiffnesses were considerably improved with the use of innovative connections compared to the standard specimens. In recent years, Martins et al. investigated behaviors of beam-to-column connections in various types of profiles using a diversity connection system: I-sharped profile using stainless cleats [47]; novel connection system for tubular profiles [64].

Most of the research on bolted PGFRP frame connection systems has been focused on their quasi-static monotonic behavior, with only a few authors exploring their cyclic behavior. Mosallam [65] conducted cyclic testing on one bolted and one bonded beam-to-column connection that incorporated a proprietary composite auxiliary part. Zhang et al. [66] studied the behavior of bonded and bolted beam-to-column connections with steel sleeve auxiliary parts and various connection typologies. Still, their loading history was defined based on the ANSI/AISC 341-16 procedures for steel structures [67]. While some of the connections were able to dissipate energy and exhibit ductility most previous studies could have comprehensively evaluated the parameters that define a joint's cyclic response. In contrast, Martins et al. [64] tested a series of bolted beam-to-column connections between pultruded PGFRP tubular profiles under a loading history defined by the ECCS protocol for steel structures [68]. In [64], the authors evaluated various parameters related to the hysteretic behaviors of the connections, such as the dissipated energy evolution and accumulation, allowing for a more direct comparison of the performance of each connection. Based on their findings, Martins et al. identified the connection system that exhibited the most favorable cyclic behavior. It was subsequently used in sway tests on 2-dimensional frames [69] and incorporated into the Click House emergency building prototype [64]. The Click House project developed and provided emergency accommodation in the EU, built based on a tubular PGFRP profile. PGFRP houses can offer superior performance at a competitive cost in several aspects, including their light weight, ease of transportation, and quick and effortless assembly and disassembly. Additionally, they offer flexibility in terms of reutilization, while also meeting the requirements for structural safety, thermal performance, and durability, which results in lower maintenance costs. However, it should be noted that the steel components used in these projects were highly customized and thus challenging to produce and install on a larger scale.

The present thesis briefly explores the potential enhancements to box-section beam-to-column (tubular profile) connections using Glass Fiber Sheets (GFS) as a strengthening material via bolted joints. As discussed earlier in this paper, GFS is a suitable material that can

effectively increase the connection's strength. The experiments evaluated the performance of member connections subjected to cyclic loads with stainless steel parts, including cleats and through-section bolts. This approach holds great potential as a competitive composite structural solution to traditional construction techniques.

2.6. Research gaps in previous studies and presenting novel solutions

As mentioned earlier in this chapter, PGFRP has emerged as a sophisticated and widely applicable material for constructing structures. Additionally, GFSs have enhanced the strength of bolted connections in PGFRP. However, despite these advancements, there remain certain research gaps in current studies, which are outlined below:

1. The current design of pultruded GFPR connections is based on several commonly used standards. ACMA [35] and EUROCOMP [36] standards recommend calculating the capacity of bolted joints with up to three rows of bolts, utilizing the limit states design (LRFD) for tension members, compression members, flexure-shear combined forces, torsion plates, and built-up member bolted connections. Some aspects have not been mentioned in those standards:
    - There is no instruction for the case of strengthening by GFSs within existing standards.
    - There is no indication of tightening forces, which may decrease over time during the performance of the structures.
    - Furthermore, debonding failure has not yet to be considered in the standards, but often occurred in specimens that were strengthened by GFSs.
2. Based on the findings of previous studies, it can be concluded that while certain researchers have put forth methods for strengthening PGFRP connections, there is a need to develop more practical and effective techniques to overcome the limitations of advanced PGFRP materials.
    - There have been limited instances where authors have utilized GFS to enhance the strength of bolted connections in PGFRP structures in previous studies.
    - No research has been conducted to investigate the behavior of PGFRP multi-bolted connections when using GFS as a strengthening method.

This study proposes a novel and straightforward method for strengthening PGFRP

connections using glass fiber sheets (GFSs) to address those issues. Various types of GFSs were employed to assess the strengthening effects of PGFRP connections. The following chapter will delineate the enhancement resulting from alterations in connection geometries, number of bolts, and bolt diameter. Furthermore, the influence on the connection strength of tightening force, and bonding strength in PGFRP to was also evaluated.

Furthermore, a full-scale experiment was conducted on a beam-to-column connection to assess the practical effectiveness of the GFS method in construction. The testing results were evaluated based on maximum loading and failure behaviors to conclude the suitability of the proposed strengthening solution.

CHAPTER 3
MULTI- BOLTED CONNECTION OF PGFRP ON STRENGTHENING BY GFS

3.1. Introduction

This chapter investigates the effectiveness of Glass Fiber Sheets (GFSs) in strengthening multi-bolted connections in PGFRP materials. The study comprises 72 experimental specimens that were subjected to various conditions, including different GFS layers, numbers of bolts, and end distances. The GFS layers used for strengthening the PGFRP connections were 0°/90° and ±45° glass woven roving, as well as a chopped strand mat (CSM), all of which were manufactured through the Vacuum Assisted Resin Transfer Molding (VaRTM) technique. The end distances selected for this study were 2*d* and 3*d*, where d represents the bolt diameter of 12mm (M12) for all connections.

3.2. Material properties experiment

3.2.1. Pultruded GFRP

The original PGFRP material is FS1005, a commercial product of Fukui Fibertech Co., Ltd (Toyohashi, Aichi, Japan). It has a thin shape with a total thickness of 5 mm and a width of 100 mm (the weight/ length is 880g/m). The PGFRP product is composed of 2 phases of the fiber part: continuous one-direction glass roving (CD) and glass fiber mat (GFM). Both fiber parts were generated from E-glass roving as the raw material. The unsaturated polyester resin was used to make the resin part.

The original material flat bar is shown in Figure 3.1(a), with 0.5mm thickness of GFM in two side surface parts and 4mm thickness of the CD part.

3.2.2. GFSs

The study used three types of glass fiber sheets (GFS) to investigate the effects and tendency of strengthening methods. Two types of laminate were used for making GFS-strengthened material: $0/90^0$ woven roving (580 g/m2) (ERW580-554A) and CSM 450 (g/m2) (ECM450-501, provided by Central Glass Co., Ltd., Tokyo, Japan). Firstly, three layers of $0/90^o$ were placed, then cut to[0/90] or rotated onto $\pm 45^o$ to make [±45] lamination. Similarly, [CSM] was created by cutting the CSM laminate. After cutting and stacking, glass fiber sheets were conducted in VaRTM to reduce the thickness of fiber layers, as shown in Figure.3.2.

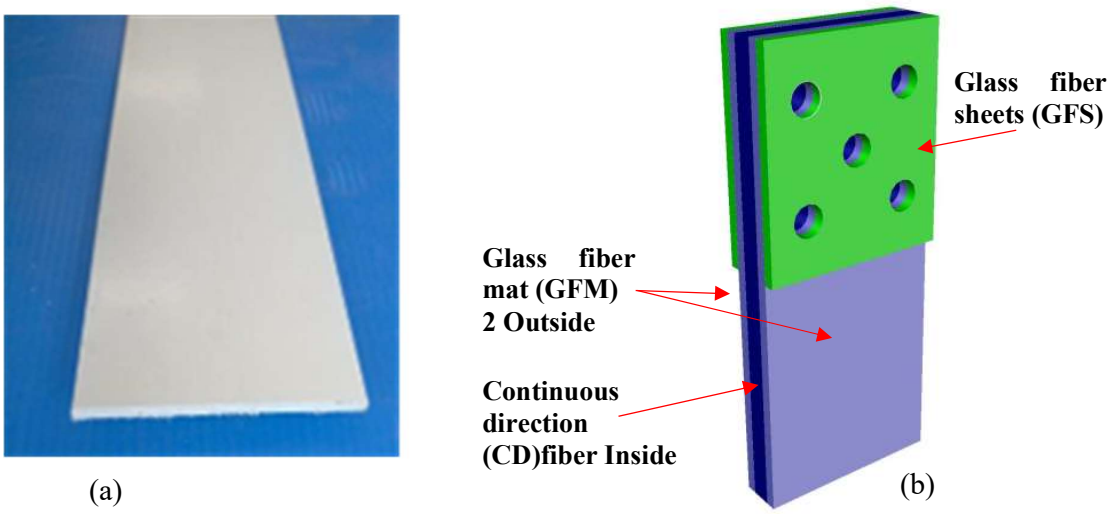

Figure 3.1 PGFRP before and after molding to making specimens:

(a) PGFRP material sheet; (b) Specimens after strengthening by GFS

The VaRTM technique confers various benefits over alternative molding methods, including cost-effectiveness and straightforward molding for multiple shapes. Additionally, one of the most notable advantages of the VaRTM method is its ability to produce a thin lamination with a high fiber content. In this study, the glass fiber sheets were impregnated with epoxy resin (E205, a product of Konishi, Osaka, Japan) using the VaRTM method.

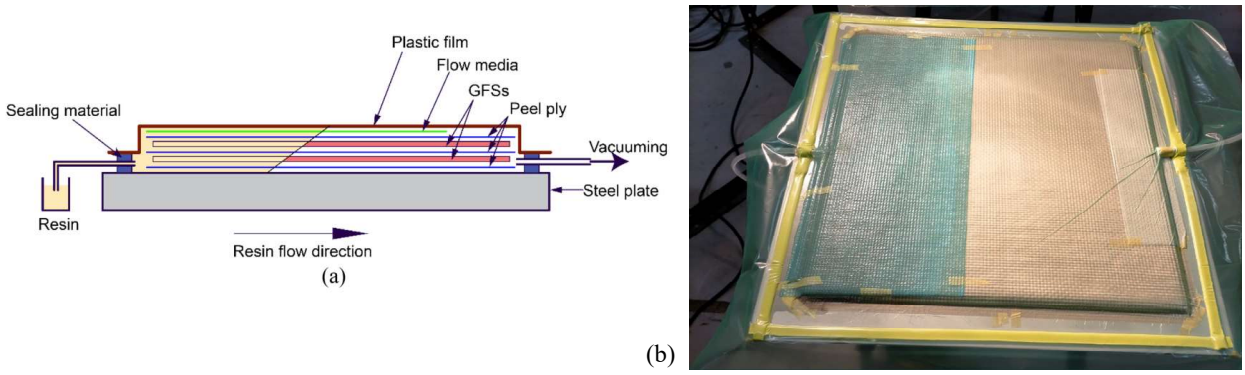

Figure 3.2 Schematic sectional view of the VaRTM to mold GFS:

(a) the molding process; (b) Molding GFS on site

The VaRTM sequence typically involves the following steps:

a) Preform preparation: The fiber reinforcement (such as glass or carbon fibers) is

arranged in a predetermined pattern and placed in the mold. The preform may be composed of a single layer or multiple layers, depending on the desired properties of the final composite material.

b) Mold sealing: The mold is sealed using a vacuum bag or a flexible membrane to create a vacuum-tight seal. The mold and preform are placed in an oven or on a heated tool to ensure that the preform is at the desired temperature for resin injection.

c) Resin injection: The liquid resin is injected into the preform under vacuum using a series of inlet and outlet ports. The resin flows through the preform, impregnating the fibers and filling any voids.

d) Curing: The resin is cured by applying heat or through a chemical reaction, depending on the type of resin used. The curing process typically takes several hours, and the temperature and pressure must be carefully controlled to ensure that the resin fully cures, and the composite material is strong and durable.

e) Demolding: Once the composite material is fully cured, the mold is opened, and the part is removed. The excess resin and flash are trimmed, and the part is ready for use.

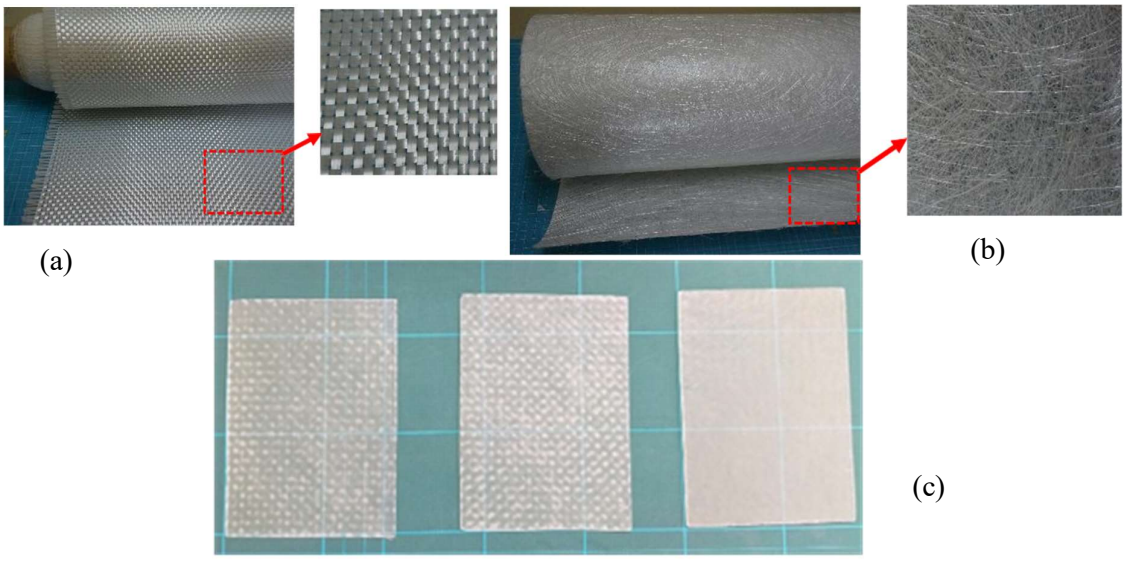

Figure 3.3 GFS before and after molding to making specimens:

(a) laminate 0/90; (b) laminate CMS; (c) GFS sheet: [0/90]; [±45]; [CSM]

3.2.3. PGFRP material properties testing

The properties of basic materials include GFS, two main components of GPFRP: CD and GFM layer are investigated by experiments. The results of those experiments are used to estimate and explain failure modes in connection tests. Two PGFRP pasted two faces of 2 GFS for strengthening. The bond matrix, E250 (product of Konishi, Osaka, Japan) adhesive has the elastic modulus and passion's ratio of 3 GPa and 0.37, respectively (from the manufacturer). As shown in Figure 3.1, the PGFRP is composited from 2 layers: one part outside the glass fiber mat (GFM) and another inside the continual glass fiber roving (CD). The glass fiber mat has random fiber directions and can be considered an in-plane isotropic material.

The list of basic material tests was implemented as shown in Table 3.1.

Table 3.1 List of specimens for material test

Specimens	No. of specimens	Specimen dimensions ($w \times l$) (mm)	Explanations	Standard tests
Tensile test	5	25 × 250	Tensile tests for PGFRP in the loading direction	JIS.K.7164
Shear strength	5	56 × 76	Shear strength test for PGFRP	JIS.K.7164
Shear-out CD	5	84 × 250	Shear-strength test for CD part of PGFRP	JIS.K.7164

(a) Tensile test

The tensile and shear strengths of the PGFRP plates were determined through tensile and shear tests, respectively. The present study was focused on analyzing the connection strength of GFS specimens using only the standard tensile test. The dimensions of the specimens were 25 x 250 mm for width and length, respectively, and they had a 100 mm holding grip length on both sides.

The PGFRP members have pasted aluminum plates at two ends of specimens and E250 epoxy to elongate the lengths of the specimens. Strain values were measured from strain gauges attached to both surfaces of the specimens, as shown in Figure 3.4. These values were used to determine the elastic modulus (E) for PGFRP material. Figure 3.4 (a). shows the test setup for tensile material tests. All dimensions of each specimen, including the widths of the specimens and the thicknesses of the specimens, were measured to calculate the actual cross-sectional areas of all specimens.

(a)

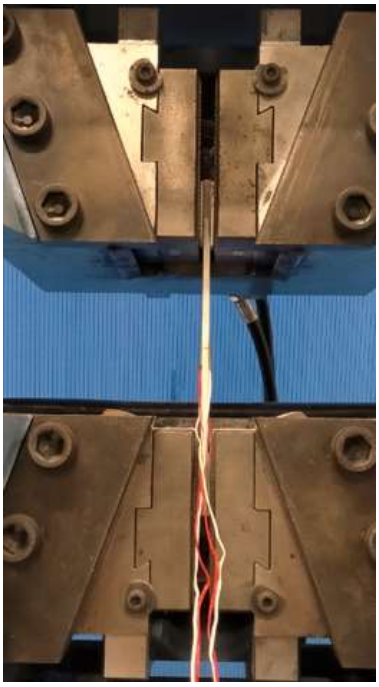

(b)

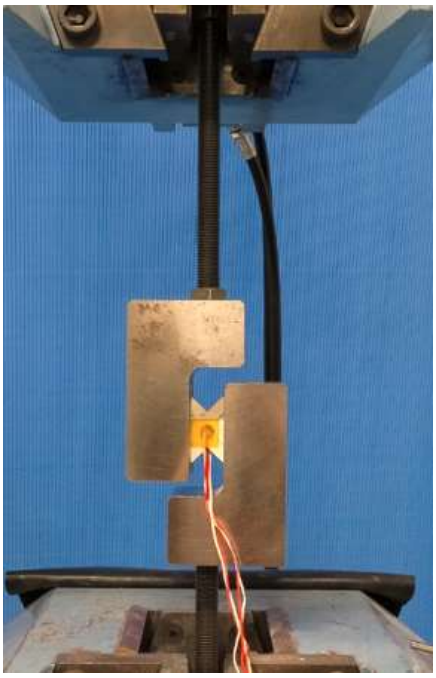

(c)

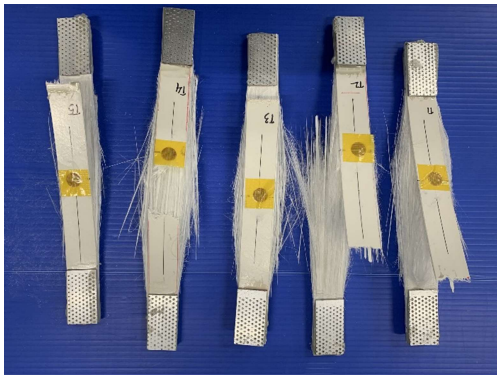

(d)

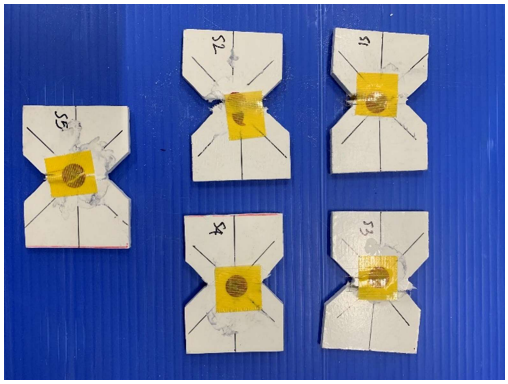

Figure 3.4 PGFRP material test

(a) Tensile test (b) Shear test (c) Tensile failure specimen (d) Shear failure specimen

The elastic modulus was calculated from two different strain points as the equation:

$$E = \frac{\Delta\tau}{\Delta\gamma} \tag{3.1}$$

Whereas $\Delta\tau$ is the different between the lower strain point is around 500 (μstrain) and the upper point is around 2500 (μstrain) and $\Delta\gamma$: is different in shear strain at those 2 points, respectively. Based on the Eq (3.1), the elastic modulus of PGFRP was determined as shown in table 3.2. Figure 3.5 shows a stress-strain relation chart with the data collected from two-direction strain gauges in testing.

Table 3.2 Results and specimen's parameter of tensile test

Parameters	Unit	T1	T2	T3	T4	T5	Average
P max	kN	39.29	43.19	71.39	68.00	65.99	57.57
Thickness	mm	5.00	5.00	5.00	5.00	5.00	
d (avg)	mm	26.29	25.81	25.90	25.64	25.81	
A	mm^2	31.43	29.05	29.50	28.20	129.05	
E- modulus	GPa	27.68	29.21	29.96	28.32	27.78	**28.59**

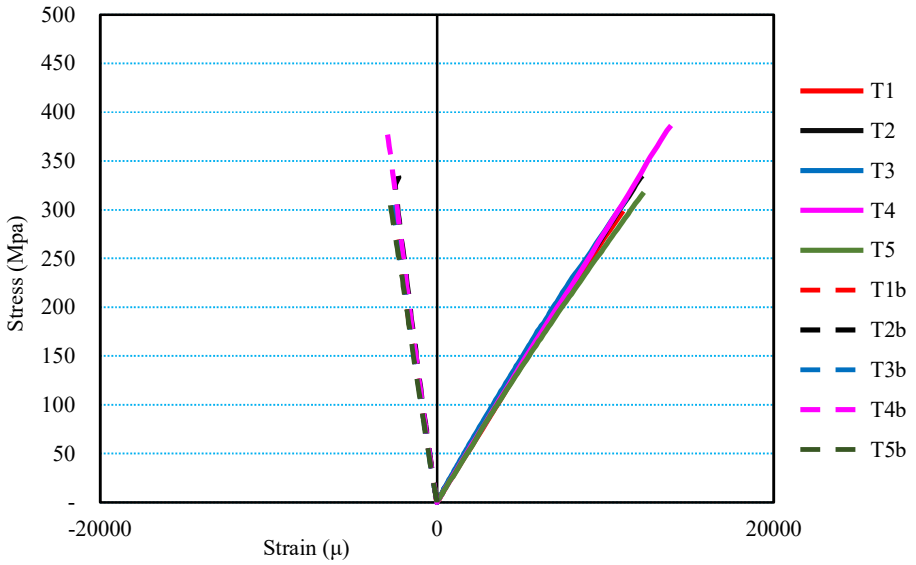

Figure 3.5 Stress-strain relations of material tensile strength test

(b) Shear strength test

To evaluate the shear strengths of the PGFRP members, we utilized the V-notched rail shear method as specified in ASTM-D7078. Five specimens of PGFRP were tested, as shown in Figure 3.4(b), using the V-notched test setup. The V-notched shear specimens had dimensions of 56x76 mm, and two directional strain gauges were attached to both surfaces of the specimens to measure the shear strains. The strain gauges were placed at ±45 degrees. Each tested material type consisted of five specimens, and the average results for both tensile and shear strengths were calculated.

The shear strengths of the specimen with thickness t and the shear modulus of the materials were obtained as follows:

$$\tau = \frac{P}{A} = \frac{P}{td_1} \tag{3.2}$$

$$\gamma_i = |\varepsilon_{+45}| + |\varepsilon_{-45}| \tag{3.3}$$

$$G_{12} = \frac{\Delta\tau}{\Delta\gamma} \tag{3.4}$$

In these equations, P is the experimental shear load, t is the specimen thickness, d_1 is the width between notches, γ_i is the ith data engineering shear strain, ε_{+45} is the +45° ith data point strain, ε_{-45} is the –45° ith data point strain, G_{12} is the in-plane shear modulus of the materials, $\Delta\tau$ is the shear stress difference between the two strain points; and $\Delta\gamma$ is the shear strain difference between two strain points. All experiment input and output data are shown in Table 3.3 as follows. Similarly in the tensile test, Figure 3.6 depicts the stress-strain relation of the shear strength test.

Table 3.3 Failure load and parameter of specimens in shear strength test

Parameters	Unit	S1	S2	S3	S4	S5	Average	CoV
P max	kN	5.26	5.48	5.92	5.08	5.88	5.53	0.052
d_1	mm	30.88	30.45	31.14	30.67	31.45	30.92	
Thickness	mm	5.06	5.07	5.07	5.08	5.07	5.07	
τPFRP (G_{12})	MPa	33.64	35.56	37.49	32.64	36.92	**35.25**	

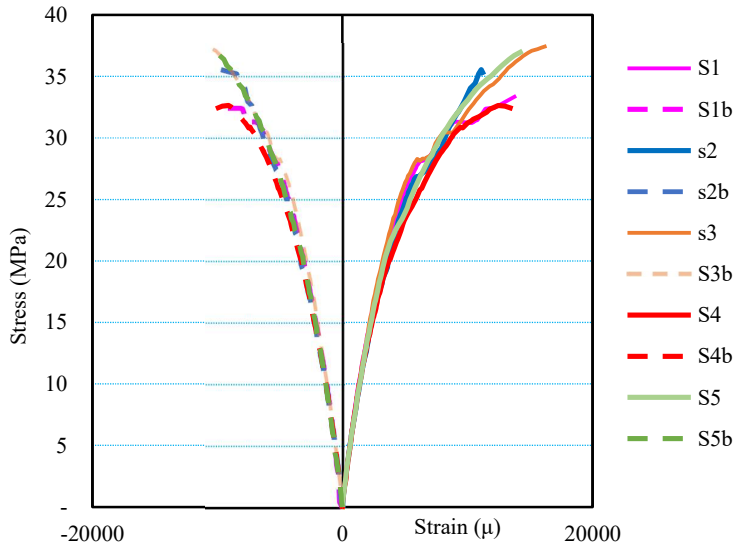

Figure 3.6 Stress-strain relations of material shear strength test

(c) Shear-out strength test

Tensile tests with pin-bearing conditions were also conducted to determine the shear-out strength of the CD parts. Figure 3.7 shows the specimen preparation for these tests. The outside

GFM parts of the pultruded profiles were removed by the sanding method. After that, the real thickness of the remaining CD parts was measured again to determine the shear-out strength of the CD parts. The shear-out strength values were calculated corresponding to the shear-out tests of the specimens having end distances of $e = 3d$.

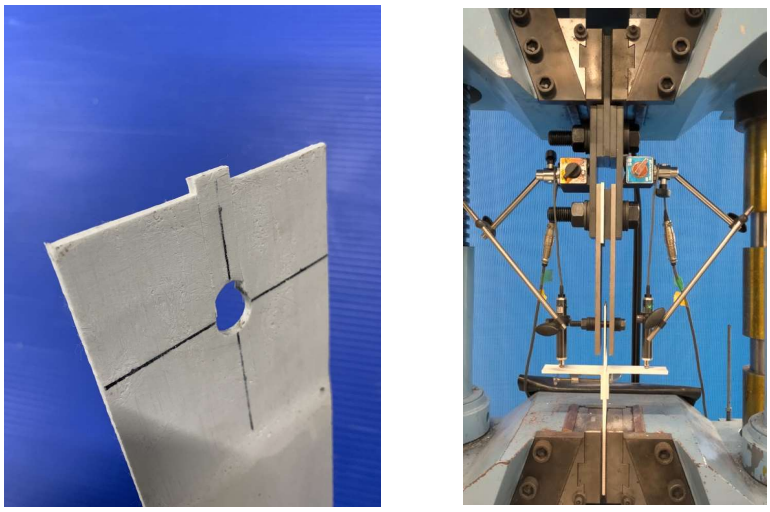

(a) Failure specimen of the shear-out test. (b) Test set-up

Figure 3.7 Test setup and failure specimens for the shear-out strength test

The equation can determine the shear-out stress as below:

$$\tau_{CD=} = \frac{P}{2et} \tag{3.5}$$

Whereas P is ultimate load; e is end-distance: dimension from center bolt hole to loaded end of specimens; t present to the thickness of specimens. The shear-out results test is shown in Table 3.4.

Table 3.4 Failure load in shear-out test

Specimens	Parameters	Unit	SO1	SO2	SO3	SO4	SO5	Average	C.o.V
SO_{CD}	Pmax	kN	2.10	2.08	2.89	3.25	2.84	2.63	
	Thickness	mm	3.22	3.09	2.96	3.29	3.10	3.13	
	d (avg)	mm	84.00	84.00	84.00	84.00	84.00	84.00	
	τCD	MPa	7.77	8.01	11.64	11.75	10.91	10.01	0.17

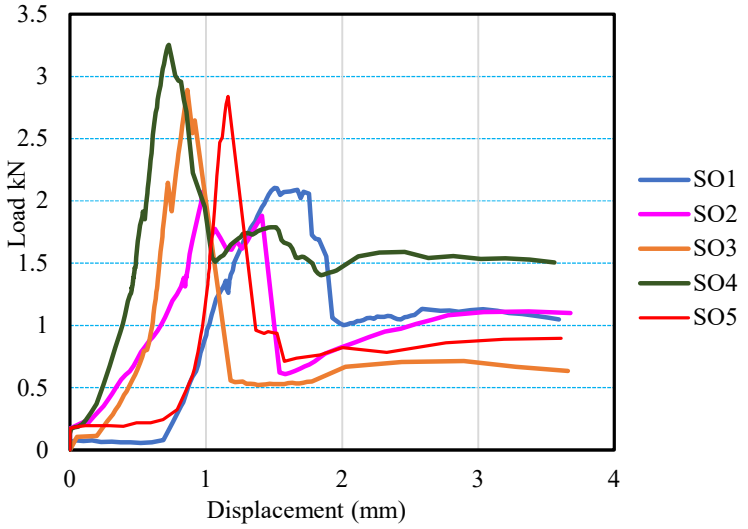

Figure 3.8 Load- displacement relations of material shear strength test

The material properties of the GFS testing were previously determined in a separate investigation, as reported in [44,45]. Table 3.5 provides a comprehensive list of all the specimens used for the material tests conducted by Nhut [44,45].

Table 3.5 List of specimens for material test

Specimens	No. of specimens	Specimen Dimensions ($w \times l$)(mm)	Explanations	Standard tests
T0/90	5	25 × 250	Tensile tests for 0°/90° GFS	JIS.K.7164
T45	5	100 × 200 (modified)	Tensile tests for ± 45° GFS	JIS.K.7164
TCSM	5	25 × 250	Tensile tests for CSM GFS	JIS.K.7164
C0/90	5	25 × 125	Compressive tests for 0°/90° GFS	JIS.K.7018
C45	5	25 × 125	Compressive tests for ± 45° GFS	JIS.K.7018
CCSM	5	25 × 125	Compressive tests for CSM GFS	JIS.K.7018

3.3. Connection strength test

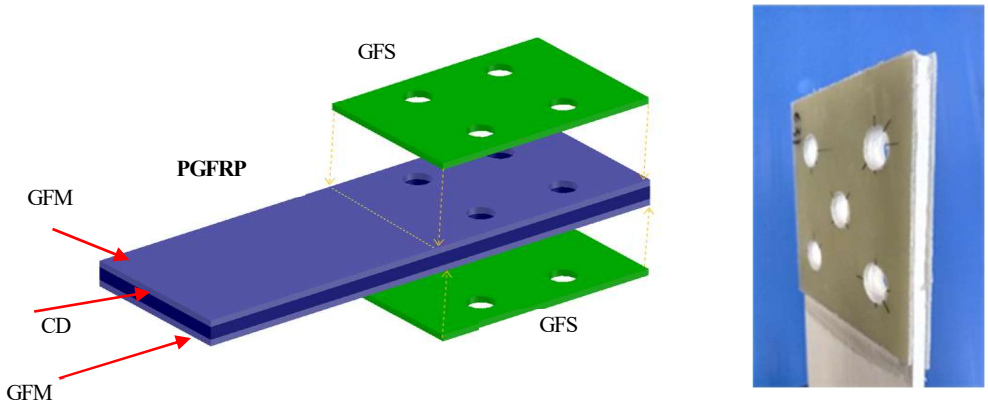

Figure 3.9 Material and specimens: (a) PGFRP; (b) specimens.

3.3.1. Specimens and testing diagram

The dimensions of specimens were designed to meet the minimum criteria of ACMA pre-standard [35]. The inner edge of PGFRP flat plates was taken with 84 mm width sheet to be used to produce specimens in the connection experiment. GFSs were pasted onto two surfaces of PGFRP using E250 adhesive (Provided by Konishi company, Japan), as shown in Figure 3.9(b). The detail of strengthening specimens is shown in the diagram in Figure 3.10.

In Figure 3.10, a universal testing machine (1000 kN) was used for connection testing. The load application system consisted of the following:

- The main part of the machine with a load capacity of 1000 kN (point A)
- Crosshead at the top (point B1) and bottom (point B2). The top cross head was clamped to a steel plate in the holding frame (C) while the bottom was clamped directly to specimens (D)
- The holding frame (C) was installed from the steel plate system and connected by two M30 bolts. In the upper row of steel plates, the M30 bolt was tightened (point C1). In the lower row tape, the M30 bolt connects plates as a pin-bearing type (point C2).
- The specimens (D) connect with two steel plates of the holding frame by the M12 bolt. The number of M12 bolts depends on the designated parameter of the specimen: two, four or five bolts.
- Two displacement transducers (E) built in vertically at two sides of the specimens.

The testing was conducted as a monotonic test under tensile loading with a resolution of 0.02 kN/ second, until the maximum displacement of the crosshead reached 30mm. Alongside the testing study, testing results in previous research were referred to predict the ultimate load, and for all configurations of connection systems.

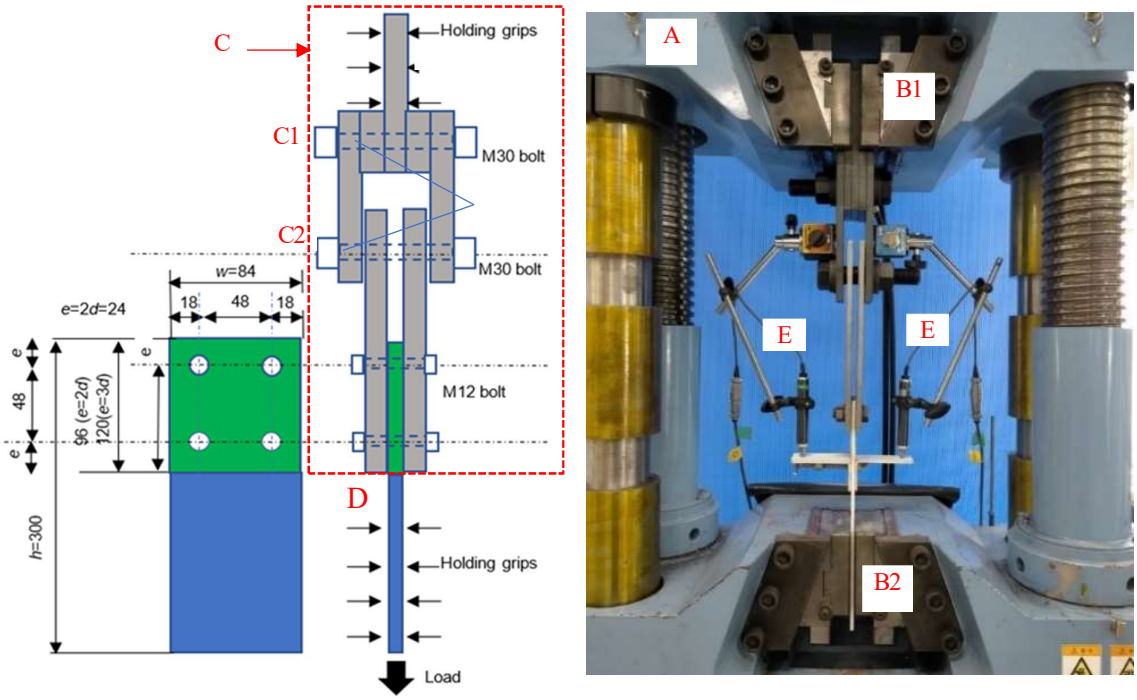

Figure 3.10 Connection test setup.

3.3.2. Testing program

The detailed parameters of specimens are shown in Table 3.6. The definitions are as follows:

• [Glass fiber] $_{T\text{-}N}$ denotes the type of glass fiber sheet made to strengthening specimens: $0/90^0$ GFS, $\pm45^0$, or CSM.

• $NS_{N\text{-}T}$ is a non-strengthening specimen (original PGFRP).

• *T* denotes the dimension of end distance (*e*) by ratio with bold size (*d*) ($e = 2d$ and $e = 3d$).

• *N* presents the quantity of bolts ($N = 2$, 4, or 5).

The M12 bolt with diameter d=12 mm and bolt hole diameter d_n=14mm was used in the

connection testing.

Table 3.6 Specimens list in the connection test

Specimen	End Distance (mm)	No. of Bolts	avg of t_{GF} (mm)	No. of Specimens
$[NS]_{2-2}$	24	2		3
$[NS]_{3-2}$	36	2		3
$[NS]_{2-4}$	24	4		3
$[NS]_{3-4}$	36	4		3
$[NS]_{2-5}$	24	5		3
$[NS]_{3-5}$	36	5		3
$[0/90]_{2-2}$	24	2	1.21	3
$[0/90]_{3-2}$	36	2	1.22	3
$[0/90]_{2-4}$	24	4	1.26	3
$[0/90]_{3-4}$	36	4	1.26	3
$[0/90]_{2-5}$	24	5	1.26	3
$[0/90]_{3-5}$	36	5	1.26	3
$[\pm45]_{2-2}$	24	2	1.24	3
$[\pm45]_{3-2}$	36	2	1.25	3
$[\pm45]_{2-4}$	24	4	1.23	3
$[\pm45]_{3-4}$	36	4	1.23	3
$[\pm45]_{2-5}$	24	5	1.23	3
$[\pm45]_{3-5}$	36	5	1.23	3
$[CSM]_{2-2}$	24	2	1.49	3
$[CSM]_{3-2}$	36	2	1.45	3
$[CSM]_{2-4}$	24	4	1.48	3
$[CSM]_{3-4}$	36	4	1.47	3
$[CSM]_{2-5}$	24	5	1.49	3
$[CSM]_{3-5}$	36	5	1.50	3

3.4. Experimental results

3.4.1. Strengthening effects

Generally, based on the results of connection testing, it can be concluded that GFS-strengthened specimens had better connection capacity compared to non-strengthened specimens. The effectiveness of the strengthening increased as the end distance increased. Additionally, the maximum load of [±45] specimens was lower than [0/90] and [CSM] specimens in almost every parameter of the number of bolts and end distance, and the joint capacity witnessed a marked increase when changing from two to four bolts.

The details of the maximum loads of the joint strength tests are presented in Table 3.6. In Figure 3.11, the average results for parameter specimens are illustrated case by case. The result demonstrated that the connection capacity of GFS specimens was better in comparison

with the NS specimens in the whole parameter series. The P_{st} /P_{NS} ratio, which measures the effectiveness of the strengthening or non-strengthened specimens, changes from 1.61 to 2.77.

In consideration of the strengthening effect by types of GFSs, as shown in Table 3.6 and Figure 3.11, the maximum load of [±45] specimens was lower than [0/90] and [CSM] specimens in almost every parameter of number bolt and end distance. We were expanding the end distance produced increasing connection strength. All specimens obtained a higher ultimate load when the end-distance *e=2d* was changed to *e=3d*, with the upper line graph presented for 3d specimens.

The joint capacity witnessed a marked increase when changing from two to four bolts. When reversing four bolts to five bolts, the connection strength rose slightly. However, the connection strength was almost unchanged when a bolt was added, from four to five bolts in the [±45] GFS specimens, which will be explained in the next chapter.

Table 3.6 Maximum connection load in testing

(a) Ultimate load of [0/90] GFS strengthening specimens (unit: kN)

Specimens	$\mathbf{[0/90]_{2\text{-}2}}$	$\mathbf{[0/90]_{3\text{-}2}}$	$\mathbf{[0/90]_{2\text{-}4}}$	$\mathbf{[0/90]_{3\text{-}4}}$	$\mathbf{[0/90]_{2\text{-}5}}$	$\mathbf{[0/90]_{3\text{-}5}}$
1	24.08	37.45	51.26	69.56	64.26	66.63
2	28.34	35.18	47.52	55.80	63.43	68.69
3	31.71	37.15	56.80	57.26	62.11	72.41
avg	28.05	36.59	51.86	60.87	63.27	69.25
C.o.V	13.63%	3.37%	9.00%	12.41%	1.72%	4.23%
P_{st}/P_{NS}	2.77	2.05	2.05	1.67	1.77	1.82

(b) Ultimate load of [±45] GFS strengthening specimens (unit: kN)

Specimens	$\mathbf{[\pm45]_{2\text{-}2}}$	$\mathbf{[\pm45]_{3\text{-}2}}$	$\mathbf{[\pm45]_{2\text{-}4}}$	$\mathbf{[\pm45]_{3\text{-}4}}$	$\mathbf{[\pm45]_{2\text{-}5}}$	$\mathbf{[\pm45]_{3\text{-}5}}$
1	27.31	32.39	61.23	62.84	50.38	56.74
2	24.87	34.30	51.86	59.30	56.64	53.73
3	26.21	34.67	46.76	53.07	55.73	56.49
avg	26.13	33.79	53.28	58.40	54.25	55.65
C.o.V	4.67%	3.62%	13.77%	8.47%	6.24%	3.00%
P_{st}/P_{NS}	2.58	1.89	2.11	1.61	1.77	1.82

(c) Ultimate load of [CSM] GFS strengthening specimens

Specimens	$[CSM]_{2-2}$	$[CSM]_{3-2}$	$[CSM]_{2-4}$	$[CSM]_{3-4}$	$[CSM]_{2-5}$	$[CSM]_{3-5}$
1	21.17	41.03	49.32	59.94	57.65	69.02
2	24.02	38.50	57.11	57.55	60.06	64.89
3	27.40	31.27	54.98	61.10	56.40	58.70
avg	24.20	36.93	53.80	59.53	58.03	64.20
C.o.V	12.88%	13.71%	7.48%	3.04%	3.21%	8.09%
P_{st}/P_{NS}	2.39	2.07	2.13	1.64	1.62	1.69

(d) Ultimate load of non-strengthening specimens (unit: kN)

Specimens	NS_{2-2}	NS_{3-2}	NS_{2-4}	NS_{3-4}	NS_{2-5}	NS_{3-5}
1	10.46	17.62	23.77	38.15	39.35	36.75
2	10.16	18.12	23.53	36.82	34.53	38.46
3	9.81	17.86	28.48	34.16	33.56	38.62
avg	10.14	17.87	25.26	36.38	35.81	37.94
C.o.V	3.18%	1.38%	11.06%	5.58%	8.65%	2.73%

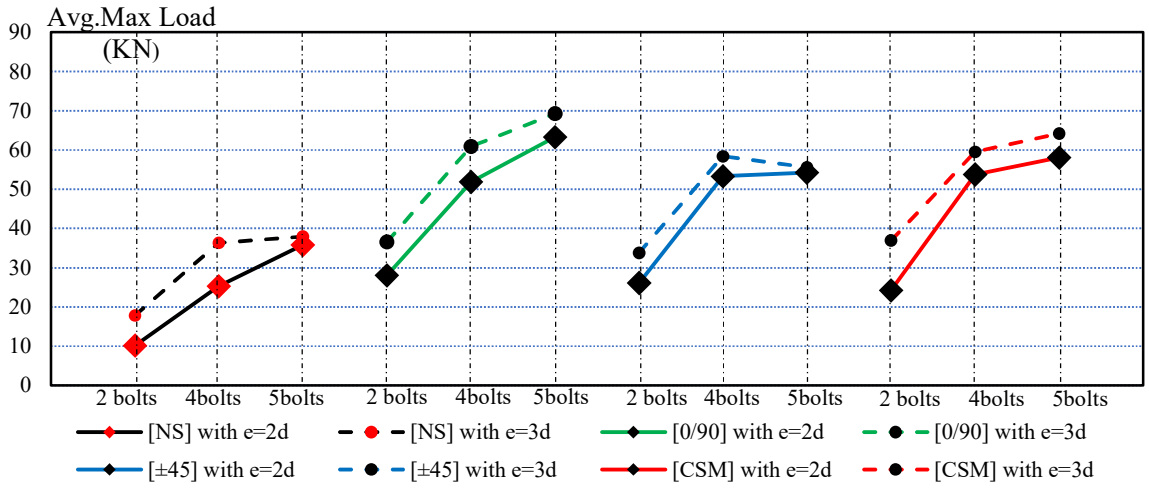

Figure. 3.11 Average ultimate load of specimens.

In comparison, between the GFSs types in strengthened specimens, [0/90] specimens obtained the highest improvement in connection strength with e=3d and five bolts.

3.4.2. Failure modes in specimens

The fundamental failure modes were defined in ACMA [35]. In correspondence with the loading-displacement data obtained in the experiment, the failure modes were listed as shown in Table 3.7 and were defined as follows:

Table 3.7 The failure mode of specimens

Specimens	Failure Mode	Specimens	Failure Mode	Specimens	Failure Mode	Specimens	Failure Mode
$[0/90]_{2\text{-}2}$	M1	$[\pm45]_{2\text{-}2}$	M1	$[CSM]_{2\text{-}2}$	M1	$NS_{2\text{-}2}$	M4
$[0/90]_{3\text{-}2}$	M1	$[\pm45]_{3\text{-}2}$	M1	$[CSM]_{3\text{-}2}$	M1/M2	$NS_{3\text{-}2}$	M4
$[0/90]_{2\text{-}4}$	M3	$[\pm45]_{2\text{-}4}$	M3	$[CSM]_{2\text{-}4}$	M2	$NS_{2\text{-}4}$	M4
$[0/90]_{3\text{-}4}$	M3	$[\pm45]_{3\text{-}4}$	M3	$[CSM]_{3\text{-}5}$	M2	$NS_{3\text{-}4}$	M4
$[0/90]_{2\text{-}5}$	M3	$[\pm45]_{2\text{-}5}$	M3	$[CSM]_{2\text{-}5}$	M2	$NS_{2\text{-}5}$	M5
$[0/90]_{3\text{-}5}$	M3	$[\pm45]_{3\text{-}5}$	M3	$[CSM]_{3\text{-}5}$	M2	$NS_{3\text{-}5}$	M5

- MODE 1 (M1): Cleavage failure in the surface of GFS/GFM and small shear-out in CD.
- MODE 2 (M2): Net-tension failure in the surface of GFS/GFM and shear-out in CD.
- MODE 3 (M3): Debonding failure in GFS/GFM and shear-out in CD.
- MODE 4 (M4): Shear-out failure in whole sections.
- MODE 5(M5): Block shear failure in GFS layer, and shear-out in CD.

Considering the differences in failure modes that occurred in the specimens, it can be concluded that the failure mode varies depending on the type of GFS and mechanical parameters. The failure in non-strengthening specimens (M4, M5) is unlike the modes obtained in strengthening specimens (M1, M2, M3). The types of failure modes also vary in specimens under pasting GFS. Although both M1 and M3 were present for failure in [0/90] and [±45], M1 was observed only in 2-bolt specimens while debonding failure (M3) appeared in 4 or 5-bolt specimens. Only [CSM] specimens witnessed net-tension failure mode (M2). Based on the failure modes observed in Figure 3.12, it was determined that not only M3 but also M2 had instances of debonding. This demonstrates that the bond strength between the GFM and CD layers in the original PGFRP material is crucial in determining the strength of the connection in the strengthened specimens. The debonding area will be used to calculate the debonding load as an element load in the continuous section, using equations that have been proposed to predict the connection strength of the specimens.

Moreover, based on observed failure modes in all specimens that occurred shear-out

failure in the CD layer, the thickness (mm) of the failure section varied from around 2 to 4 mm. This is because of instability and uncontrollability in the behavior of fiber and resin part in PGFRP material under shear force. Consequently, the strength of connection in the experiment witnessed a fluctuation in ultimate load.

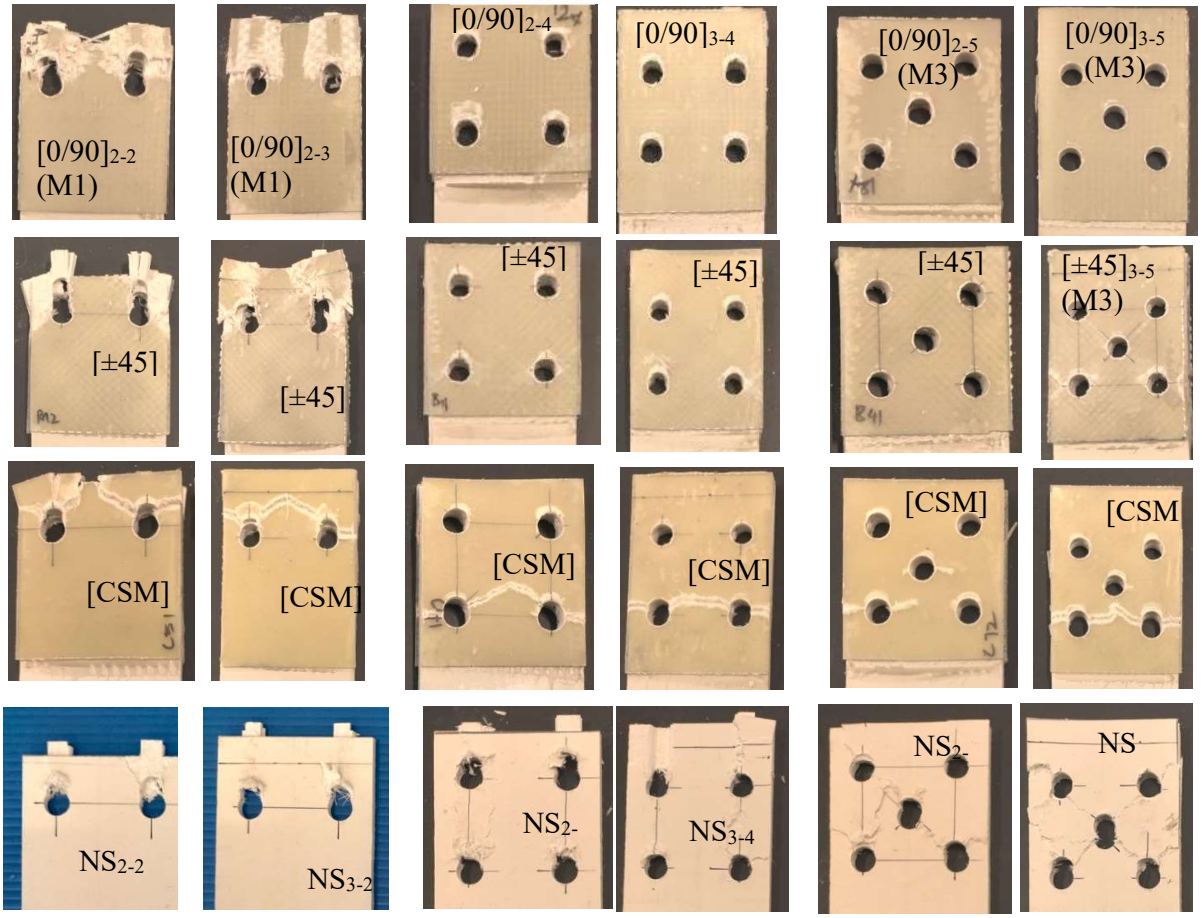

Figure 3.12 The failure obtained after the experiment in all specimens.

3.4.3. Load-displacement of the specimens

The initial points in the lines were moved and adjusted in the graph to provide a better overall view of all the load-relative displacement relationships. Figure 3.13 (a, b) shows the load-displacement relations of two bolts specimens. After reaching the maximum load, loading in [0/90] and [±45] GFS specimens with two bolts were kept for a period before dropping. This is because bearing failure occurred in GFSs (MODE 5). In the other failure modes, the bearing load rapidly decreased after reaching the ultimate load. The maximum load corresponding to the point of stiffness reduction was called damage load [10]. In the case of four bolts and five bolts specimens, which are illustrated by Figure 3.13 (c, d, e, and f) the bearing failure did not

occur in the GFSs of [0/90] and [±45]. Since the de-bonding failure has occurred in the GFSs of [0/90] and [±45], it can be concluded that the bonding strength is smaller than the bearing strength in four or five bolts' specimens.

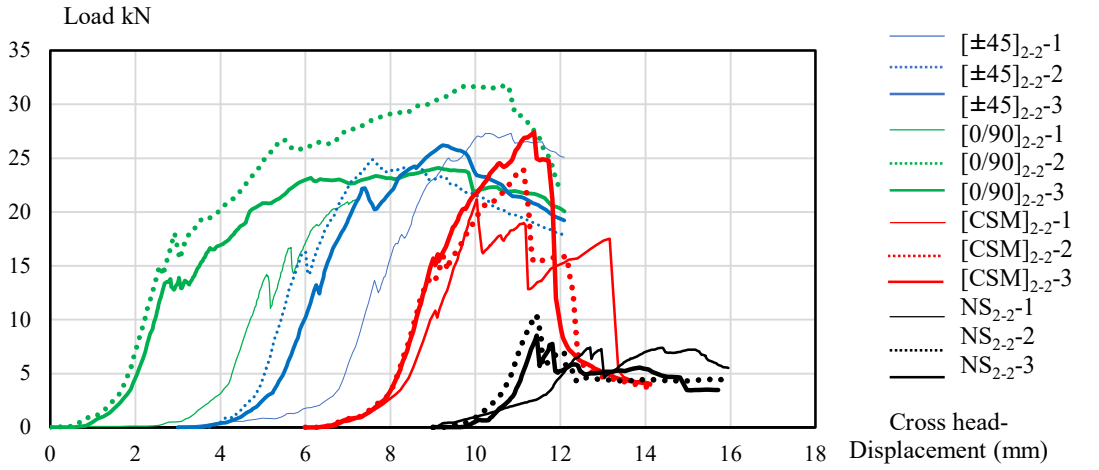

(a) 2 bolts and *e*=2*d*

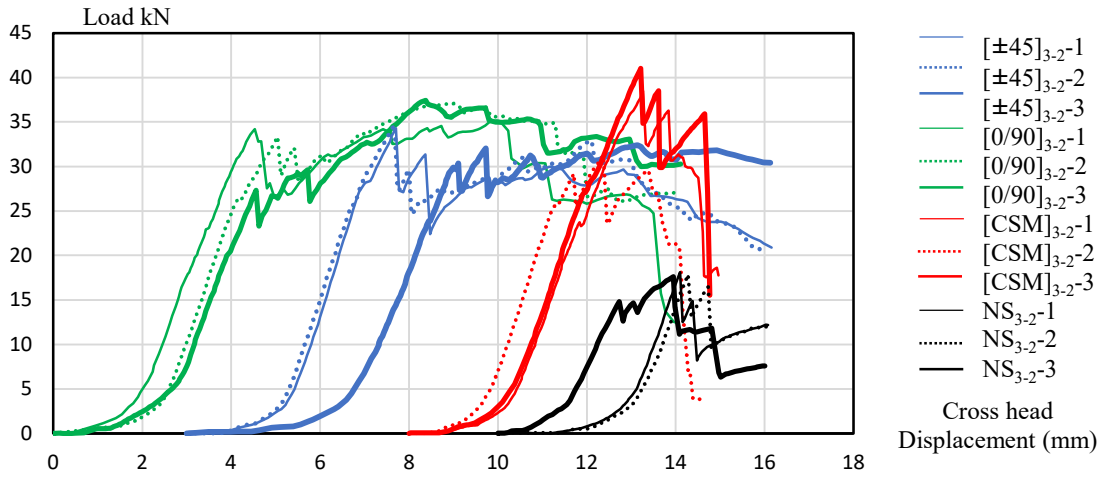

(b) 2 bolts and *e*=3*d*

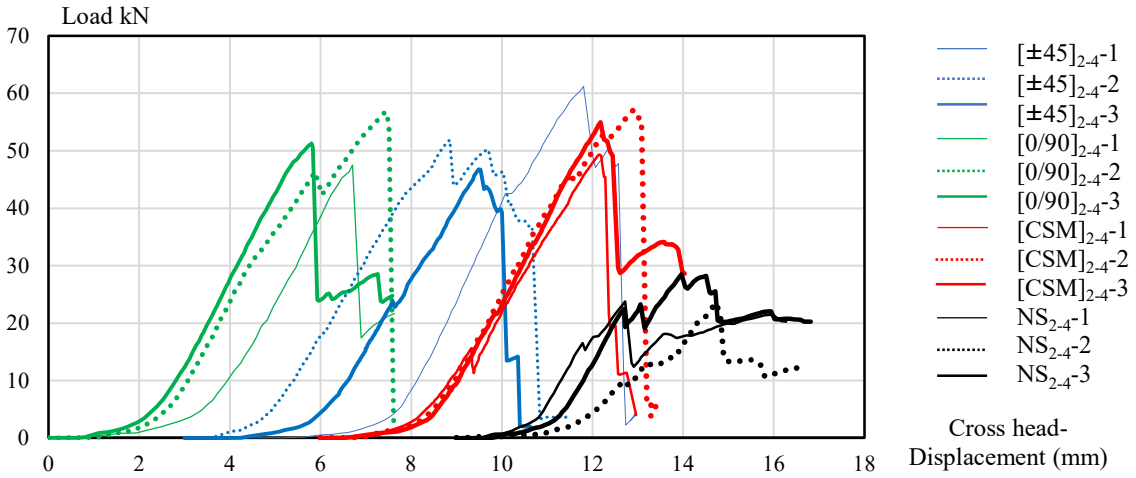

c) 4bolts and *e=2d*

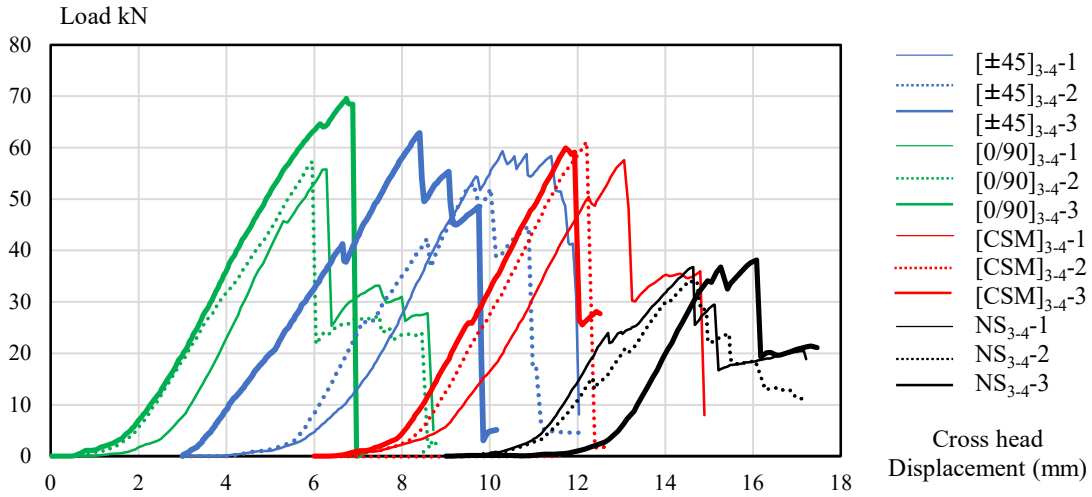

(d) 4bolts and *e*=3*d*

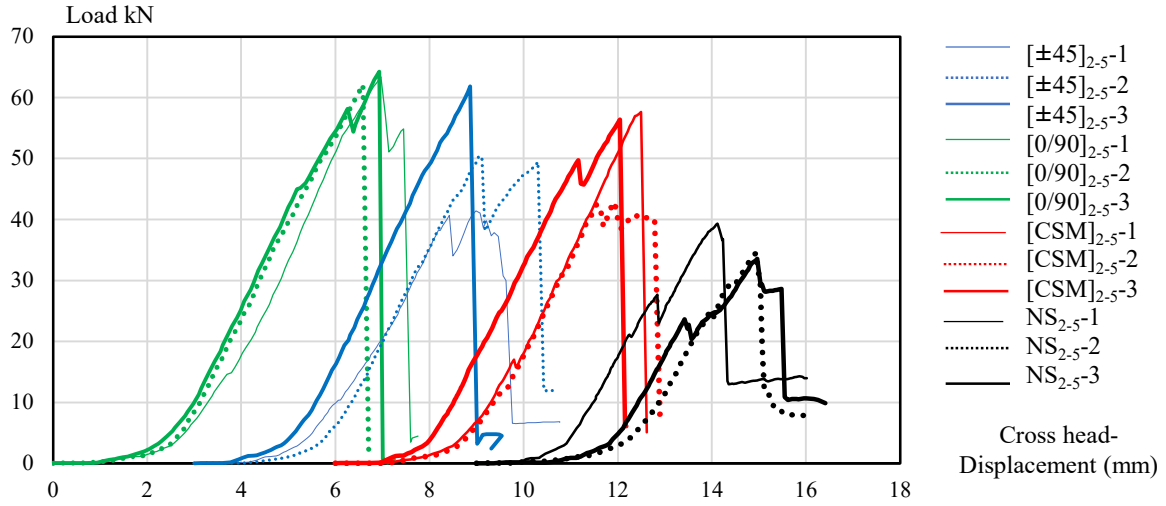

(e) 5bolts and *e*=2*d*

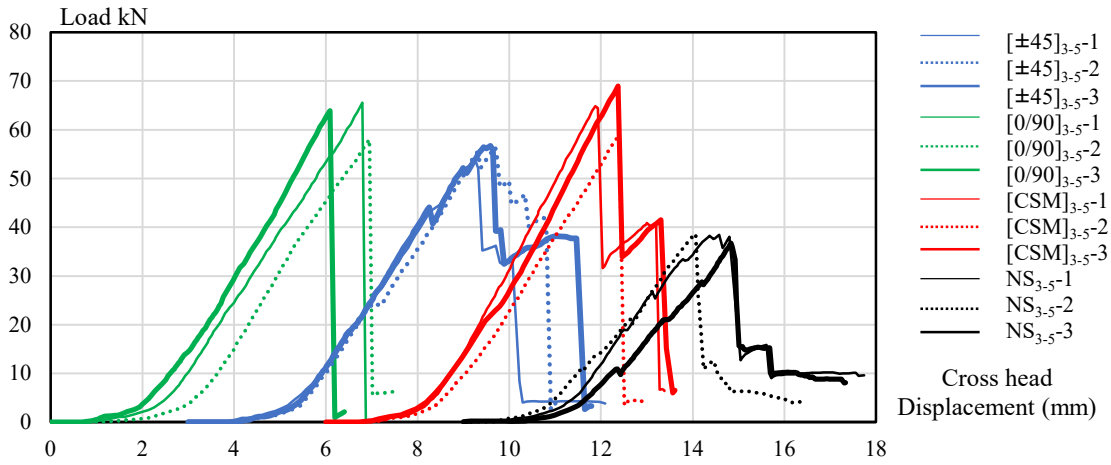

(f) 5bolts and *e*=3*d*

Figure 3.13 Load-cross head displacement relations in the PGFRP connections of all specimens

3.4.4. Evaluation of strengthening effect by types of GFSs

Regarding the specimens illustrated by line graphs in Figure 3.13, the maximum load of GFSs was higher than that in NS specimens in all types of GFSs. The effectiveness of the specimens after strengthening is also demonstrated by [Pst/PNS] ratio, varying from 1.4 to 2.1. Table 6 a, b [CSM] effective ratio is lower than in any other GFSs, at 40% with five bolts specimens.

Table 3.8 Strengthening effective of GFS

(a) *e=2d* specimens

No. bolt	[±45]	[0/90]	[CSM]
2	158%	177%	139%
4	111%	105%	113%
5	77%	77%	62%

(b) *e=3d* specimens

No. bolt	[±45]	[0/90]	[CSM]
2	89%	105%	107%
4	61%	67%	62%
5	82%	82%	69%

3.4.5. Evaluation of strengthening effect by the number of bolts

It significantly increases connection strength when changing bolt quantity from two to four bolts. The effectiveness was also noticeable in NS when changing four bolts to five bolts. However, the strengthening effect was trivial in GFS specimens when changing from 4 to 5 bolts. In [0/90], [±45] GFS type, the ultimate load in 4 bolts connection specimens was higher than in 5 bolts-specimens because the bonding area was decreased by one more bolt hole area. In [CSM] specimens, the tensile strength of GFS did not significantly change when adding one more bolt from 4 bolts to 5 bolts. Due to the cross area of the failure section, the main factor that makes net-tension failure, was no change, the ultimate load in [CSM]was not changed in these cases. On the other hand, the NS specimens obtained the failure mode change from MODE 1 (2 and 4 bolts) to MODE 2: 5 bolts (block shear). The length of the long shear area was increased in case 5 bolts. Consequently, it made better strength in comparison with two or four bolts.

3.4.6. Evaluation strengthening effect related to end-distance

Besides the effect of the number of bolts and the type of GFS, the end distance e was also investigated in this study. Table 3.9 provides the percentage of increasing strength when changing from end-distance *e=2d* to *e=3d.*

In the case of two bolts, all specimens were shown a high effect with an increasing ratio ranging from 10.9% to 30.9%. The added end distance made the failure-out section of the CD layer was longer. The reason above made maximum load stronger in *e=3d* specimens.

In the type of four or five bolts' specimens, only [±45] with four bolts specimens shows an increase in connection strength (around 12% increase).

The bonding strength of CD and GFS layer was a major element when evaluating MODE 2 and MODE 5. These represent a failure mode that occurred in 4 or 5 bolts specimens (except [CSM] specimens). The distribution and area of effective bonding will be continuously investigated as a supplement for more understanding of this issue.

Table 3.9 Comparison of the strengthening effect of *3d* end -distance specimens to *2d* end-distance specimens

No. bolt	[±45]	[0/90]	[CSM]	NS
2	10.9%	19.5%	30.9%	17.5%
4	12.6%	0.3%	3.3%	8.7%
5	7.6%	4.0%	3.2%	5.0%

3.5. Conclusion

The findings of this chapter indicate that applying glass fiber sheets to the connection area of the bolted connection in PGFRP significantly enhances its mechanical properties, as verified by the experimental results. The ultimate loads of GFS-strengthened connections increased from 1.61 to 2.77 times compared with non-strengthened specimens. Diffident failure modes were found in different types of specimens. Five basic failure modes were found in the experimental analysis. The failure mode depends on the GFS material and the geometries of the specimens. In [0/90] and [±45], debonding failure appeared in whole four- and five-bolt specimens, while in two-bolt specimens, cleavage failure occurred as the typical mode. In [CSM] specimens, net-tension failure was witnessed in all two-, four-, and five-bolt specimens.

CHAPTER 4

THE INFLUENCE OF BONDING STRENGTH AND PROPOSED EQUATION FOR CONNECTION STRENGTH PREDICTION

4.1. Introduction

The strength of the bond between Glass Fiber Mat (GFM) and Continuous direction fiber (CD) layers in Pultruded GFRP material is a crucial factor that influences the ultimate strength of the connection in strengthened specimens. This chapter presents an investigation of the bonding strength in PGFRP, utilizing a combination of theoretical formulae and experimental techniques. The outcomes of these analyses enable the estimation of connection strength using proposed equations.

4.2. Experimental program

The specimen was produced from two PGFRP plates (with a 10 mm gap) with the dimensions $L \times W$=350 x 80 mm, and two GFS plates, which were pasted on both sides. The specimens' dimensions and details are shown in Figure 4.1(a)**.** On both surfaces of the GFS, one thick sheet of GFS (80 x 60mm) was added to prevent local failure from occurring at the gap. The glue material, E250 adhesive, had an elastic modulus and Poisson's ratio of 3 GPa and 0.37, respectively (from the manufacturer). Five samples were in bond testing in each specimen [0/90] and [±45]. The [CSM] specimens were not considered for the bond strength test due to their GFS layers causing net-tension failures before debonding. Tensile testing was selected to investigate the strength of bonding resistance force.

In Figure 4.1(b), similar to earlier described in connection testing, a 1000 kN universal testing machine was arranged. The experiment was conducted where a tensile load was applied to the specimens at a rate of 0.02 kN per second. The test continued until either the specimen failed, or the displacement of the crosshead reached approximately 20 mm.

4.3. Experimental results

The failure specimens [0/90] and [±45] are presented in Figure 4.2 (a) and Figure 4.2 (b), respectively**.** The failure occurred on at least one side of the outside surfaces of PGFRP connections. The result of the maximum load is described in Table 4.1.

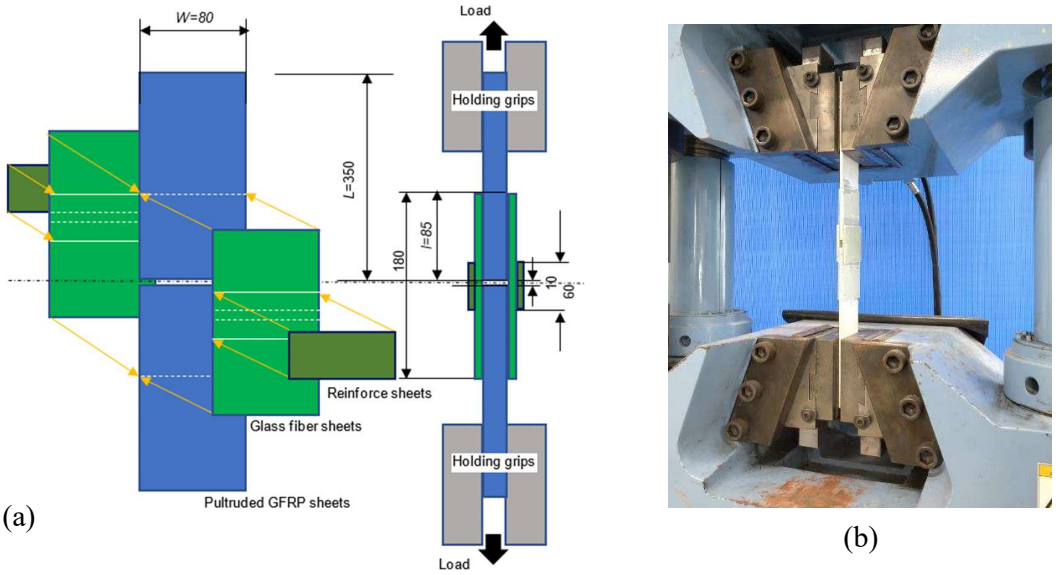

Figure 4.1 Bond strength test: (a) specimens and diagram; (b) setting up in the tensile test.

The bond strength, which prevents debonding failure between CD and GFM layers, can be determined by the following equation:

$$F_{bd} = \frac{P}{2Wl} \tag{4.1}$$

Where P is the ultimate load, W=80 mm, and l=85mm correspond to the width and length of the area covered by GFS in the PGFRP connections.

(a)Debonding in all surfaces of [0/90]

(b)Deformation in surface of [±45] GFSs

Figure 4.2 Failure in bond strength test (a) in [0/90] specimens; (b) in [±45] specimens.

In Table 4.1 the result of bond strength in [0/90] was higher than [±45] in the whole case of specimens. This tendency can be explained by observing the failure modes. In [0/90] specimens, debonding occurred in all GFS areas, as shown in Figure 4.2 (a). In [±45], the local deformation occurred before completely debonding the whole area, as shown in Figure 4.2 (b), thus decreasing the maximum loads. The lower force transfer can be explained by fiber direction when the [±45] specimens inclined 45^0 with the force direction. However, in the connection strength experiment, it was acceptable not to consider fiber direction effectiveness

on bond strength because of bolt-hole re-distributed tensile stress in the GFS surface. The value of [0/90] bond strength, by the assumption, can be taken to estimate the connection strength with the proposal equation in all GFS specimens: [±45]; [0/90], and [CSM].

Table 4.1 Results of the bond strength test

Specimens	**0/90$_1$**	**0/90$_2$**	**0/90$_3$**	**0/90$_4$**	**0/90$_4$**
Load (kN)	57.46	52.98	56.78	51.94	48.82
Avg (kN)	53.60				
C.o.v	3.19%				
F_{bd} (MPa)	3.94				

Specimens	**±45$_1$**	**±45$_2$**	**±45$_3$**	**±45$_4$**	**±45$_5$**
Load (kN)	37.44	35.86	39.84	37.42	36.92
Avg (kN)	37.50				
C.o.v	1.31%				
F_{bd} (MPa)	2.76				

4.4. The proposed equation for connection strength prediction

4.4.1. ACMA standard for non-strengthening specimens.

According to ACMA [35], the connections are to be designed as per the following equation:

$$R_u \leq \lambda \varphi R_n C_\Delta C_M C_T \tag{4.2}$$

Where:

- R_u: Ultimate connection strength due to factored loads.
- φ: Either resistance factor φ_b for steel bolt or resistance factor φ_c for FRP connections with strength formula.
- λ: Time effect factor.
- R_n: Nominal connection strength.
- C_Δ: Geometry factor that considers the connection geometry.
- C_M: Moisture condition factor.
- C_T: Temperature condition factor.

In Eq (4.2), R_n denotes nominal connection strength. In case the connection has two or three rows of bolts, the lowest value of R_{tt} , $R_{bt,}$, $R_{br,}$ $R_{nt,f,}$ $R_{sh,}$ and R_{bs} was chosen as R_n. In case only one-row bolts, R_n, is the lowest among of $R_{sh,}$ $R_{bt,}$ $R_{tt,}$ $R_{br,}$ R_{nt} and $R_{cl.}$

Where:

- R_{bt}: Bolt strength of tension
- R_{tt}: Bolt strength of through-the-thickness tension.
- R_{br}: Strength of pin-bearing.
- R_{nt}: Strength of net tension.
- R_{sh}: Strength of shear-out.
- R_{cl}: Cleavage strength.
- $R_{nt,f}$: Net tension strength at first bolt row.
- R_{bs}: Strength of Block- shear in case the concentric load.
- $R_{bs,e}$: Strength of Block shear in case eccentric load.

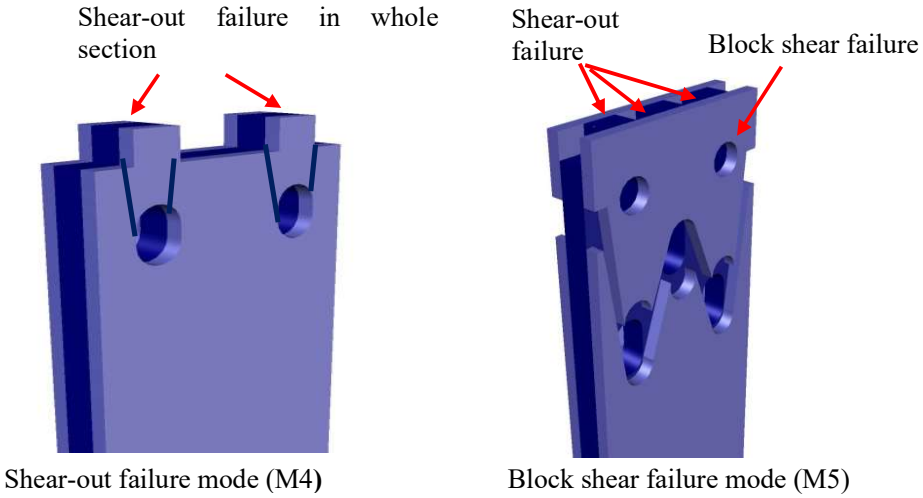

Figure 4.3 Failure modes in non-strengthening specimens.

In the case of non-strengthening specimens (NS), the ultimate joint load can be calculated and used to predict failure mode following Eq (4.2). The two kinds of failure modes that occurred in NS specimens were shear-out failure (M4) with two- and four-bolt specimens and block shear (M5) with five-bolt specimens. Therefore, based on ACMA [35], the nomination strength (R_n) can be determined as shear-out strength (R_{sh}) or block shear strength (R_{bs}), depending on the failure modes of specimens. In [35], the ultimate strength of block shear can be estimated by:

$$R_{bs} = 0.5(A_{ns}F_{sh} + A_{nt}F_L{}^t) \quad (4.2b)$$

For two rows (n = 2) bolts, the shear-out strength per line can predict as follow:

$$R_{sh} = 1.4\left(e - \frac{d_n}{2} + g\right)tF_{sh} \quad (4.2c)$$

Where:

- t: Thickness of PGPRP sheet
- d_n: Bolt hole diameter.
- g: distance between the bolt holes in the row bolt, in this study, g=48 mm
- e: The end-distance.
- F_{sh}: In-plane shear strength of PGFRP subjected to the shear-out failure, measured by material properties testing.
- F^t_L: Tensile strength of the material in the fiber direction, which is measured by material properties testing.

A_{ns} : The zone subjected to shear-out.

A_{nt} : The zone subjected to tension failure.

As shown in Table 4.2, using Eq (4.2b) and Eq (4.2c), the obtained result showed good agreement with maximum loading in testing. The largest value of errors was 23.99% in two bolts, and the end distance $e=3d$ ($NS_{3\text{-}2}$). This was because there was a variance in the undefined properties between the material used to propose the empirical formula of ACMA and this study's experiment.

Table 4.2 Comparison of the estimate and testing result of the connection strength in non-strengthening specimen

Specimens	Failure Mode	Nomination Strength	Estimating Value kN	Testing Result kN	Variation (%)
$NS_{2\text{-}2}$	Shear-out	R_{sh}	8.45	10.14	20.08%
$NS_{3\text{-}2}$	Shear-out	R_{sh}	14.41	17.87	23.99%
$NS_{2\text{-}4}$	Shear-out	R_{sh}	32.30	25.26	-21.80%
$NS_{3\text{-}4}$	Shear-out	R_{sh}	38.26	36.38	-4.92%
$NS_{2\text{-}5}$	Block shear	R_{bs}	33.98	35.81	5.38%
$NS_{3\text{-}5}$	Block shear	R_{bs}	38.33	37.94	-1.01%

In this experiment, except for the debonding failure (M3), the failure mode occurred within the listed nomination strength found in Eq (4.2). However, the PGFRP, after being strengthened with GFS had different behavior. In the continuous section, the report proposed by Mosallam [52] was examined in the calculation. By referring to and customizing those theories, this study proposed the enhancement of estimated connection strength under the applied strengthening method by GFS.

4.4.2. The efficiency of the bolted joint

The efficiency of a composite bolted joint was discussed by Dastin [70]. Joint efficiency (η) of the PGFRP connection was determined by the connection capacity of the member and strength of unjointed continuous member of the same size, or

$$\eta = \frac{S_j}{S_m} = \frac{P_{ult}}{twF_{nt}} \tag{4.3}$$

Where:

η: Joint efficiency.

S_j: Ultimate joint strength.

S_m: Maximum load of unjointed PGFRP members with the same parameter.

P_{ult}: Ultimate joint load.

t: Member thickness.

w: Member width.

F_{nt}: Tensile strength of the PGFPR member.

d_n: Hole diameter.

Rosner [71] modified by semi-empirical and consists of two major failure modes of the PGFRP joint.

(a) Net-Tension Criterion

$$\eta = \frac{1}{\left[1 + C\left(K_{te} - 1\right)\right]}\left(1 - \frac{nd_n}{w}\right) \tag{4.4}$$

Where: η, d_n, and w are as defined in Eq (4.3).

K_{te} is the isotropic stress concentration factor for the same joint geometry that was proposed by Hart-Smith [72] for composite joints with multiple holes. In the loaded hole:

$$K_{te} = \frac{g}{d_n} + 0.5\left(1 - \frac{d_n}{g}\right)\theta \tag{4.5}$$

Where:

$$\theta = \left(\frac{g}{e} - 1\right) \text{ For: } \frac{e}{g} \leq 1$$

Where:

θ: The nondimensional factor, $\theta = g/e$ for a multi-bolted connection.

g: The distance between the bolt holes in the row bolt

C: Stress concentration reduction factors for PGFRP, and

$$K_{tc} - 1 = C\left(K_{te} - 1\right) \tag{4.6}$$

Where:

K_{tc}: Stress concentration factor was obtained at connection occur failure, determined by:

$$K_{tc} = \frac{F_{nt} t\left(w - d_n\right)}{P} \tag{4.7}$$

Where:

F_{nt} and w are as defined in Eq (4.3)
P: Tension load when the bolted connection fails due to the net tension mode.

(b) Bearing/Cleavage Failure Criterion

Regarding Hassan [73], the bearing or cleavage failure criterion can be determined by

the following function:

$$\eta = \frac{1}{\left[1 + C\left(K_{te} - 1\right)\right]}\left(1 - \frac{nd_n}{w}\right)\left(\frac{6}{5} - \frac{3}{5}\frac{d_n}{e}\right)^{\nu} \tag{4.8}$$

Where:

- ν = 2 for single-row bolts connection (in this research, this case corresponds with two-bolt specimens).
- ν = 1 for multiple bolt rows in a single column (this case was not available in this study).
- ν = 0 for connection with two rows and two columns of bolts. In this paper: four- or five-bolt specimens. Consequently, the e/d ratio did not affect the ultimate load, and the failure mode was net tension.

(c) Ultimate loading for the element load

After determining η, the ultimate load of net-tension or cleavage can be predicted via the efficiency of the bolted joint. Dastin [70] described this as follows:

$$P_{ult} = \eta\ (twF_{nt}) \tag{4.9}$$

In Eqs (4.4) and (4.8), it is necessary to determine the *C* factor, which depends on K_{te} and K_{tc}. The isotropic stress concentration factor for the similar connection parameter- *Kte*, can be obtained as described in Eq (4.5). *Ktc* can be calculated by the result of ultimate load in net-tension failure mode, which appeared in [CSM] specimens but did not occur with [0/90] and [±45] specimens in the connection test. In additional testing, under the expansion of the end distance of specimens (e=10d), net-tension failure occurred in [0/90] instead of debonding failure mode, as presented in Figure 4.4. The result of the C value for each specimen and the efficiency of bolted joints are shown in Table 4.3.

Table 4.3 The efficiency of the bolted joint η value

Specimens	C value	Net Tension	Cleavage	Failure Mode
		η	η	(Lower η)
$[0/90]_{2\text{-}2}$	0.24	0.40	0.29	Cleavage
$[0/90]_{3\text{-}2}$	0.27	0.40	0.37	Cleavage
$[45]_{2\text{-}2}$	0.26	0.39	0.28	Cleavage
$[45]_{3\text{-}2}$	0.28	0.39	0.36	Cleavage
$[CSM]_{2\text{-}2}$	0.24	0.40	0.29	Cleavage
$[CSM]_{3\text{-}2}$	0.22	0.43	0.40	Cleavage/net tension

Since in whole GFS strengthened specimens, debonding also occurred partly in the area between the GFM and CD layer of PGFRP, the bonding strength was considered in the proposal estimating equation for connection strength as an element load.

In the experiment, [CSM]3-2 specimens were recorded in net tension failure mode. Notwithstanding, in Table 4.3, the η value of cleavage was lower than the η value of tension. This tendency is due to η value of the tension and cleavage not being too distinct in certain specimens. The failure mode appearances in [CSM]3-2 also combined net-tension and cleavage failure. Thus, the net tension load was combined with connection strength.

Regarding the instruction of Mosallam [52], the design and analytical procedure are proposed as follows:

- Step 1. Input parameter and using Eq (4.4) for net tension, and Eq (4.8) for cleavage or the bearing criterion, the η values can be calculated.

- Step 2. Joint efficiency be considered as the lowest η value in step 1

- Step 3. The ultimate loading is estimated by Eq (4.9).

- Step 4. The predicted strength of the connection, and the failure mode corresponded as lowest obtained value η in Step 2.

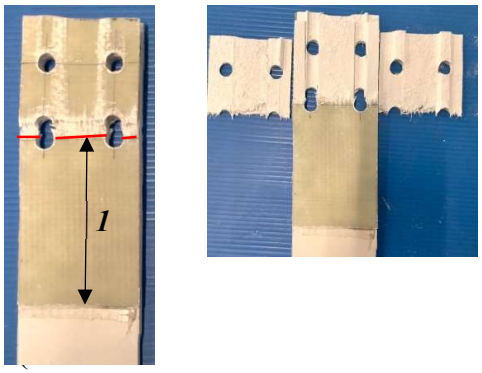

Figure 4.4 Failure in extended GFS area specimens after tensile testing. (a) GFS extended length 10*d* specimens; (b) failure inside the layer of GFS extended 10*d*.

4.4.3. Explanation of failure modes

The main failure modes that occurred in strengthening specimens: net-tension (or cleavage) and debonding in whole GFS sheets. Bonding strength prevents the debonding between the CD and GFM parts, while tensile strength prevents net-tension failure. When the bonding strength was larger than the tensile load, debonding (in the whole area) did not occur, and net tension or cleavage appeared. In contrast, debonding became the failure mode if tensile strength exceeded the bonding strength. The effective bonding load was calculated by effective area and bond strength (F_{bd}) in some instances of specimens. In Figure 4.5, the effective area of bonding strength before failure is denoted by yellow highlighting. The effective area of bonding strength was defined as the area from the first bolt row to the loaded end. This was because Mosallam [52] investigated the first-row bolt as a criteria line where failure can occur with net tension or cleavage/bearing.

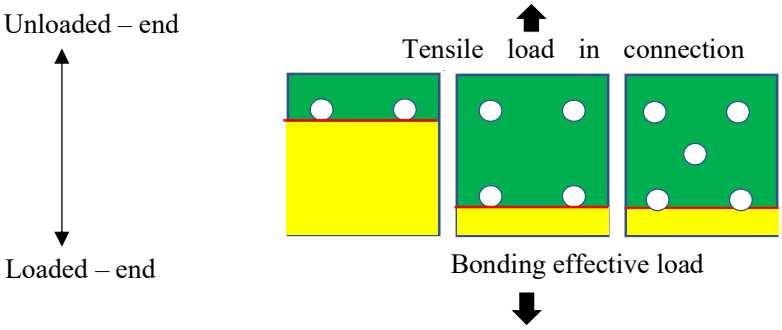

Figure 4.5 Effective area of bonding strength in GFS sheets.

By applying Eqs (4.4), (4.8), and (4.9), the ultimate loading for net tension or cleavage can be determined. The result shown in Table 4.4 has demonstrated the assumption of the relation between tensile load (P_{ult}) and effective bonding load (P_{bde}) in predicting the ultimate

failure load of connection. The lower loading in the calculation can be used to predict corresponding failure modes. For example, in $[0/90]_{2\text{-}2}$ specimens, since $P_{ult} < P_{bde}$, the cleavage or net tension will occur. Then, as presented earlier, by predicted joint efficiency- η values in two cases, cleavage was found as the failure mode of the specimens. All the predictions of failure modes found in Table 4.4 showed good matching with failure mode in the testing.

Moreover, the failure modes of $[0/90]_{3\text{-}5}$ appeared partly with net tension at the first-row bolts. The tendency above could be explained by referring to the value of P_{bde} and P_{ult} of $[0/90]_{3\text{-}5}$ specimens with a slight difference between the two-element strength. Therefore, the failure mode was hybrid and could change from debonding to net-tension failure. If we extend the end-distance of GFS in the loaded end, the value P_{dbe} will exceed P_{ult}, and net tension can occur, as shown in Figure 4.4.

Table 4.4 Prediction of failure modes for specimens

Specimens	Bonding Effective Load (kN)			P_{ult} (kN)	Failure Mode	Experimental Failure Mode
	F_{bd}	A_{bd}	P_{bde}			
$[0/90]_{2\text{-}2}$	3.94	5460.00	**43.02**	**28.65**	Clg or Net	Cleavage
$[0/90]_{3\text{-}2}$	3.94	6468.00	**50.96**	**36.89**	Clg or Net	Cleavage
$[0/90]_{2\text{-}4}$	3.94	1428.00	**11.26**	**19.83**	De-bond	De-bond
$[0/90]_{3\text{-}4}$	3.94	2436.00	**19.2**	**19.74**	De-bond	De-bond
$[0/90]_{2\text{-}5}$	3.94	1428.00	**11.26**	**19.83**	De-bond	De-bond
$[0/90]_{3\text{-}5}$	3.94	2436.00	**19.2**	**19.74**	De-bond	De-bond
$[\pm45]_{2\text{-}2}$	3.94	5460.00	**43.02**	**28.32**	Clg or Net	Cleavage
$[\pm45]_{3\text{-}2}$	3.94	6468.00	**50.96**	**37.11**	Clg or Net	Cleavage
$[\pm45]_{2\text{-}4}$	3.94	1428.00	**11.26**	**19.83**	De-bond	De-bond
$[\pm45]_{3\text{-}4}$	3.94	2436.00	**19.2**	**19.74**	De-bond	De-bond
$[\pm45]_{2\text{-}5}$	3.94	1428.00	**11.26**	**19.83**	De-bond	De-bond
$[\pm45]_{3\text{-}5}$	3.94	2436.00	**19.2**	**19.74**	De-bond	De-bond
$[CSM]_{2\text{-}2}$	3.94	5460.00	**43.02**	**15.83**	Clg or Net	Cleavage
$[CSM]_{3\text{-}2}$	3.94	6468.00	**50.96**	**21.47**	Clg or Net	Net-tension
$[CSM]_{4\text{-}2}$	3.94	1428.00	**11.26**	**10.90**	Net-tension	Net-tension
$[CSM]_{4\text{-}3}$	3.94	2436.00	**19.2**	**11.61**	Net-tension	Net-tension
$[CSM]_{5\text{-}2}$	3.94	1428.00	**11.26**	**10.90**	Net-tension	Net-tension
$[CSM]_{5\text{-}3}$	3.94	2436.00	**19.2**	**11.61**	Net-tension	Net-tension

In Table 4.4:

- Clg or Net: Cleavage failure or net-tension failure, respectively.
- P_{utl}: The ultimate load of net-tension or cleavage (kN) determined by Eq (4.9) and the procedure presented in the previous part.
- P_{bde}: Bonding effective load (kN), and

$$P_{bde} = 2\, F_{bd} A_{bde} \tag{4.10}$$

Where:

- $F_{bd:}$: Bond strength
- A_{bde}: Bonding effective area as illustrated in Figure 4.5

4.4.4. Proposal formula to predict connection strength

(a) General formula

$$P_e = Min\{P_{nt,} P_{cl}\} + P_{bd} + P_{SOCD} \quad (4.11)$$

Where:

- $P_{e:}$ Estimate for connection strength.
- $P_{nt:}$ Estimate load of net tension failure in GFS, GFM layer.
- $P_{cl:}$ Estimate load of cleavage failure in GFS, GFM layer.
- $P_{bd:}$ Bonding load.
- P_{SOCD}: Shear-out load of the CD layer.

(b) Two-bolt connection case

Based on the observation, those values can be omitted since the debonding, and shear-out failure did not completely occur. Eq (11) becomes

$$P_e = Min\{P_{nt,} P_{cl}\} \quad (12)$$

Where: P_{nt} and P_{cl} were determined as P_{ult} ultimate load by Equation (4.9) and following the design procedure.

(c) [CSM] type with four and five bolts

In two-row bolts, net-tension failure could appear in only two kinds of failures: net-tension or cleavage, as explained in earlier section**.** Moreover, the failure mode of [CSM] four- and five-bolt specimens were determined as net-tension. The general formula Eq (4.11) can be applied as follows:

$$P_e = P_{nt} + P_{bd} + P_{SOCD} \quad (4.13)$$

Where:

- $P_{bd:}$ Bonding load (kN), with debonding area A_{bd} failure, as illustrated in Figure 4.6 , and:

$$P_{bd} = 2\, F_{bd} A_{bd} \quad (4.14)$$

where A_{bd} is the debonding area, which was defined as the zone where the GFS/GFM layer had a debonding failure. The debonding area depended on the failure mode, which can be predicted as outlined in the previous section. In net-tension failure specimens (MODE2),

the upper loaded hole zone was the debonding area. On the other hand, in MODE 3, debonding occurred in the whole GFS/GFM area. Therefore, all the strengthening areas were calculated as the debonding area in MODE3.

- P_{soCD}: Shear-out load of CD (kN), and

$$P_{SOCD} = T_{SOCD} \times A_{SO} = T_{SOCD} \times 2 \times 2e\left(d + t_{CD}\right) \quad (4.15)$$

Where:

- T_{SOCD}: Shear-out strength of CD (MPa), which was determined by material property testing.
- A_{SO}: Shear-out area of CD (mm^2)
- t_{CD}: The thickness of CD (mm)
- d: diameter of bolt= 12 (mm)
- e: end-distance of specimens as described earlier

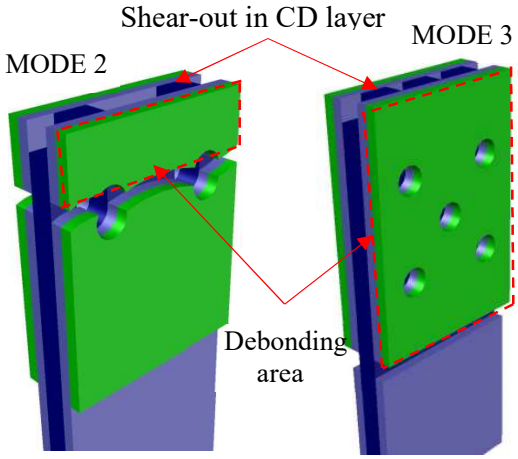

Figure 4.6 Failure modes in strengthened specimens and the debonding area.

(d) [0/90] and [±45] with four bolts

Net-tension failure did not occur in [0/90] and [±45] with four- and five-bolt specimens. When investigating failure specimens, it is different in the failure sequence between the four-bolt and five-bolt types. The bearing in the outside layer and shear-out in the CD layer appeared initially in four bolts. After that, debonding occurred. Therefore, the ultimate load in four-bolt specimens can be estimated with the following equation:

$$\boldsymbol{P_e = P_{bd}} \quad (4.16)$$

(e) [0/90] and [±45] with five bolts

In the five-bolts specimen, the failure modes were as follows: shear out in CD, and

debonding occurring simultaneously. Thus, the connection strength was determined by two combined element loads:

$$P_e = P_{bd} + P_{SOCD} \quad (4.17)$$

In Eq (4.16) and Eq (4.17):

P_{SOCD} was as explained in (15).

P_{bd}: Debonding load (kN), as explained in Eq (4.14).

The bond strength was calculated by GFS area after deducting the area of bolt holes because this area was subject to shear-out failure load, as shown in Figure 4.7. The width of the deducted area was considered by bolt diameter, d=12 mm. In the calculation, the material properties were determined in accordance with the experiments presented in Nhut [44,45].

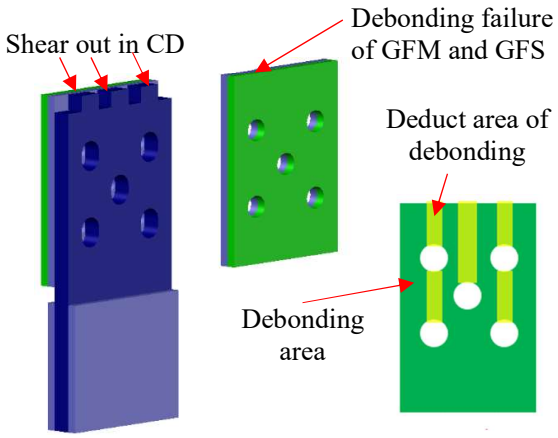

Figure 4.7 Three-dimensional configuration of separated failure mode in specimens.

Table 4.5 Summary of the proposed equation for predicting connection strength

Specimens	Type of GFS	Prediction Formula	Equation
Two bolts		$P_e = Min\{P_{nt}, P_{cl}\}$	(4.12)
Four bolts/five bolts	[CSM]	$P_e = P_{bd} + P_{nt} + P_{SOCD}$	(4.13)
Four bolts	[0/90]; [±45]	$P_e = P_{bd}$	(4.16)
Five bolts	[0/90]; [±45]	$P_e = P_{bd} + P_{SOCD}$	(4.17)

Table 4.6 Estimation of the ultimate loads of PGFRP connections compared to the experimental results

Specimens	Estimated	Result	Error
$[0/90]_{2\text{-}2}$	28.65	28.05	-2.11%
$[0/90]_{3\text{-}2}$	36.89	36.59	-0.80%
$[0/90]_{2\text{-}4}$	47.66	51.86	8.8%
$[0/90]_{3\text{-}4}$	60.90	60.87	0.0%
$[0/90]_{2\text{-}5}$	60.30	63.27	4.9%
$[0/90]_{3\text{-}5}$	81.18	69.25	-14.7%
$[\pm45]_{2\text{-}2}$	28.32	26.13	-7.73%
$[\pm45]_{3\text{-}2}$	37.11	33.79	-8.94%
$[\pm45]_{2\text{-}4}$	47.66	53.28	11.8%
$[\pm45]_{3\text{-}4}$	60.90	58.40	-4.1%
$[\pm45]_{2\text{-}5}$	60.30	54.25	-10.0%
$[\pm45]_{3\text{-}5}$	81.18	55.65	**-31.4%**
$[CSM]_{2\text{-}2}$	21.79	24.20	11.04%
$[CSM]_{3\text{-}2}$	32.73	36.93	12.85%
$[CSM]_{2\text{-}4}$	56.12	53.80	-11.2%
$[CSM]_{3\text{-}4}$	64.37	59.53	**-21.2%**
$[CSM]_{2\text{-}5}$	50.83	58.03	4.9%
$[CSM]_{3\text{-}5}$	57.75	64.20	-6.9%

Table 4.6 shows good agreement together between prediction and test results in terms of connection strength. However, a maximum error was found in $[\pm45]_{3\text{-}5}$ specimens, which is a big deviation from a 31.4% error. As described previously, the net tension failure partly appeared before debonding failure appeared, then it decreased the ultimate load of $[\pm45]_{3\text{-}5}$ specimens.

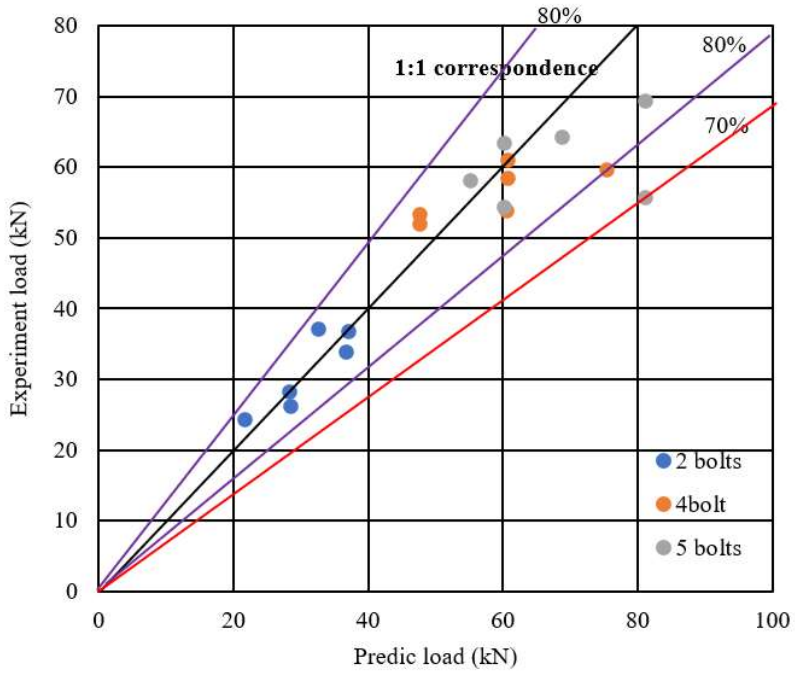

Figure 4.8 Comparison between the experiment and the predicted result of bolted joint loading.

Figure 4.8 illustrates the deviation between the experiment and the predicted ultimate joint loading. Using the proposed formula, the occurred shear out thickness in CD layer be simplified and assumed equal to the thickness of CD part (t_{CD}) 4mm. However, there are unstable in the shear section when shear-out failure happens in specimens. It means that, the value of the shear-out area (A_{SOCD}) is varied, then made a large diffidence in the estimated result and testing value (more than 20%) in 2 specimens Table 4.6.

4.5. Conclusion

Bond strength, which is a property in PGFRP manufacturing progress, was also a factor that affected the capacity of connection in the strengthened specimens. Bond strength can be measured by material testing. After that, the result was taken into estimating the connection strength. Depending on the failure mode of specimens, the effective area of bonding strength was separately measured.

The failure modes can be predicted by taking minimum values of two component strengths: The ultimate load of net-tension or cleavage and effective bonding strength.

The result of testing in non-strength specimens showed good matching with the estimated value from calculations using the equation of ACMA standards.

The proposed equations to calculate the connection strength for the strengthened PGFRP specimens showed good matching with the testing results. The deviation between the estimation and testing results of connection strength varied from 0.2% to 14.18% (except for five bolts, e=3d in [±45] GFS specimens). A general procedure was also proposed in order to apply the appropriate equations in estimating.

The C coefficient of the GFS and GFM layers in this study was referred from additional testing. It is necessary to conduct a particular experiment to determine more accurately the C value for all types of GFS specimens.

To prevent instantaneous failure, the end distance in the GFS sheet can be extended in the loaded end to prevent the debonding load. Meanwhile, net-tension failure can be prevented by increasing the width or thickness of the GFS sheet. Further investigation of this issue is required in future studies.

To comprehensively assessment effective of the strengthening method, the finite element method is recommended to be performed to compare with the result of the testing and the proposed predict strength formula. Consequently, it is important to carry out additional testing to determine the properties of materials sufficiently. Further studies in typical connection of PGFRP structure (beam, column) under strengthening by GFS should be investigated with the design configuration referred to findings of this research.

CHAPTER 5

THE INFLUENCE OF TIGHTENING FORCE ON BOLTED CONNECTION UNDER STRENGTHENING BY GFSs

5.1. Introduction

As discussed in Chapter 3, Glass Fiber Sheets (GFS) were proven to be effective in strengthening PGFRP materials. This chapter focuses on investigating the impact of bolt-tightening force on the strength of PGFRP connections. Similar to the previous chapter, the study comprised 72 experimental specimens that were subjected to different conditions, including different GFS layers, numbers of bolts, and end-distances. The GFS layers employed for strengthening the PGFRP connections were 0°/90° and ±45° glass woven roving, along with a chopped strand mat (CSM). The end-distances selected for this study were 2*d* and 3*d*, where d represented the bolt diameter of 12mm (M12) for all connections. The applied tightening force for all specimens was 21Nm.

5.2. Experimental study

a) Connection system

In this study, a 21N.m torque force was applied when setting up bolt connections for specimens (ISO 6789-1:2017). Nevertheless, for the design of bearing-type connections, it is assumed that there is no force transferred through friction between the connected elements.

b) Bolts and bolt holes

Table 5.1 Minimum requirements for bolted connection geometries

Notation	Definition	Minimum required spacing (or distance in terms of bolt diameters)
e_{min}	End distance Single row of bolts Two or three bolt rows	Tension load *4d* *2d*
	End distance All connections	Compression load *2d*
$e_{2,min}$	Edge distance	*1.5d*
s_{min}	Pitch spacing	*4d*
g_{min}	Gage spacing	*4d*
$g_{2,min}$	Gage spacing with staggered bolts	*2d*

Where:

- *d* is the nominal diameter of the bolt.

- Minimum e_{min} may be reduced to $2d$ when the connected member has a perpendicular element attached to the end that the connection force is acting towards.

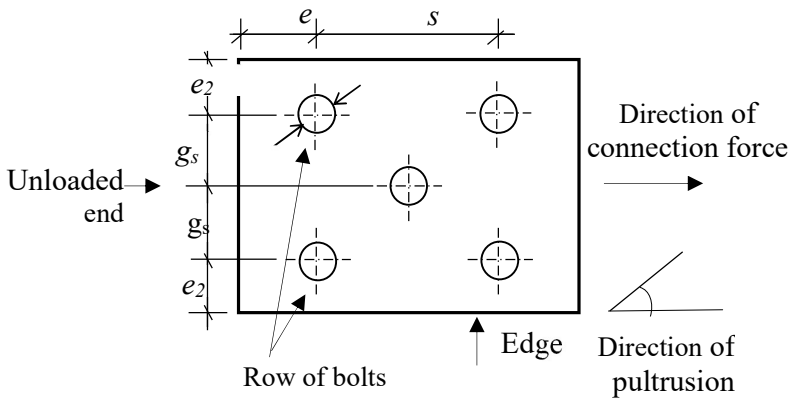

Figure 5.1. Connection definition

ACMA [35] instructed bolts shall be of carbon or stainless steel with specifications in accordance with ASTM standards A307, A325 or F593. Bolts shall be in the range of diameters, d, from 3/8 in. (9.53 mm) up to, and including, 1 in. (25.4 mm). The bolt length shall be such that the end of the bolt extends beyond or is at least flush with the outer face of the nut when properly installed. The length of the bolt shank with thread that is bearing with FRP material should be at most 1/3 of the thickness of the plate component. Bolts shall be torqued to the snug-tightened condition. The slope parts in contact with the washer the bolt head and the nut shall be equal to or less than 1:20 with respect to a plane that is perpendicular to the bolt axis.

The nominal hole diameter, d_n, shall be 1/16 in. (1.6 mm) larger than the nominal bolt diameter, d. Holes must be drilled or reamed. Oversized holes greater than 1/16 in. (1.6 mm) larger than the bolt shall not be permitted, and slotted holes shall not be aligned in the primary direction of connection force.

Bolts, bolt holes and connection geometries were determined based on the minimum requirements of ACMA standard [35] as in Figure 1 and Table 1. In this study, the bolt M12 and bolt hole size is 13.5 mm.

c) Prediction of modes of failure

Figure 5.2 shows the primary in-plane failure of plate-to-plate connection with (a) to (e) and shows different failure modes of single-bolted connections or multi-bolted connection s[13].

The other failure modes illustrated in Figure 5.2 are not desirable because their failure mechanisms are sudden. Under most geometrical arrangements it is found that bolted connections with two and three rows of bolts will have faster failure modes of either net tension (Hassan et al., 1997) [14] or a form of block shear (Prabhakaran et al., 1996) [45].

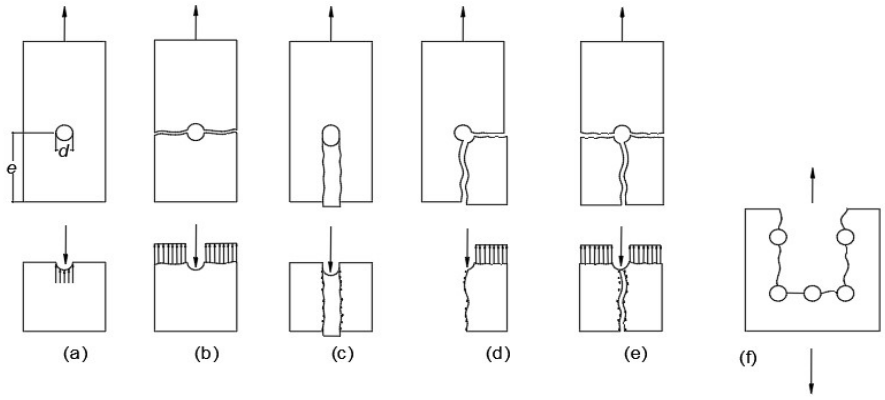

Figure 5.2. The failure mode of Bolted connection and simplified stress distributions

(a) bearing, **(b)** net tension, **(c)** shear-out, **(d)** cleavage **(e)** net tension 'splitting', **(f)** block shear

The detailed parameters of specimens are shown in Table 5.1. The definitions are as follows:

• [Glass fiber] $_{T\text{-}N}$ denotes the type of glass fiber sheet made to strengthening specimens: 0/90º GFS, ±45º, or CSM.

• $NS_{N\text{-}T}$ is a non-strengthening specimen (original PGFRP).

• T denotes the dimension of end distance (e) by ratio with bold size (d) ($e = 2d$ and $e = 3d$).

• N presents the quantity of bolts (N = 2, 4, or 5).

The M12 bolt with diameter d=12 mm and bolt hole diameter d_n=14mm was used in the connection testing.

By reference Tohnichi company torque handbook, an application of 21 Nm tightening force was affected through a manual torque wrench, while controlling the moment capacity using an analog meter. The remaining conditions were set up in a manner akin to those described in Chapter 3. This methodology is in line with academic standards for precision and rigor in experimental procedures.

Table 5.2 Specimens in the connection test

Specimen	End Distance (mm)	No. of Bolts	avg of t_{GF} (mm)	No. of Specimens
$[NS]_{2-2}$	24	2		3
$[NS]_{3-2}$	36	2		3
$[NS]_{2-4}$	24	4		3
$[NS]_{3-4}$	36	4		3
$[NS]_{2-5}$	24	5		3
$[NS]_{3-5}$	36	5		3
$[0/90]_{2-2}$	24	2	1.21	3
$[0/90]_{3-2}$	36	2	1.22	3
$[0/90]_{2-4}$	24	4	1.26	3
$[0/90]_{3-4}$	36	4	1.26	3
$[0/90]_{2-5}$	24	5	1.26	3
$[0/90]_{3-5}$	36	5	1.26	3
$[\pm45]_{2-2}$	24	2	1.24	3
$[\pm45]_{3-2}$	36	2	1.25	3
$[\pm45]_{2-4}$	24	4	1.23	3
$[\pm45]_{3-4}$	36	4	1.23	3
$[\pm45]_{2-5}$	24	5	1.23	3
$[\pm45]_{3-5}$	36	5	1.23	3
$[CSM]_{2-2}$	24	2	1.49	3
$[CSM]_{3-2}$	36	2	1.45	3
$[CSM]_{2-4}$	24	4	1.48	3
$[CSM]_{3-4}$	36	4	1.47	3
$[CSM]_{2-5}$	24	5	1.49	3
$[CSM]_{3-5}$	36	5	1.50	3

5.3. Experimental failure modes and capacity of specimens

5.3.1. Strengthening effectiveness

Table 5.2 displays the ultimate loads obtained from the connection strength test, while the line graphs in Figure 5.2 illustrate the average results of three samples for each designed specimen. The maximum load achieved by GFSs was found to surpass that of NS specimens across all types of GFSs, with fixed parameters for bolt number and end-distance. In the results, the specimens also demonstrated strengthening effectiveness despite a decrease in the Pst /PNS ratio, which ranged from 1.4 to 2.1, compared to the non-tightening cases reached 2.7. Notably, in Table 5.2 (a, b), the [CSM] effective ratio was observed to be lower than any of the other GFSs, measuring at 40% for specimens with 5 bolts.

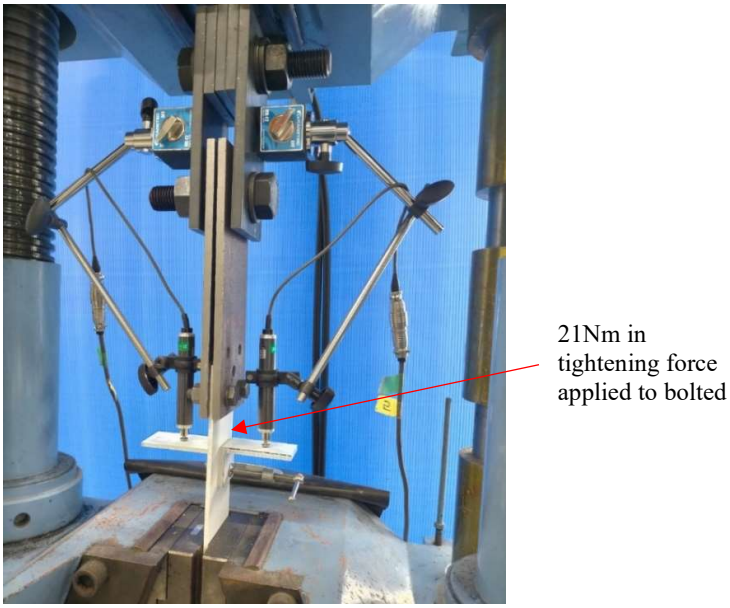

Figure 5.3 Test setup with tightening force applied in the bolted connection

Table 5.3 The ultimate loads of PGFRP connections and strengthening effects of GFSs.

a) Ultimate load of [0/90] GFS strengthening specimens

Specimens	$[0/90]_{2\text{-}2}$	$[0/90]_{3\text{-}2}$	$[0/90]_{2\text{-}4}$	$[0/90]_{3\text{-}4}$	$[0/90]_{2\text{-}5}$	$[0/90]_{3\text{-}5}$
1	44.708	51.782	72.33	79.668	78.10	83.424
2	38.194	49.212	84.82	75.412	71.68	76.98
3	42.146	48.486	80.64	83.464	76.96	75.324
Average load	**41.683**	**49.827**	**79.267**	**79.515**	**75.581**	**78.576**
C.O.V	3.28	1.73	6.35	4.02	3.42	4.27
Pst/P_{NS}	2.12	2.15	1.88	1.74	1.44	1.43

b) Ultimate load of [45] GFS strengthening specimens

Specimens	$[\pm45]_{2\text{-}2}$	$[\pm45]_{3\text{-}2}$	$[\pm45]_{2\text{-}4}$	$[\pm45]_{3\text{-}4}$	$[\pm45]_{2\text{-}5}$	$[\pm45]_{3\text{-}5}$
1	40.316	43.876	74.39	89.8	89.31	87.08
2	40.514	46.216	75.30	90.232	74.83	91.028
3	41.794	45.948	84.53	83.644	76.71	80.936
Average load	**40.875**	**45.347**	**78.075**	**87.892**	**80.283**	**86.348**
C.O.V	0.80	1.280	5.61	3.68	7.87	5.08
Pst/P_{NS}	2.08	1.96	1.85	1.92	1.53	1.57

c) Ultimate load of [CSM] GFS strengthening specimens

Specimens	$[CSM]_{2-2}$	$[CSM]_{3-2}$	$[CSM]_{2-4}$	$[CSM]_{3-4}$	$[CSM]_{2-5}$	$[CSM]_{3-5}$
1	36.972	45.508	70.18	79.064	72.92	74.82
2	32.582	47.018	72.57	77.88	77.04	78.292
3	38.25	48.6	77.08	70.084	72.07	76.048
Average load	**35.935**	**47.042**	**73.275**	**75.676**	**74.008**	**76.387**
C.O.V	2.97	1.54	3.50	4.87	2.65	1.76
Pst/P_{NS}	1.83	2.03	1.74	1.65	1.41	1.39

d) Ultimate load of non-strengthening specimens

Specimens	NS_{2-2}	NS_{3-2}	NS_{2-4}	NS_{3-4}	NS_{2-5}	NS_{3-5}
1	20.562	24.452	44.726	40.820	48.276	54.060
2	18.887	23.034	42.288	48.368	56.388	52.700
3	19.617	21.904	39.254	48.064	52.420	58.148
Average load	**19.689**	**23.130**	**42.089**	**45.751**	**52.361**	**54.969**
C.O.V	0.839	1.27	2.74	4.27	4.05	2.83

In the table 5.2:

- P_{st}: denotes the ultimate loads of strengthened specimens.
- P_{NS}: denotes the ultimate loads of NS specimens.

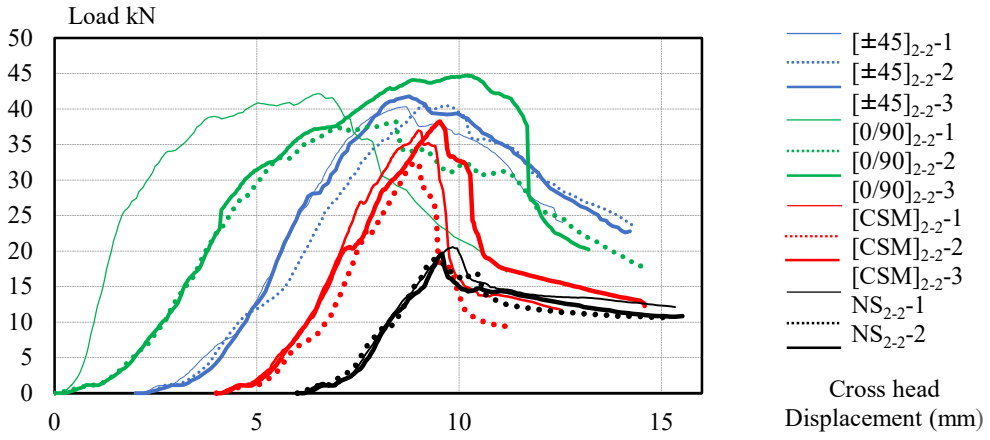

(a) 2 bolts and e=2d

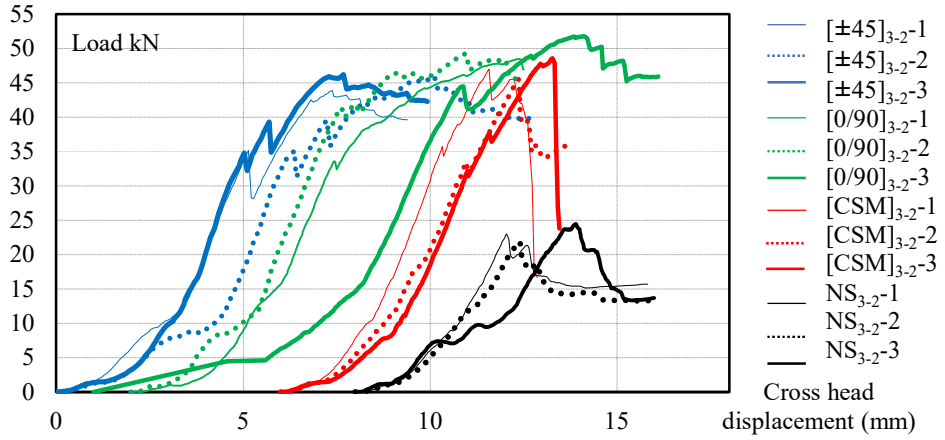

(b) 2 bolts and *e*=3*d*

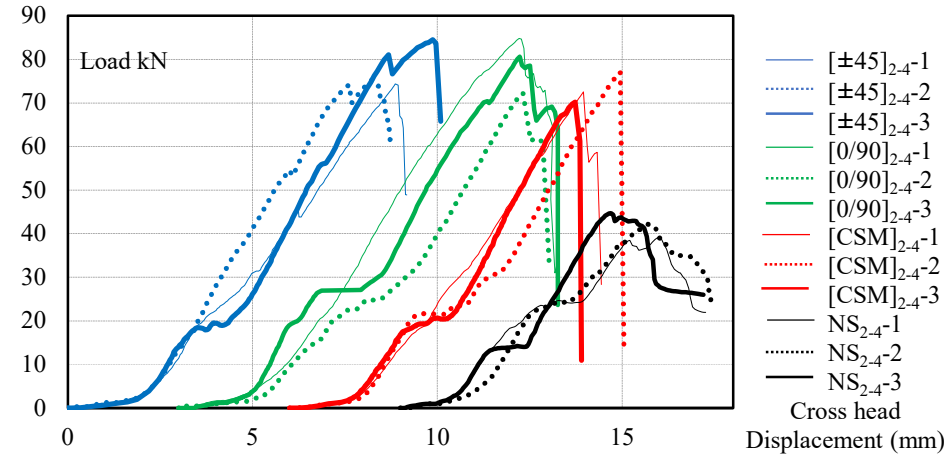

(c) 4bolts and *e*=2*d*

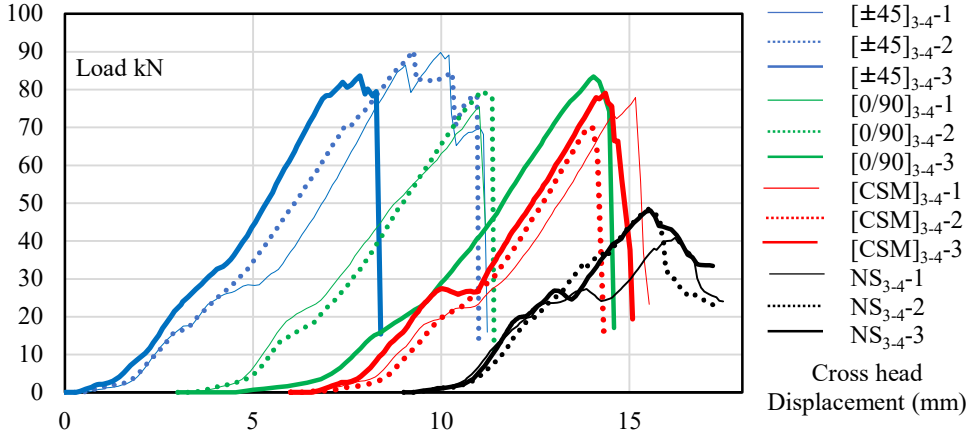

(c) 4bolts and *e*=3*d*

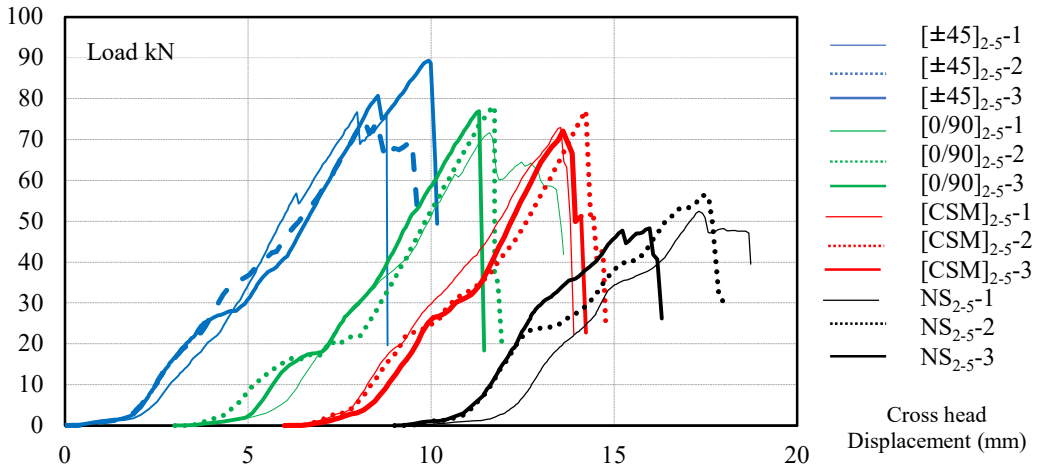

(e) 5bolts and e=2d

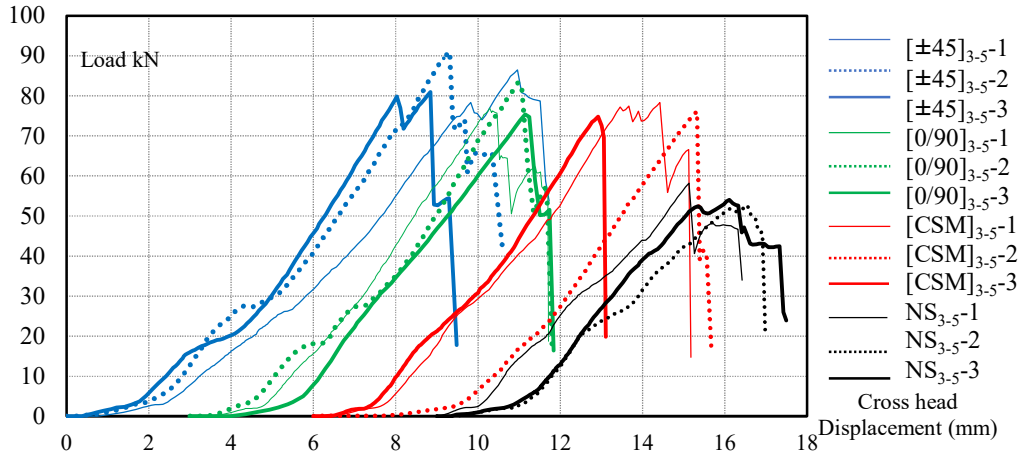

(f) 5bolts and e=3d

Figure 5.4 Load-cross head displacement relations in all specimens

According to the load development shown in Figure 5.2, there is a clear difference in the behavior of two bolted connections under the influence of tightening force. The load gradually increases before and after reaching the maximum value, indicating the effect of the tightening force. However, this phenomenon was not observed in the non-tightening specimens. Therefore, it can be concluded that the tightening force significantly influences the load behavior of bolted connections.

Table 5.3 presents the variation in maximum load values between the application of case tightening force and non-tightening force in bolted connections. The average maximum loading values in the [±45] and [NS] orientations demonstrate a significant increase in connection

capacity, whereas the variations recorded in [CMS] and [0/90] were relatively lower.

Table 5.4 Comparison of ultimate loads between non-tightening and tightening specimens

Specimens	$[0/90]_{2\text{-}2}$	$[0/90]_{3\text{-}2}$	$[0/90]_{2\text{-}4}$	$[0/90]_{3\text{-}4}$	$[0/90]_{2\text{-}5}$	$[0/90]_{3\text{-}5}$
Non-tightening force	28.05	36.59	51.86	60.87	63.27	69.25
Tightening force	41.68	49.83	79.27	79.52	75.58	78.58
Various	49%	53%	19%	36%	31%	13%
Specimens	$[\pm45]_{2\text{-}2}$	$[\pm45]_{3\text{-}2}$	$[\pm45]_{2\text{-}4}$	$[\pm45]_{3\text{-}4}$	$[\pm45]_{2\text{-}5}$	$[\pm45]_{3\text{-}5}$
Non-tightening force	26.13	33.79	53.28	58.40	54.25	55.65
Tightening force	40.88	45.35	78.08	87.892	80.28	86.35
Various	56%	47%	48%	34%	51%	55%
Specimens	$[CSM]_{2\text{-}2}$	$[CSM]_{3\text{-}2}$	$[CSM]_{2\text{-}4}$	$[CSM]_{3\text{-}4}$	$[CSM]_{2\text{-}5}$	$[CSM]_{3\text{-}5}$
Non-tightening force	24.20	36.93	53.80	59.53	58.03	64.20
Tightening force	35.94	47.04	73.28	75.68	74.01	76.39
Various	36%	28%	27%	27%	19%	48%
Specimens	$NS_{2\text{-}2}$	$NS_{3\text{-}2}$	$NS_{2\text{-}4}$	$NS_{3\text{-}4}$	$NS_{2\text{-}5}$	$NS_{3\text{-}5}$
Non-tightening force	10.14	17.87	25.26	36.38	35.81	37.94
Tightening force	19.69	23.13	42.09	45.75	52.36	54.97
Various	94%	67%	46%	29%	26%	45%

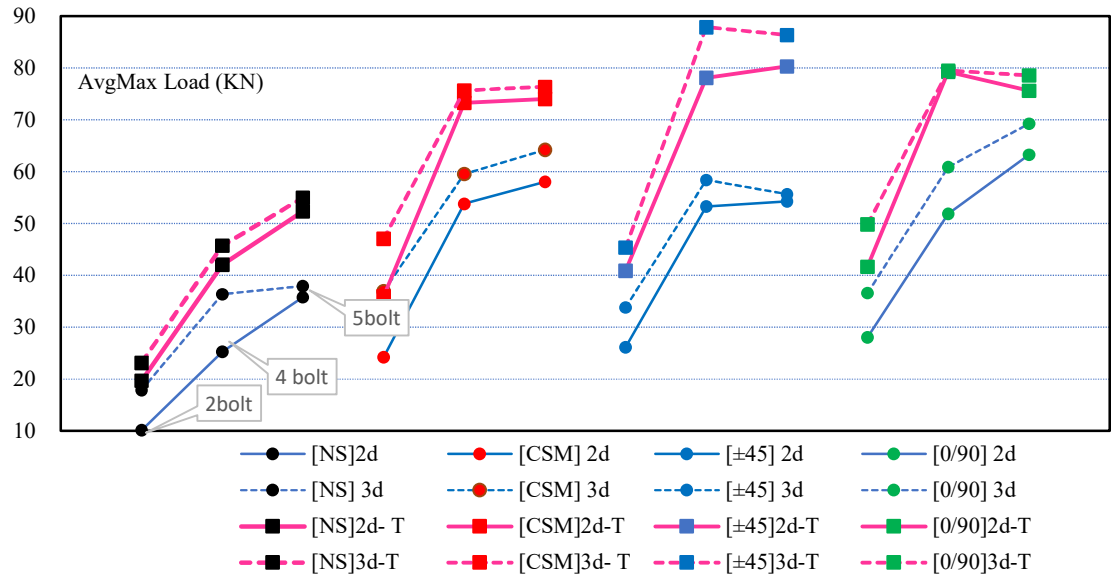

Figure 5.5 Average Ultimate load in all specimens tightening and non-tightening force

On the other hand, it should be noted that the [±45] orientation exhibits the highest absolute variation in the maximum load in compare values before and after the application of tightening force for bolts. There were illustrated in Figure 5.5, which shows two series of specimens with and without fastened bolted connections. The [specimen]-T presented for

specimens that apply tighten force in bolts. Based on these results, it can be concluded that connection strength behavior in GFS depends on the surface or fiber direction under the influence of tightening force.

5.3.2. Failure modes and comparison to non-tightening force specimens

The variation in the increase of connection strength for each GFS type can also be observed in the different failure modes that occurred. The experiment identified five main types of failure modes, which are simulated in 3D view in Figure 5.5. Experiment result pictures are listed in Figure 5.6, showing each typical specimen's perspective and front view. It should be noted that the failure modes were a combination of 2 or 3 elements, as shown in Table 5.4.

Table 5.5 The failure mode of specimens

Specimens	**Failure Mode**	**Specimens**	**Failure Mode**	**Specimens**	**Failure Mode**	**Specimens**	**Failure Mode**
$[0/90]_{2\text{-}2}$	M1	$[\pm45]_{2\text{-}2}$	M1	$[CSM]_{2\text{-}2}$	M1	$NS_{2\text{-}2}$	M4
$[0/90]_{3\text{-}2}$	M1	$[\pm45]_{3\text{-}2}$	M1	$[CSM]_{3\text{-}2}$	M1/M2	$NS_{3\text{-}2}$	M4
$[0/90]_{2\text{-}4}$	M3	$[\pm45]_{2\text{-}4}$	M3	$[CSM]_{2\text{-}4}$	M2	$NS_{2\text{-}4}$	M4
$[0/90]_{3\text{-}4}$	M3	$[\pm45]_{3\text{-}4}$	M3	$[CSM]_{3\text{-}5}$	M2	$NS_{3\text{-}4}$	M4
$[0/90]_{2\text{-}5}$	M3	$[\pm45]_{2\text{-}5}$	M3	$[CSM]_{2\text{-}5}$	M2	$NS_{2\text{-}5}$	M5
$[0/90]_{3\text{-}5}$	M3	$[\pm45]_{3\text{-}5}$	M3	$[CSM]_{3\text{-}5}$	M2	$NS_{3\text{-}5}$	M5

The brief description of failure modes can be defined as follows:

- MODE 1 (M1): Shear-out or bearing in the surface of GFS/GFM and small shear-out in CD. This mode was taken in [0/90] and [±45] GFS specimens with 2 bolts.
- MODE 2 (M2): Net-tension failure in the surface of GFS/GFM and shear-out in CD. It was obtained in all CSM-strengthened specimens (2,4 and 5 bolts). It consists of net-tension in GFS and GFM parts and shear-out in the GFM part.
- MODE 3 (M3): Debonding failure in GFS/GFM and shear-out in CD. This failure mode occurred in 4 and 5 bolts with [0/90] and [±45] GFS specimens.
- MODE 4 (M4): Shear-out failure in whole sections in 2 bolts and 4 bolts with non-strengthened specimens (NS).

- MODE 5(M5): Shear-out inside (CD layer) and block shear failure outside (GFM layer) occurred in 5 bolts -NS specimens.

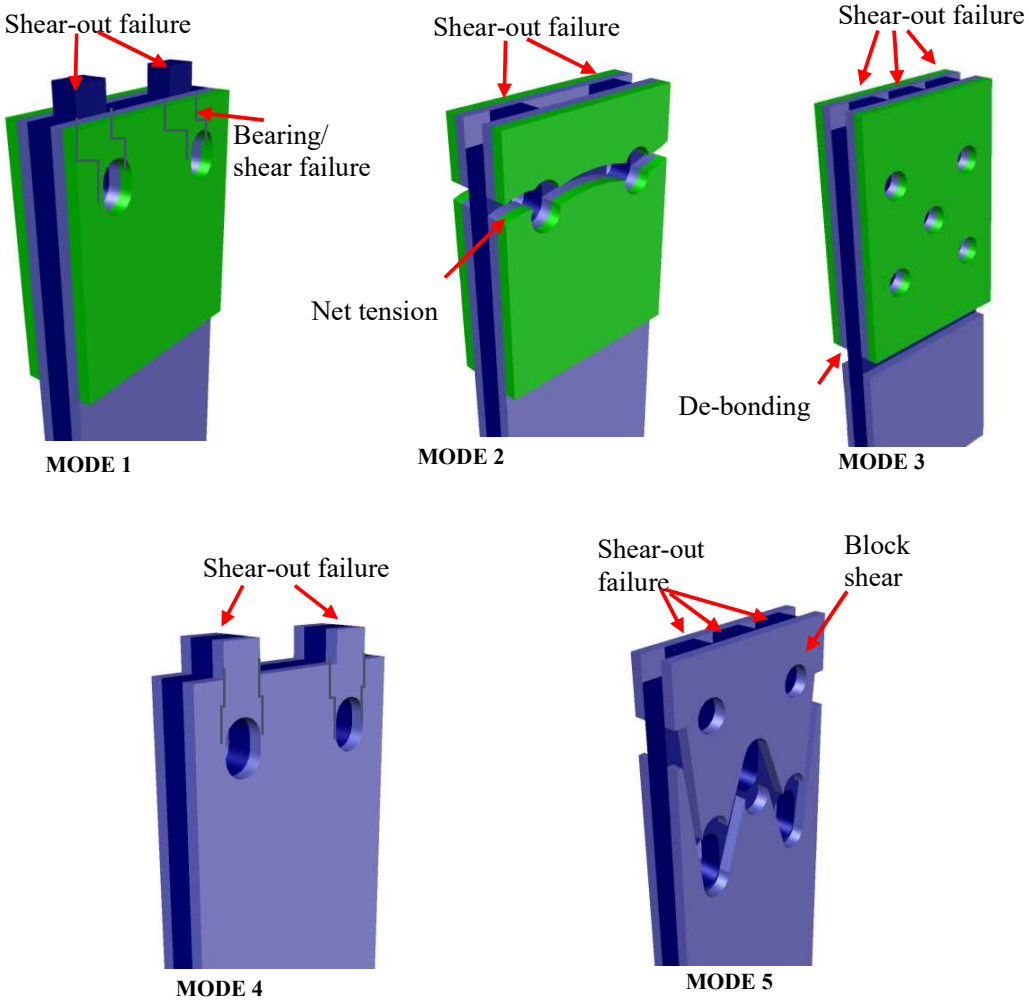

Figure 5.6 Failure modes of the PGFRP connections

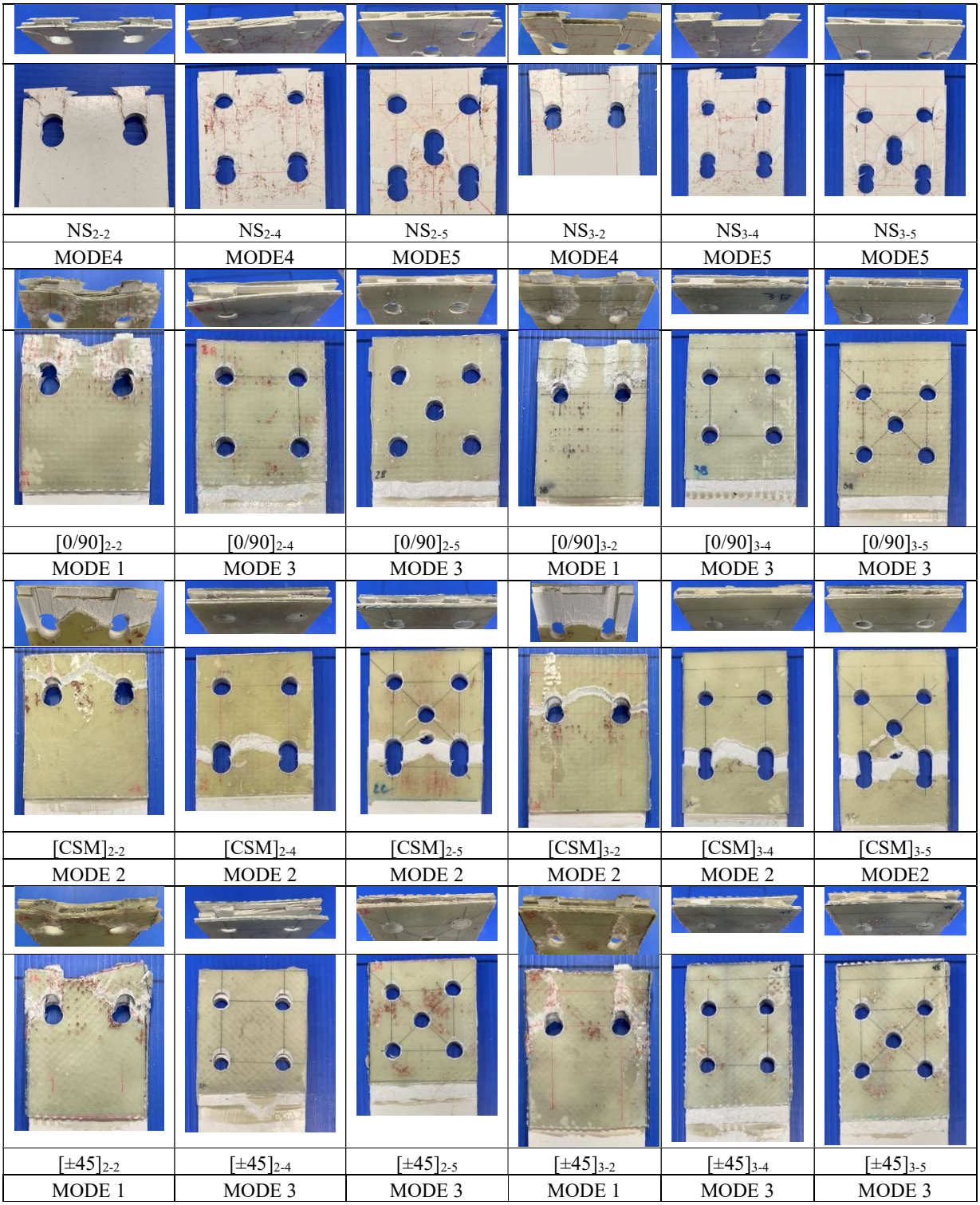

Figure 5.7. Typical failure modes of the PGFRP connections in the experiments

The tendency of failure modes is explained based on the result of load-cross head displacement as shown in Figure 9. Overall, the failure modes displayed similar behavior to that of the non-tightening force, except for MODE 1 which exhibited shear out in GFM and GFS instead of clearance. This can be attributed to the influence of the applied tightening force on the bolt and load transfer to the two steel plates, which distributes the load across the entire surface of the GFS. As a result, the behavior of the fiber in the GFS was altered, leading to differences in the type of failure observed.

MODE 4 occurred in all thicknesses of NS 2 and 4 bolts. The result met with previous studies' results investigated the failure mode in the base plate PGFRP. The shear-out strength of the CD layer is much less than in comparison with bearing or tensile strength. Therefore, shear out failure mode has an appearance in CD and leads to GFM layer shear-out meanwhile the loading increases.

From MODE1, MODE 2 and MODE3 based on the observation, debonding failure occurred in whole specimens. During the loading development, each component will fail with the mode depending on order of its component strength size, as indicated in Appendix 1.

The other mode in NS is MODE 5: block shear failure mode occurred with three-bolt rows in five bolts specimens. In Appendix 1, block shear strength was considered the weakest. After block shear failure occurred, the second component failure came with the shear-out of the inside layer (CD) corresponding with the order of strength size.

Debonding failure witnessed in MODE 3 occurred in the whole GFS strengthening area. According to the ASCE [15] principle, bonding strength tends to rise to the combined strength of bearing or shear-out strength of GFM/GFS before debonding. However, due to debonding in the whole surface of the GFM/GFS area, only the CD layer was a shear-out failure in the final, corresponding to the weakest value.

By a similar method, failure mode, MODE 4 in the [CSM] specimens can be explained. The net-tension failure occurred after loading reached the lowest combined strength and tensile strength. CD layer inside also shear-out consequently. In e=2d and 2 bolts specimens, the tensile and shear strength in GFM/GFS are equivalent, thus leading to the “hybrid mode”: shear out and net-tension failure co-occurred.

5.3.3 Evaluation of strengthening effect by number of bolts

The increase in connection strength is significant when the number of bolts is changed from 2 to 4. The effectiveness is also noticeable in the NS when changing from 4 to 5 bolts. However, the strengthening effect is trivial in GFS specimens when changing from 4 to 5 bolts. In the [0/90], [±45] GFS type, the ultimate load in the 4 bolts connection specimens is higher than in the 5 bolts-specimens because the bonding area is decreased by one more bolt hole area. In the [CSM] specimens, the tensile strength of GFS did not significantly change when adding 1 more bolt from 4 bolts to 5 bolts. This is because the main factor that causes net-tension failure, i.e., the cross area of the failure section, did not change, hence, the ultimate load in [CSM] did not change in these cases. On the other hand, the NS specimens exhibited a change in failure mode from MODE 1 (2 and 4 bolts) to MODE 2: 5 bolts (block shear). The length of the along shear area increased in the case of 5 bolts, resulting in better strength than 2 or 4 bolts.

Table 5.5 Comparison of the strengthening effect of *3d* end -distance specimens to *2d* end-distance specimens

No. bolt	[±45]	[0/90]	[CSM]	NS
2	10.9%	19.5%	30.9%	17.5%
4	12.6%	0.3%	3.3%	8.7%
5	7.6%	4.0%	3.2%	5.0%

5.3.4 Strengthening effect related to end-distance.

Besides the effect of the number of bolts and the type of GFS, the end distance *e* was also investigated in this study. Table 5.5 provides the percentage of increasing strength when changing from end-distance *e=2d* to *e=3d.*

In the case of 2 bolts, all specimens were shown a high effect with an increasing ratio ranging from 10.9% to 30.9%. The added end-distance made the failure-out section of CD layer longer. The reason above made the maximum load stronger in *e=3d* specimens.

In the type of 4 or 5 bolts specimens, only [±45] with 4 bolts specimens shows an increase in connection strength (around 12% increase).

In addition, the relative increasing values in ultimate load were trended lower in the 4 or 5 bolts specimens in comparison with the 2 bolts specimen. This is because of the absolute value of the ultimate load in 2 bolts is much lower than in the other. Therefore, it is more effective when increasing by extending end-distance in 2 bolts specimens than the 4 or 5 bolts

specimens.

The bonding strength of the CD and GFS layer was a major element when evaluating MODE 2 and MODE 5. These represent a failure mode occurred in 4 or 5 bolts specimens (except [CSM] specimens). The distribution and area of effective bonding will be continuously investigated as a supplement for more understanding of this issue.

5.4. Conclusion

This chapter has presented an investigation into the strengthening of multi-bolted PGFRP using GFS under the application of tightening force for bolts. The results of the connection testing have demonstrated that the strengthening method by GFS remains effective under various conditions of PGFPR bolted connection. Despite the variations in the application of the tightening force, all other parameters were maintained at a similar level as the non-tightening case described in Chapter 3.

Even though the maximum load increased in all types of specimens compared to the case without applied tightening, the effectiveness before (NS) and after strengthening with GFSs (P_{st}/P_{NS}) slightly decreased. The failure modes were explained by measuring the strength of the individual elements and then calculating to find lowest combined strength. However, due to the complexity of the tightening force's effect, equations for prediction ultimate load of connection could not be proposed.

It is necessary to conduct additional investigations in various connection parameters: the number of bolts and different tightening forces apply to a more comprehensive understanding of GFS strengthening multi-bolted PGFRP connection.

Appendix

Appendix 1a

Material properties									
Fail. mode	Specimens	Bearing strg of GFM (Mpa)	Bearing strg of GFS (Mpa)	Bearing strength of (CD Mpa)	Shear out strg of CD (Mpa)	Shear out strg of (GFM)	Shear strg of GFS (Mpa)	Tensile strg of PGFRP (Mpa)	Tensile strg of GFS (Mpa)
MODE 1	[0/90] 2 bolts 2d	199.71	146.03	260.49	11.68	81.91	86.00	536.00	420.00
	[0/90] 2bolts 3d	199.71	146.03	260.49	11.68	81.91	86.00	536.00	420.00
MODE 3	[0/90] 4 bolts 2d	199.71	146.03	260.49	11.68	81.91	86.00	536.00	420.00
	[0/90] 4 bolts 3d	199.71	146.03	260.49	11.68	81.91	86.00	536.00	420.00
	[0/90] 5 bolts 2d	199.71	146.03	260.49	11.68	81.91	86.00	536.00	420.00
	[0/90] 5 bolts 3d	199.71	146.03	260.49	11.68	81.91	86.00	536.00	420.00
MODE 1	[45] 2 bolts 2d	199.71	154.56	260.49	11.68	81.91	94.92	536.00	169.00
	[45] 2 bolts 3d	199.71	154.56	260.49	11.68	81.91	94.92	536.00	169.00
MODE 3	[45] 4 bolts 2d	199.71	154.56	260.49	11.68	81.91	94.92	536.00	169.00
	[45] 4 bolts 3d	199.71	154.56	260.49	11.68	81.91	94.92	536.00	169.00
	[45] 5 bolts 2d	199.71	154.56	260.49	11.68	81.91	94.92	536.00	169.00
	[45] 5 bolts 3d	199.71	154.56	260.49	11.68	81.91	94.92	536.00	169.00
MODE 2	[CSM] 2 bolts 2d	199.71	199.71	260.49	11.68	81.91	81.91	536.00	164.80
	[CSM] 2 bolts 3d	199.71	199.71	260.49	11.68	81.91	81.91	536.00	164.80
	[CSM] 4 bolts 2d	199.71	199.71	260.49	11.68	81.91	81.91	536.00	164.80
	[CSM] 4 bolts 3d	199.71	199.71	260.49	11.68	81.91	81.91	536.00	164.80
	[CSM] 5 bolts 2d	199.71	199.71	260.49	11.68	81.91	81.91	536.00	164.80
	[CSM] 5 bolts 3d	199.71	199.71	260.49	11.68	81.91	81.91	536.00	164.80
MODE 4	NS 2 bolt 2d	199.71		260.49	11.68	81.91		536.00	
	NS 2 bolt 3d	199.71		260.49	11.68	81.91		536.00	
	NS 4 bolt 2d	199.71		260.49	11.68	81.91		536.00	
	NS 4 bolt 3d	199.71		260.49	11.68	81.91		536.00	
MODE 5	NS 5 bolt 2d	199.71		260.49	11.68	81.91		536.00	
	NS 5 bolt 3d	199.71		260.49	11.68	81.91		536.00	

The principal equation can obtain the Component strength::

$$P_i = \tau_i A$$

- τ_i : component strength in Appendix 1a: properties of material that referred from Nhut [44, 45] and the material testing
- *A:* is the net area subject to each component's strength:
  - Bearing strength: $A = dtn$

with d and n are the bolt diameter and the number of bolts, and t is the thickness of component layers.

- Shear strength; tensile strength: $A = tL$

With t; T is the thickness and total length of subject component layers

Appendix 1b

Specimens' parameters								
Fail. mode	Specimens	Width w mm	End distance e mm	Length of GFS l mm	No of bolts n nos	Thk of CD t_{CD} *(mm)*	Thk of GFS t_{GFS} *(mm)*	Thk of GFM t_{GFM} *(mm)*
MODE 1	[0/90] 2 bolts 2d	84.00	24.00	96.00	2.00	4.00	1.26	0.50
	[0/90] 2 bolts 3d	84.00	36.00	120.00	2.00	4.00	1.29	0.50
MODE 3	[0/90] 4 bolts 2d	84.00	24.00	96.00	4.00	4.00	1.25	0.50
	[0/90] 4 bolts 3d	84.00	36.00	120.00	4.00	4.00	1.26	0.50
	[0/90] 5 bolts 2d	84.00	24.00	96.00	5.00	4.00	1.26	0.50
	[0/90] 5 bolts 3d	84.00	36.00	120.00	5.00	4.00	1.25	0.50
MODE 1	[45] 2 bolts 2d	84.00	24.00	96.00	2.00	4.00	1.21	0.50
	[45] 2 bolts 3d	84.00	36.00	120.00	2.00	4.00	1.20	0.50
MODE 3	[45] 4 bolts 2d	84.00	24.00	96.00	4.00	4.00	1.23	0.50
	[45] 4 bolts 3d	84.00	36.00	120.00	4.00	4.00	1.24	0.50
	[45] 5 bolts 2d	84.00	24.00	96.00	5.00	4.00	1.23	0.50
	[45] 5 bolts 3d	84.00	36.00	120.00	5.00	4.00	1.24	0.50
MODE 2	[CSM] 2 bolts 2d	84.00	24.00	96.00	2.00	4.00	1.65	0.50
	[CSM] 2 bolts 3d	84.00	36.00	120.00	2.00	4.00	1.61	0.50
	[CSM] 4 bolts 2d	84.00	24.00	96.00	4.00	4.00	1.61	0.50
	[CSM] 4 bolts 3d	84.00	36.00	120.00	4.00	4.00	1.59	0.50
	[CSM] 5 bolts 2d	84.00	24.00	96.00	5.00	4.00	1.57	0.50
	[CSM] 5 bolts 3d	84.00	36.00	120.00	5.00	4.00	1.59	0.50
MODE 4	NS 2 bolt 2d	84.00	24.00	96.00	2.00	4.00		0.50
	NS 2 bolt 3d	84.00	36.00	120.00	2.00	4.00		0.50
	NS 4 bolt 2d	84.00	24.00	96.00	4.00	4.00		0.50
	NS 4 bolt 3d	84.00	36.00	120.00	4.00	4.00		0.50
MODE 5	NS 5 bolt 2d	84.00	24.00	96.00	5.00	4.00		0.50
	NS 5 bolt 3d	84.00	36.00	120.00	5.00	4.00		0.50

Appendix 1c

Component strength (kN)							
Fail. mode	Specimens	P_{brCD}	$P_{brGFM/GFS}$	P_{soCD}	$P_{soGFS/GFM}$	$P_{ntGFS/GFM}$	$P_{ntPGFRP}$
MODE 1	[0/90] 2 bolts 2d	25.01	13.62	4.48	28.65	68.45	300.16
	[0/90] 2bolts 3d	25.01	13.80	6.72	43.62	69.68	300.16
MODE 3	[0/90] 4 bolts 2d	50.01	27.05	13.45	68.72	67.84	300.16
	[0/90] 4 bolts 3d	50.01	27.25	15.69	83.62	68.50	300.16
	[0/90] 5 bolts 2d	62.52	34.06	13.45	69.28	68.50	300.16
	[0/90] 5 bolts 3d	62.52	33.82	15.69	82.94	67.84	300.16
MODE 1	[45] 2 bolts 2d	25.01	13.77	4.48	29.92	32.13	300.16
	[45] 2 bolts 3d	25.01	13.70	6.72	44.60	31.94	300.16
MODE 3	[45] 4 bolts 2d	50.01	27.84	13.45	73.18	32.51	300.16
	[45] 4 bolts 3d	50.01	28.04	15.69	89.06	32.78	300.16
	[45] 5 bolts 2d	62.52	34.80	13.45	73.18	32.51	300.16
	[45] 5 bolts 3d	62.52	35.06	15.69	89.06	32.78	300.16
MODE 2	[CSM] 2 bolts 2d	25.01	20.61	4.48	33.81	39.68	300.16
	[CSM] 2 bolts 3d	25.01	20.23	6.72	49.78	38.95	300.16
	[CSM] 4 bolts 2d	50.01	40.41	13.45	80.12	38.91	300.16
	[CSM] 4 bolts 3d	50.01	40.07	15.69	95.87	38.58	300.16
	[CSM] 5 bolts 2d	62.52	49.61	13.45	78.67	38.21	300.16
	[CSM] 5 bolts 3d	62.52	50.09	15.69	95.87	38.58	300.16
MODE 4	NS 2 bolt 2d	25.01	4.79	4.48	7.86		300.16
	NS 2 bolt 3d	25.01	4.79	6.72	11.80		300.16
	NS 4 bolt 2d	50.01	9.59	13.45	19.00		300.16
	NS 4 bolt 3d	50.01	9.59	15.69	22.93		300.16
MODE 5	NS 5 bolt 2d	62.52	11.98	13.45	23.59		300.16
	NS 5 bolt 3d	62.52	11.98	15.69	27.52		300.16

ASCE [35], Sub-section 8.3.3.4. Block Shear Strength, R_{bs}

When the connection force is concentric to the group of bolts, tensile and parallel to the direction of FRP material the nominal block shear strength for the multi-bolted connection shall be given by:

$$R_{bs} = 0.5\ (A_{ns}F_{sh} + A_{nt} + F^{t}_{L})$$

$$\varphi_c = 0.45$$

where

- F_{sh} = Characteristic in-plane shear strength of FRP material appropriate to the shear-out failure

- F^{T}_{L} = Characteristic tensile strength of the FRP material in the longitudinal A_{ns} = Net area subjected to shear
- A_{nt} = Net area subjected to tension, where the bolts are staggered the total deducted in c

determining Ant shall be the greater of

(i) the maximum of the sectional area in any cross-section perpendicular to the member axis, or

(ii) $t\ (nd_n - \sum b_s)$

Where:

- $\boldsymbol{b_s}$ is the lesser of $\boldsymbol{r} = \frac{s^2}{4g_s}$ *or* $0.65gs$
- n = Number of holes extending in any diagonal or zig-zag line progressively across the member or part of the member (n_{max} = 3)
- d_n = Nominal diameter of hole

The calculated value of block shear strength of NS 5 bolt ($NS_{2\text{-}5}$ and $NS_{3\text{-}5}$) = 8.20 kN and 9.19 kN

CHAPTER 6
STRENGTHENING FOR BEAM-TO-COLUMN BOLTED CONNECTION

6.1. Introduction

In previous studies, the effectiveness of Glass Fiber Sheets (GFS) as a strengthening method has been analyzed in relation to main parameter aspects for application to multi-bolted PGFRP connections. The proposed prediction equations have also been demonstrated to be highly applicable. This chapter will focus on the application of the GFS strengthening method on beam-to-column connections, which are common components in building structures. In order to evaluate the effectiveness of the Glass Fiber Sheets (GFS) strengthening method on beam-to-column connections, a total of four full-scale specimens were tested. Two of these specimens were tested without any GFS strengthening, while the other two were strengthened using GFS. This approach was taken to allow for a clear comparison of the effectiveness of the GFS method in enhancing the strength and durability of beam-to-column connections. By comparing the results of the tests on the strengthened and non-strengthened specimens, the impact of GFS on the behavior and performance of beam-to-column connections can be analyzed.

6.2. Experimental program

6.2.1. PGFRP

The SP100 is the original PGFRP material developed by Fukui Fibertech Co., Ltd, located in Toyohashi, Aichi, Japan. The material has a square box section with dimensions of 100x100mm and a total thickness of 5.5mm, resulting in a weight of 3440g/m. The PGFRP product consists of two fiber phases, namely, continuous direction glass roving (CD) (2 layers) and glass fiber mat (GFM) (3 layers), both of which are produced using E-glass roving as the raw material. The resin component is made from unsaturated polyester resin. The original material is depicted in Figure 6.1, with the GFM on the two sides surface, and a layer embedded between two layers of the CD part.

Likewise, for the purpose of strengthening, GFSs of the same [0/90] type as described in Chapter 3 were utilized, comprising three layers of $0/90^0$ woven roving (ERW580-554A with a weight of 580 g/m2).

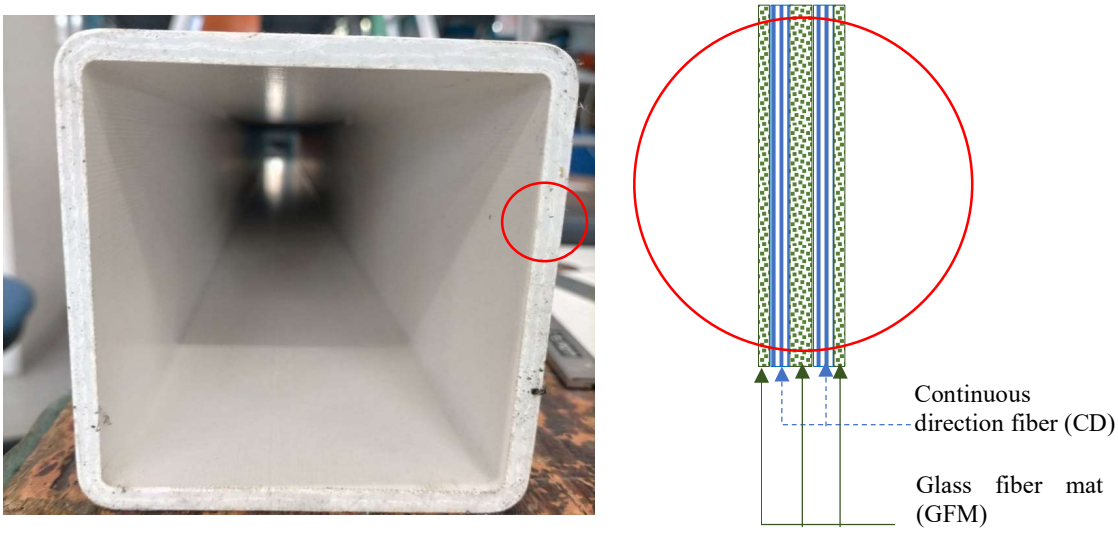

Figure 6.1 Pultruded GFRP in section view

6.2.2. Material mechanical properties test

The results of the performed tests and the standards followed are presented in Table 6.1. As expected, the material presented orthotropic behavior, with higher stiffness and strength in the longitudinal direction of the profile. The specimens for the material test were taken from cutting 1 side of square profile bar, then divided based on dimension and fiber direction. All results of the material's properties were calculated similarly to Chapter 3, with corresponding Eq (3.1), Eq (3.2), Eq (3.3) and Eq (3.4).

Table 6.1 List of specimens for material test

Specimens	No. of specimens	Specimen dimensions ($w \times l$) (mm)	Explanations	Standard tests
Tensile	5	25 × 250	Tensile tests for PGFRP in the loading direction	JISK7164
Shear strength	5	56 × 76	Shear strength test for PGFRP	JISK7164
Shear-out	5	84 × 250	Shear-strength test for whole section of PGFRP	JISK7164
Compressive	5	25×125	Compress tests for PGFRP in the loading direction	

a) Tensile test

The material properties, including the compressive strength, tensile strength elastic modulus in the loading direction (E1), and the transversal direction of loading (E2), were obtained from standard tests. The elastic modulus, tensile strength, and compressive strength

of the PGFRP were different in both directions. PGFRP specimens were cut from SP100 profiles.

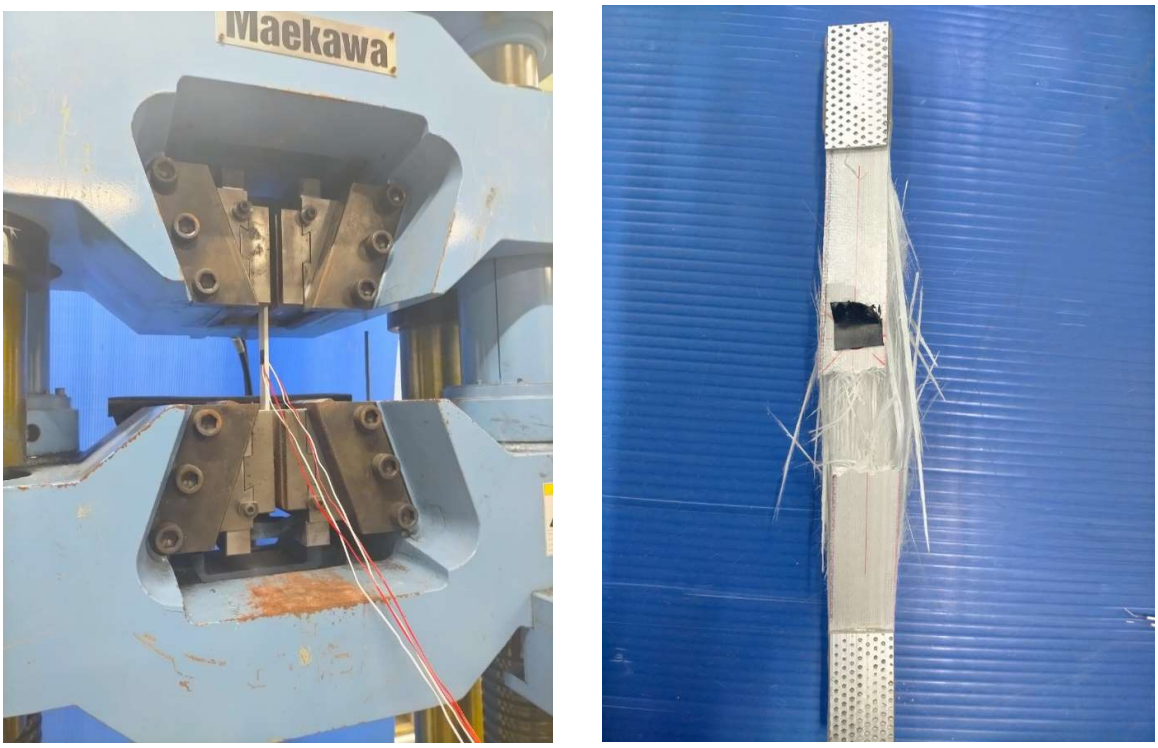

Figure 6.2 Test setup and failure specimen of tensile test

Table 6.2 Tensile test result in the fiber direction

Parameters	**Unit**	**T1**	**T2**	**T3**	**T4**	**T5**	**Avg**	**C.o.V**
P max	kN	52.45	58.42	54.16	51.22	57.31	54.71	5.0%
Thickness	mm	5.75	5.50	5.76	5.80	5.75		
d (avg)	mm	25.80	26.00	25.40	25.09	26.05		
A	mm^2	148.35	143.00	146.30	145.52	149.79		
E1- elastic modulus	GPa	23.859	27.418	23.276	25.955	31.013	**27.430**	11%

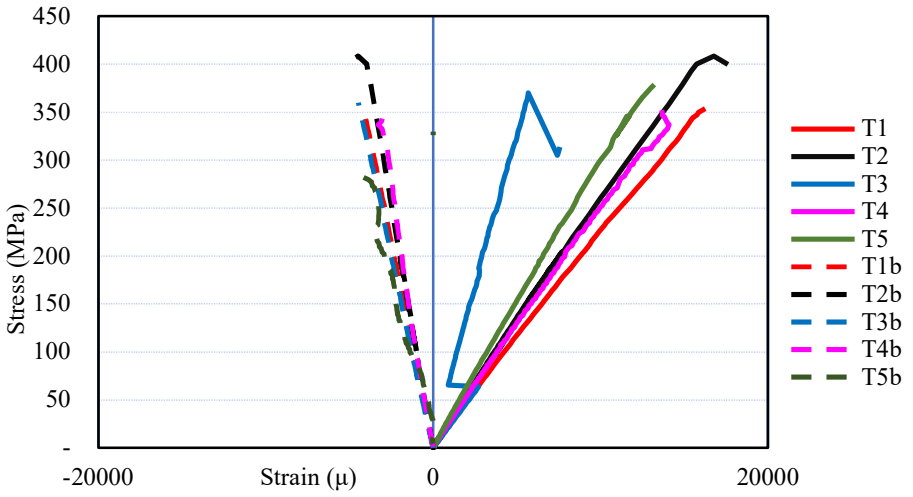

Figure 6.3 Stress-strain relations of material tensile test in the fiber direction

The dimensions of the specimens in the transversal direction tests were also modified. This is because the maximum widths of the SP100 profiles were only 100 mm; therefore, they could not be cut to the same dimensions as the standard specimens. The PGFRP members were connected with the main parts of the specimens by aluminum plates and E250 epoxy to elongate the lengths of the specimens. In the case of compressive tests for the transversal PGFRP specimens, the steel plates were inserted on both sides of the specimens to fix the machine conditions. Strain values were measured from strain gauges attached to both surfaces of the specimens, as in Figure 6.2 and Figure 6.5.

Table 6.3 Tensile test result in the transverse fiber direction

Parameters	**Unit**	**T1**	**T2**	**T3**	**T4**	**T5**	**Avg**	**C.o.V**
P max	kN	5.58	6.58	5.27	5.73	5.18	5.67	9%
Thickness	mm	5.31	5.38	5.31	5.33	5.38		
Width d	mm	25.74	25.82	25.04	25.54	26.09		
Area section	mm^2	136.68	138.91	132.96	136.13	140.36		
E2- elastic modulus	GPa	8.85	9.15	7.18	9.41	8.36	**8.59**	

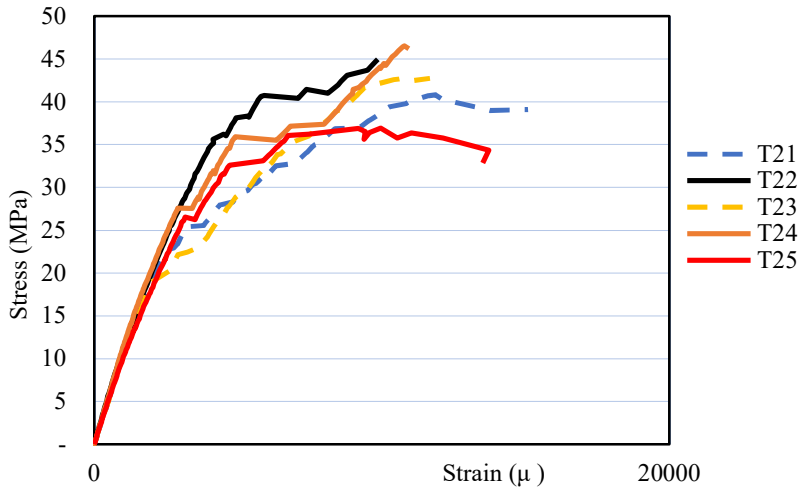

Figure 6.4 Stress-strain relations of material tensile test in the transverse fiber direction

b) Compressive test

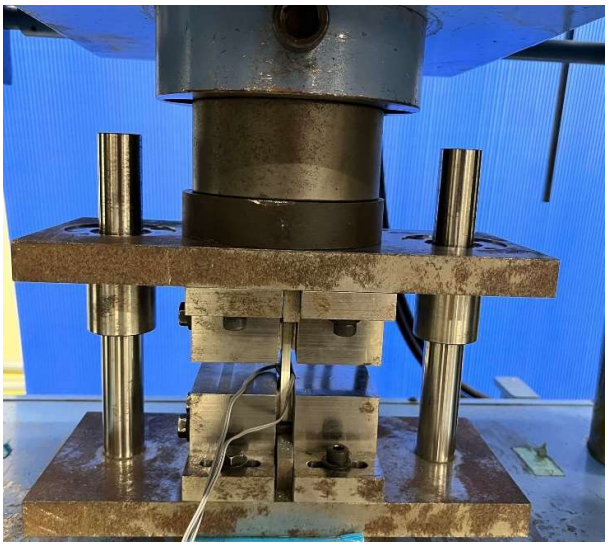

Figure 6.5 Test setup of compress test

The typical modes of failure of all specimens, the stress–crosshead displacement relations, and the properties of the PGFRP members were illustrated in Figures 6.2 and 6.5. To determine the elastic modulus (E1, E2) of all basic materials, two-directional and one-directional strain gauges were attached to both surfaces of the tensile specimens and compressive specimens, respectively. The corresponding data were presented in Tables 6.2 to 6.5.

Table 6.4 Compress test result in the fiber direction

Parameters	Unit	C11	C12	C13	C15	Avg	C.o.V
P max	kN	64.73	66.34	64.89	61.23	64.30	2.9%
Thickness	mm	5.55	5.56	5.40	5.50		
Width d	mm	25.40	25.60	25.60	25.60		
Area section	mm^2	140.97	142.34	138.24	140.80		
E1- elastic modulus	GPa	23.57	26.79	25.37	25.04	25.20	4.5%

Table 6.5 Compress test result in transverse fiber direction

Parameters	Unit	C21	C22	C23	C24	C25	Avg	C.o.V
P max	kN	14.47	16.60	13.61	14.98	13.79	14.69	7.3%
Thickness	mm	5.50	5.50	5.50	5.50	5.50		
Width d	mm	25.40	25.60	25.60	25.70	25.60		
Area section	mm^2	139.70	140.80	140.80	141.35	140.80		
E2- elastic modulus	GPa	9,78	10,36	10,47	10,445	10,44	10,30	2.5%

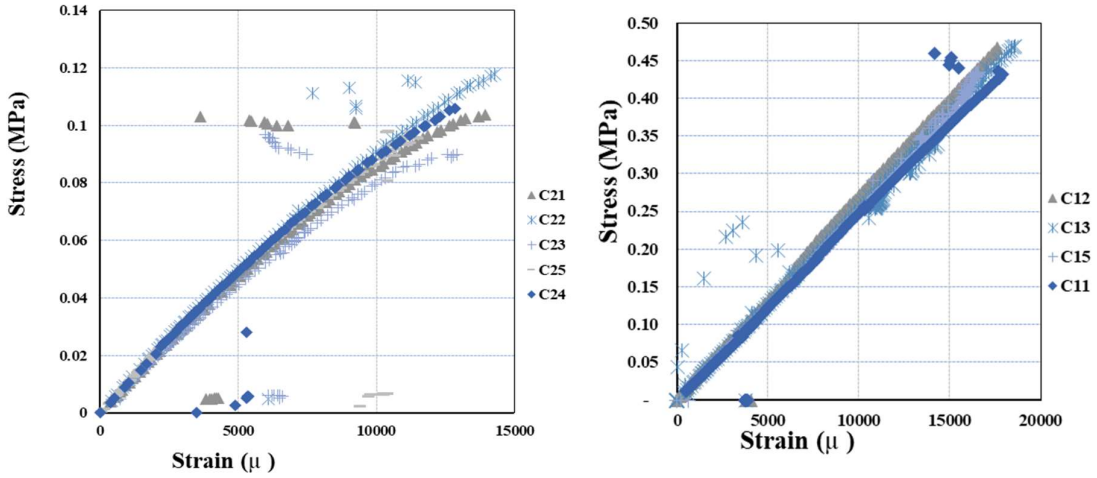

Figure 6.6 Stress-strain relations of material tensile test in fiber and transverse fiber direction

To calculate the actual cross-sectional areas of all specimens, the widths and thicknesses of each specimen were measured. The stress values of each specimen were obtained by dividing the load by cross-sectional areas. The elastic modulus of all basic materials was determined from two different strain points, namely, the lower strain point of around 500 (μ-strain) and the upper point of around 2500 (μ-strain). The elastic modulus values were approximately the same for the tensile and compressive specimens.

It is worth noting that the elastic modulus, strength, and Poisson ratio values reported in the study are average values based on every five specimens per one parameter.

c) Shear strength test

The in-plane shear strengths of the PGFRP members were calculated by the V-notched rail shear method (ASTM-D7078) as described in Chapter 3.

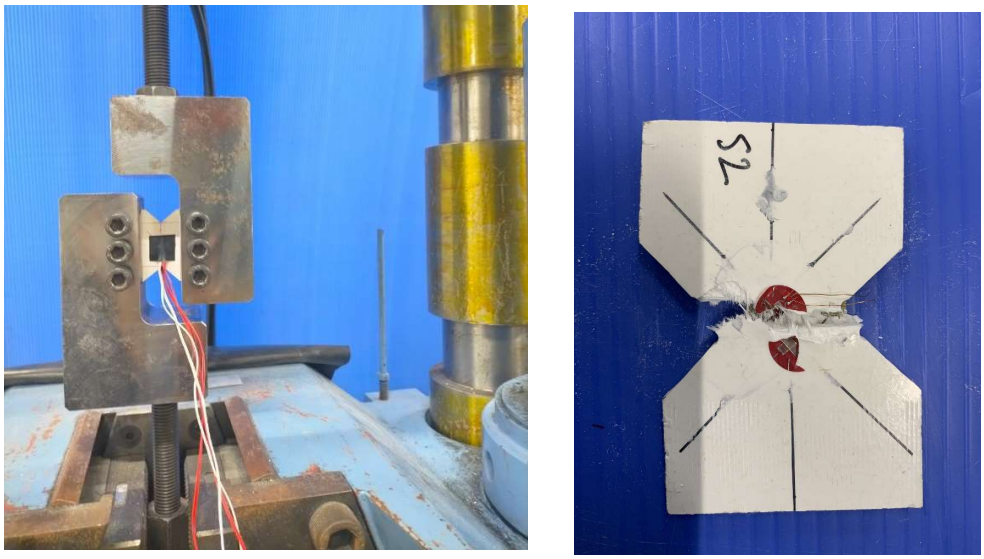

Figure 6.7 Shear strength testing setup and failure specimens

The shear strength and modulus calculations are the same process presented in Chapter 3. Figure 6.8 and Table 6.6 show the experimental results of the shear test.

Table 6.6 Shear strength test result in the fiber direction

Parameters	**Unit**	**S1**	**S2**	**S3**	**S4**	**S5**	**Avg**	C.o.V
P max	kN	9.92	9.17	9.34	9.94	9.14	14.69	7.3%
Thickness	mm	34.77	30.84	31.88	32.82	32.23		
Width d	mm	5.69	5.69	5.69	5.69	5.69		
Area section	mm^2	197.84	175.48	181.40	86.75	83.39		
G-shear modulus	MPa	50.16	52.23	51.50	53.23	49.85	10,30	2.5%

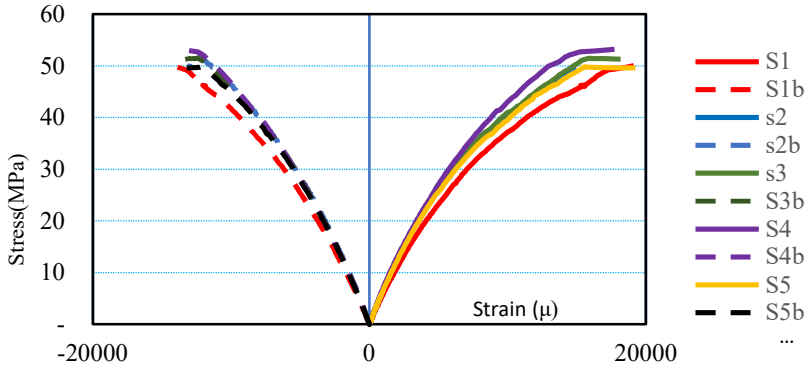

Figure 6.8 Stress-strain relations of material shear strength test

d) Shear-out and bearing strength test

To evaluate the strength of the GFRP-to-steel bolted connections, 10 specimens divided into two series were tested in a double lap configuration, as illustrated in Figure 6.9 The specimens, comprising GFRP plates trimmed from the tubular profiles used in the full-scale connection tests, had 450 mm of length, 90 mm of width and nominal thickness of 5 mm. Each GFRP plate was bolted to two steel plates, using full-threaded M8 bolts, with enough clearance between the plates to avoid friction. The bolts were centered in the transverse direction of the plates and placed at a distance from the GFRP plate's bottom edge (e) of 24 mm for the shear-out test series, and 56 mm for the bearing series. Five specimens of each series were tested in a universal testing machine using displacement control at a crosshead rate of 1 mm/min. The axial relative displacement of two points spaced by 350 mm, was measured by two displacement transducers, from TML with a stroke of 25 mm and precision of 0.01 mm. The testing method and calculation were the same as the tests described in Chapter 3.

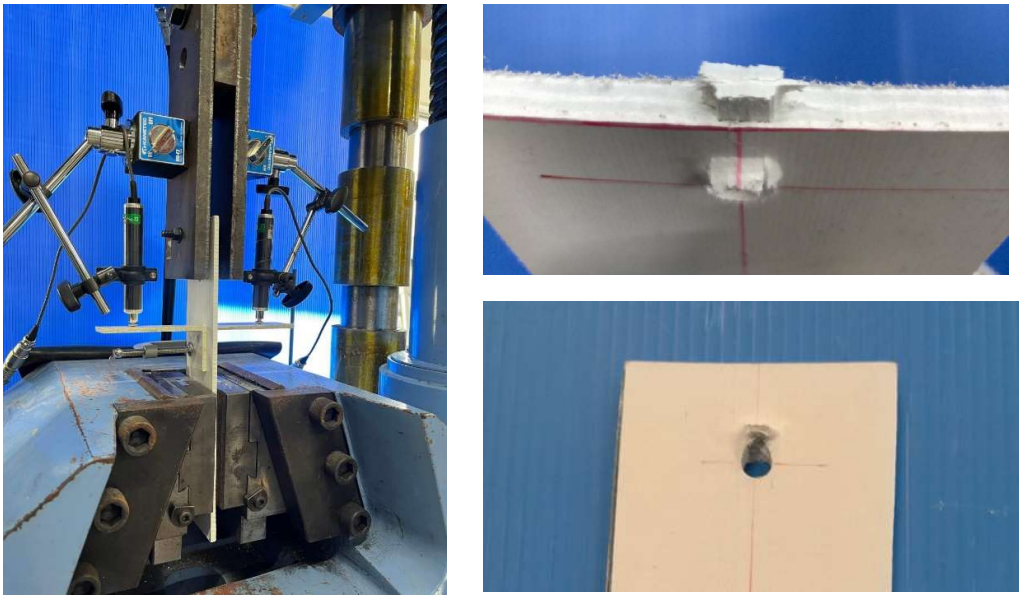

Figure 6.9 Test setup and failure specimen of tensile/ bearing test

Figure 6.9 shows the shear-out failure modes and the bearing failure modes. Tables 6.7 and 6.8 show the shear-out and bearing strengths, respectively.

Table 6.7 Shear-out strength test result in the fiber direction

Parameters	Unit	S1	S2	S3	S4	S5	Average	C.o.V
Pmax	kN	6.16	5.69	5.41	5.71	5.83	5.76	4%
Thickness	mm	5.50	5.50	5.50	5.50	5.50		
e	mm	16.00	16.00	16.00	16.00	16.00		
Shear strength τ	MPa	34.99	32.32	30.72	32.46	33.13	32.72	

Table 6.8 Bearing strength test result in the fiber direction

Parameters	Unit	B1	B2	B3	B4	B5	Average	C.o.V
Pmax	kN	8.30	9.91	11.71	9.15	8.78	9.57	12%
Thickness	mm	5.50	5.50	5.50	5.50	5.50		
d	mm	8.00	8.00	8.00	8.00	8.00		
Bear strength *F*	MPa	188.52	225.13	266.03	207.85	199.51	**217.41**	

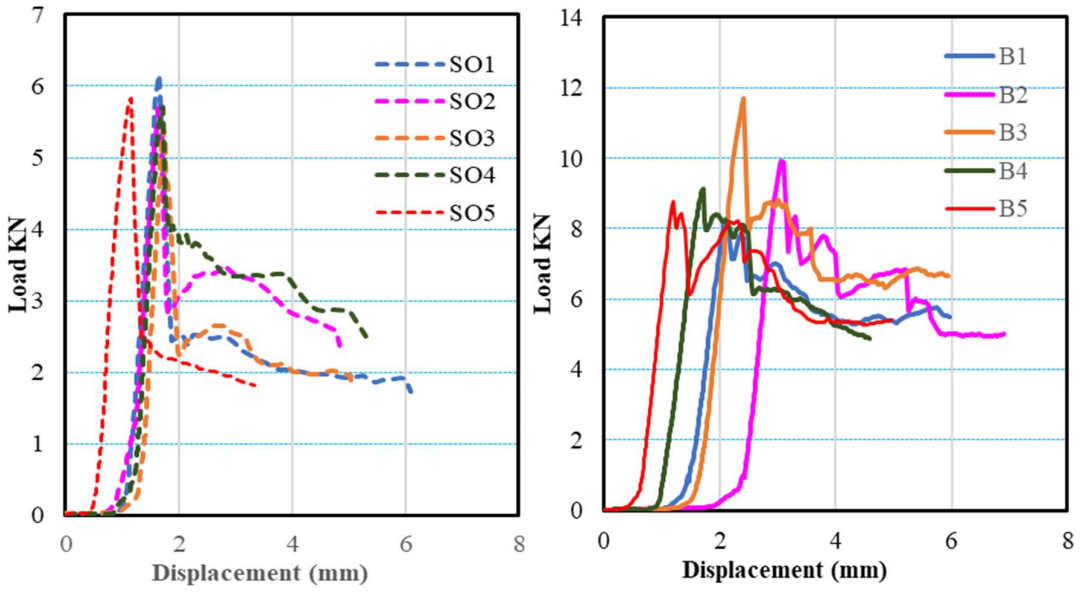

(a) Shear-out test (b) Bearing test

Figure 6.10 Load- relative displacement of material in shear-out strength and bearing test

6.2.3. Beam-to-column connection pre-test

a) Designation for experiment series

In practical industrial, PGFRP buildings, or structures may be assembled by combining individual modules, which share the adjacent beams and columns. In this study, with a square hollow section (100mm ×5.5 mm), the novel beam-to-column connection system comprises metal parts inserted/embedded in the cavity of the profiles. The beam part has a metallic tubular with 5 sides and is made by machining a stainless-steel solid cube. Then 2 sides have pre-drilled holes regarding the series designated as shown in Figure 6.11.

The column part is a steel plate which also has pre-drilled holes. The novel connection system proposed herein was tested in different configurations, namely:

- Four bolts per flange: series 1.
- Two bolts per flange: series 2A, with end distance (e) e=3d (d is present to bolt hole diameter);
- Two bolts per flange and a higher edge distance (e=7d) than that used in series 2B.

All series were idealized as semi-rigid connections: series 1 and series 2A aimed at evaluating the influence of the number of bolts used in each flange, while series 2B intended to assess the influence of the edge distance in the overall behavior of the connection, namely in its failure mode and moment distribution capacity. Two specimens were tested per series: non-strengthened by GFS and strengthened specimens.

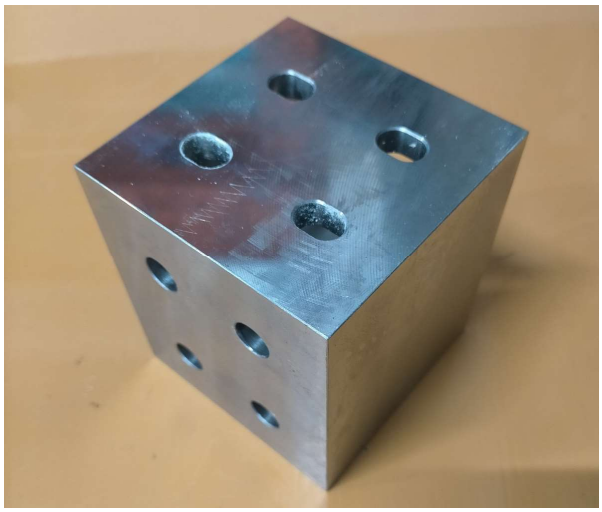

Figure 6.11 Steel box in the beam connection part

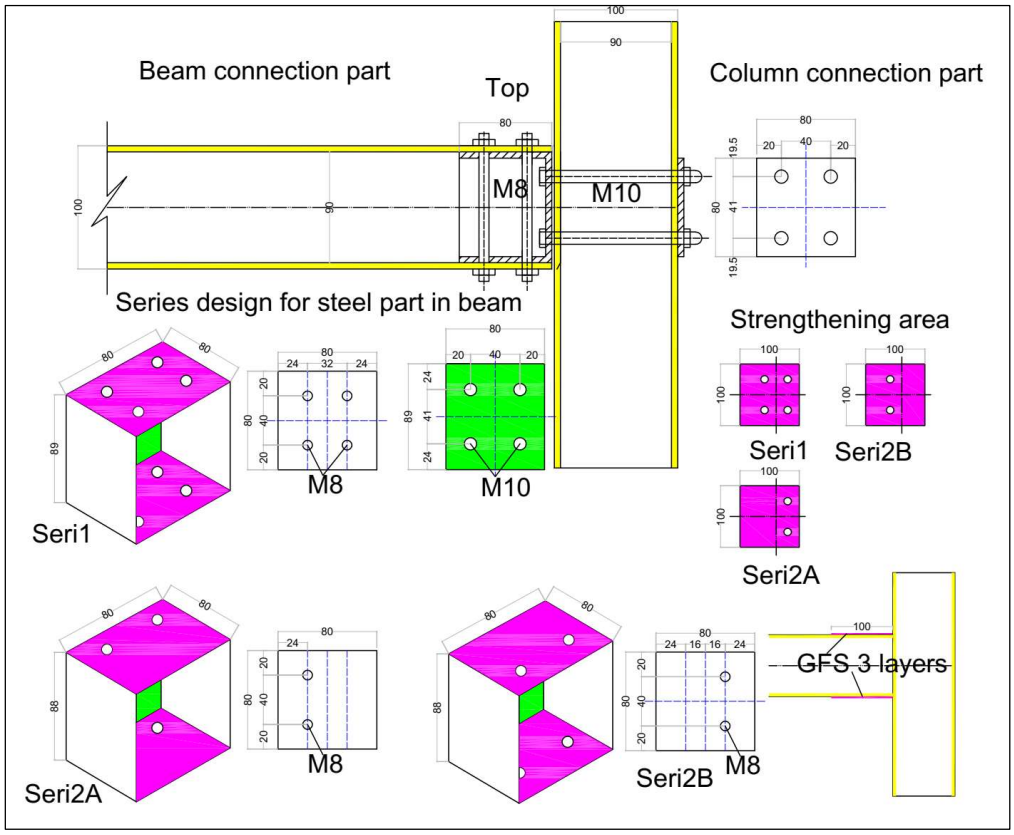

Figure 6.12 Series design and connection parameter for specimens

Steel bolts (grade class 10.9) were used in connection specimen parts which were M8 in the beam part and M10 in the connection beam to column. Bolts were fastened by a 10 Nm tightening force.

b) Test setup and procedure

The full-scale connection test specimens aim to replicate an external frame connection where only one beam is joined to the column. These specimens comprised a 950 mm long column and a 1000 mm long beam, with the joint placed at mid-height of the column.

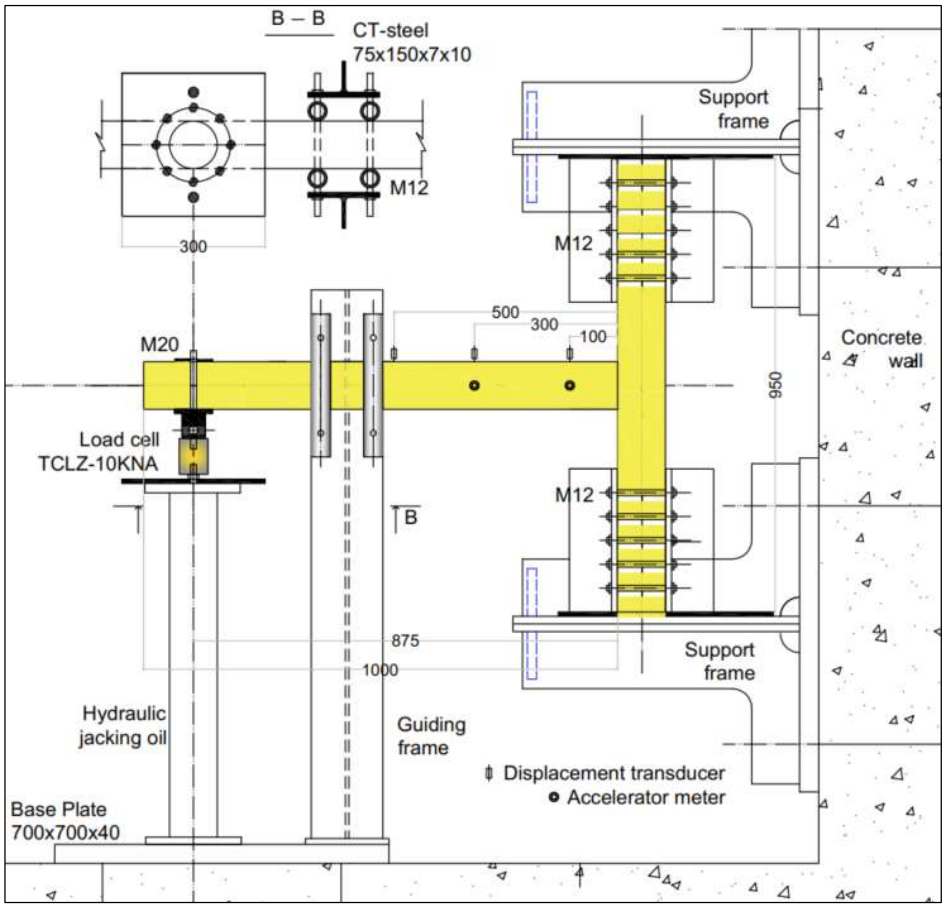

Figure 6.13 Illustrative scheme for set-up testing

Figure 6.13 depicts the beam-to-column test setup. The tests were performed in a closed steel loading frame anchored to the laboratory strong floor and concrete wall. The load was applied by a hydraulic oil jack with a capacity of 100 kN in compression and 50 kN in tension, and maximum stroke of ±250 mm. The load was measured with a *TML* load cell with capacity of 10 kN. To guarantee the verticality of the applied load, and avoid local crushing, two steel spreading plates (80×300×9 mm) were installed between the load cell and the specimens.

The load was applied under displacement control at a designated applied cyclic load which is described in detail in the next part. The vertical load was applied to the beam at 875 mm from the front face of the column profile. To ensure that the load was always applied in the same section, a steel rod was inserted through 20 mm diameter holes drilled on both beam flanges, fixing the profile to the load application system.

Two column ends of the specimens were fixed to a steel frame system, which connects

to a concrete wall. To fully fix these sections, both in terms of rotation and out-of-plane displacements, the column was arranged with steel plates-fastener bolted combined along 300 mm in both ends. Displacements were measured at the load application point by three displacement transducers, from beam-to-column connection point 100, 300 and 500 with stroke of 50, 100, and 200 mm respectively. Two accelerometers were used to measure the absolute rotation of the beam (transducer placed on the top flange of the beam, at distances of 100 and 300 mm from the column face).

c) Result and discussion

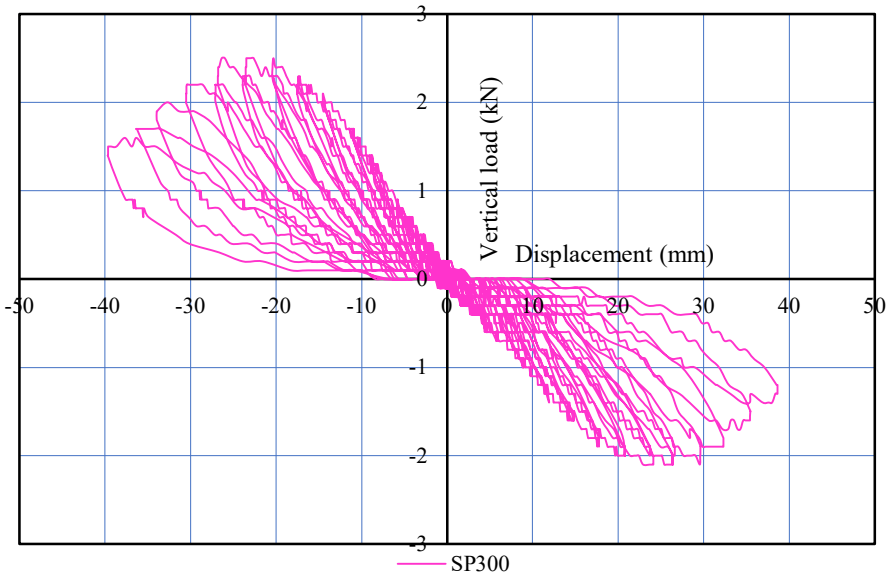

Figure 6.14 Force and relative displacement curve of non-strengthened (column) specimens on cyclic test

In the first conducted experiment, there was only one specimen of series 2A (with 2 bolts and e=2d) in non-strengthened GFS. Figure 6.14 presents representative loading vs. relative rotation curves in the test. The cyclic test curves showed considerable symmetry. However, the failure occurred on two sides of the columns in the connection part due to the steel part in the beam and back steel plate made crushing in the column surface as shown in Figure 6.15 (a). Considering the stiffness of beam systems, it is much higher than PGFRP material in the column, leading to damage first coming separately in the column. Then, the aim focuses on investigating failure modes in the beam that could not be obtained.

The reinforcement column was made using a 5mm thickness of GFS (200×100×5) to improve connection capacity. After pasted GFS in both sides of the column connection part, pre-bolted holes were drilled, and an expanded steel plate (100×100×6) was connected as the column part. Figure 6.15 (b) presents the experiment with strengthened (column) specimens and failure after testing.

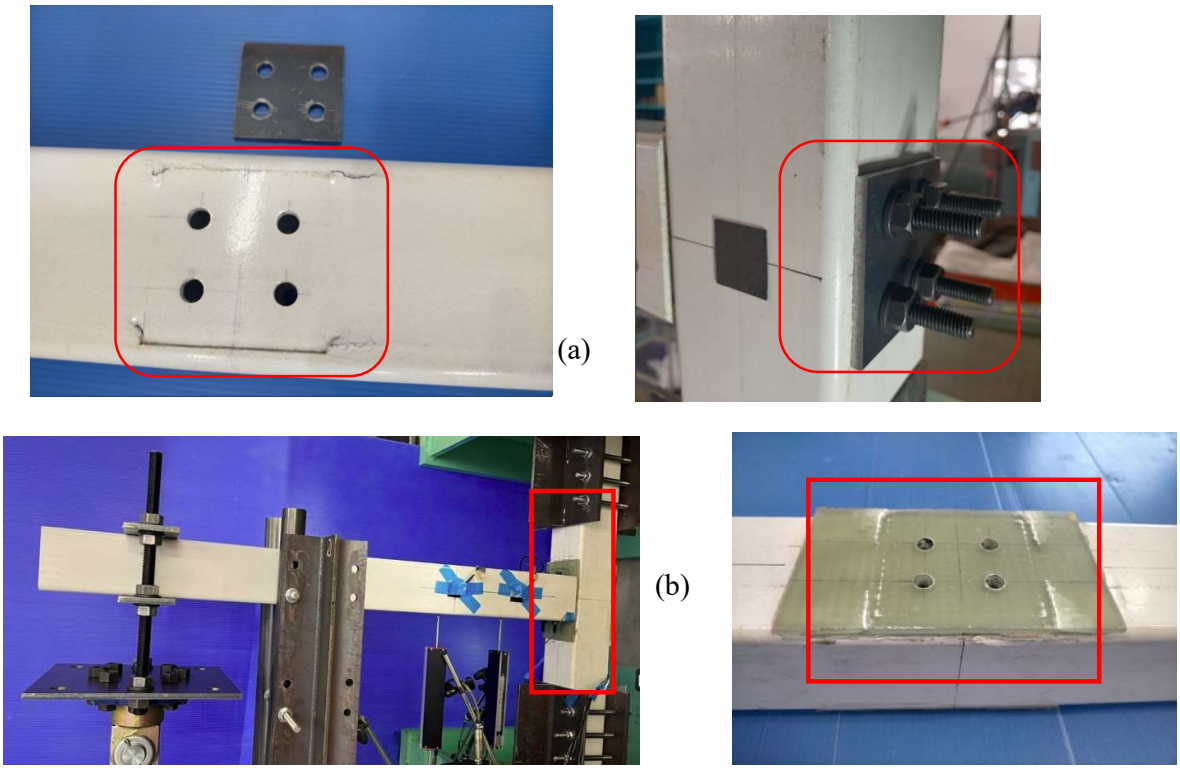

Figure 6.15 Frontal view of testing and failure specimens

The maximum bending moment of reinforced specimens (2.18 kN.m) was higher than the first testing without pasted GFS in column part (1.05 kN.m). In Figure 6.16, strengthened specimens presented higher overall stiffness, bending moment at the end of each cycle and wider hysteretic loops. In general, the behaviors of both cases can be divided into two stages: (i) until the maximum moment was achieved, the hysteretic curves presented a wider shape with less pinching; and (ii) after reaching to maximum moment, the pinching increased (iii) the stiffness gradually decreased when the absolute value of bending moment increasing. SP500, SP300 and SP100 in Figure 6.16 presented for displacement transducer allocated at the corresponding distance: 500, 300, 100 from the connection point.

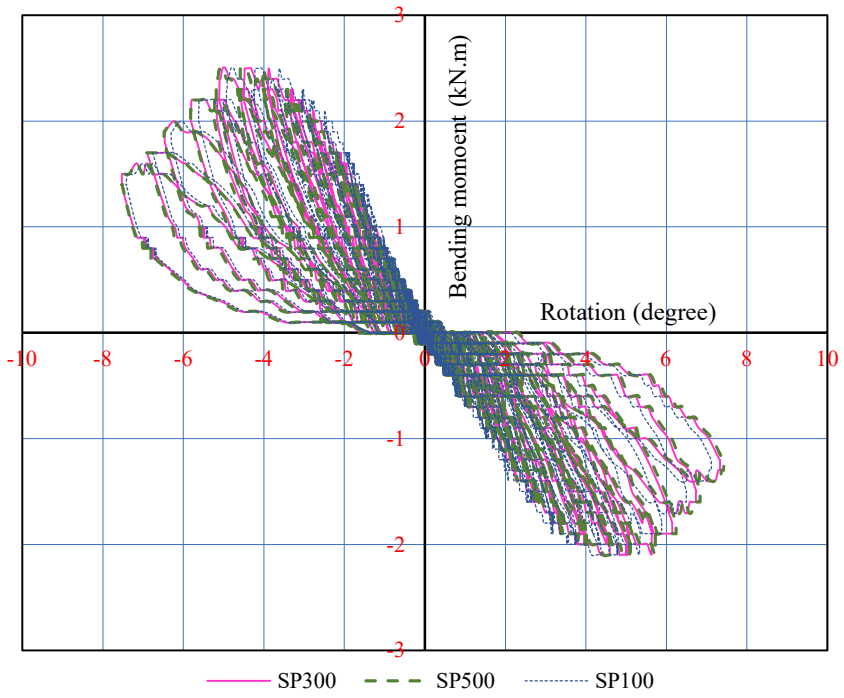

Figure 6.16 Bending moment and relative rotation curve of specimens after strengthened on cyclic test

Despite a significant increase in maximum loading and stiffness, the failure modes observed in the cyclic tests conducted on a series of reinforced connections were found to be similar to those observed in the non-strengthened tests. The strengthened specimens exhibited damage modes that occurred again in the column, as illustrated in Figure 6.15 (b). However, the crushing failure was observed in the GFS plate instead of the PGFRP as mentioned in the first connection test. This can be attributed to the fact that the out-plane shear strength of the GFS reinforcement material was lower than that of the shear force by the auxiliary steel part on the beam applied. Consequently, although the stiffness in the column improved, it did not result in a change in the failure type.

To achieve the original purpose of the experiment, which was to investigate the connection strength and failure behavior of a series of specimens, it is imperative to enhance the existing connection types with a box-shaped inner beam by another system, so that the stiffness or shear force applied to the column can be reduced. Otherwise, the desired outcome cannot be obtained.

6.2.4. Cyclic behavior of beam-to-column connection test

The loading procedure suggested by ANSI/AISC 341-16 [67] for steel structures was adopted in this study because no specific loading procedures had been defined for FRP structures. As shown in Figure 6.17, the applied cyclic displacement was determined as the multiplication of the drift angle suggested by ANSI/AISC 341-16 [67] and the length of the applied load point in the PGFRP beam (875mm). There was a total of 14 cyclic loading groups (C1 to C14) and the calculated maximum applied cyclic displacement was 100 mm in both directions. Such a traveling distance was within the ultimate stretch of the loading cell used.

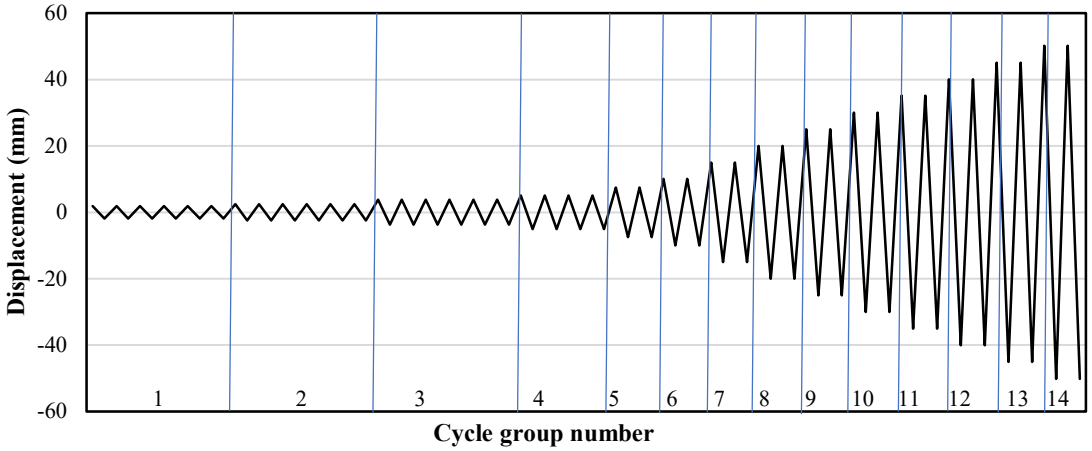

Figure 6.17 Cyclic loading procedure for load apply

Table 6.7 Detail cycle measurement

Group	Rotation	Displacement	Cycle number
	Rad	*mm*	*cycle*
1	0.00375	3.28	6
2	0.005	4.38	6
3	0.0075	6.56	6
4	0.01	8.75	4
5	0.015	13.13	2
6	0.02	17.5	2
7	0.03	26.26	2
8	0.04	35.02	2
9	0.05	43.79	2
10	0.06	52.56	2
11	0.07	61.35	2
12	0.08	70.15	2
13	0.09	78.96	2
14	0.1	87.79	2

6.2.5. Revision designation for connection test

Alternative connections were designed as detailed as shown in Figure 6.18. A couple of steel cleats (100×70×10) are the main connection parts that connect the beam at the top and bottom flanges by two bolts and to the front side of the column by four bolts. Those 4 bolts through the inner of the column and connect to the opposite side by a steel plate as an “anchor” (100×100×10).

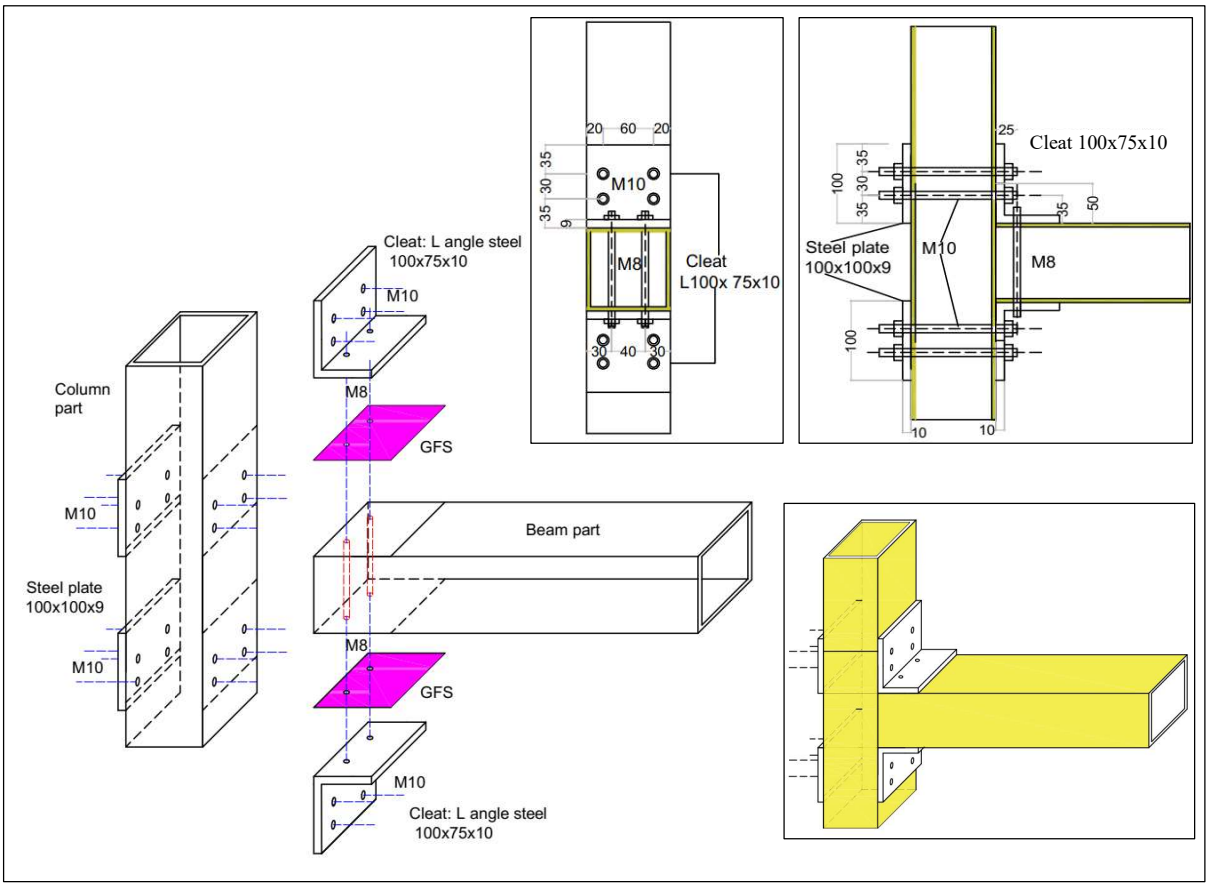

Figure 6.18 Revision specimens making progress

The tentative plan is to conduct cyclic tests on only the series 2 specimens, both with and without GFS strengthening. These tests will be designed in a manner similar to that described earlier.

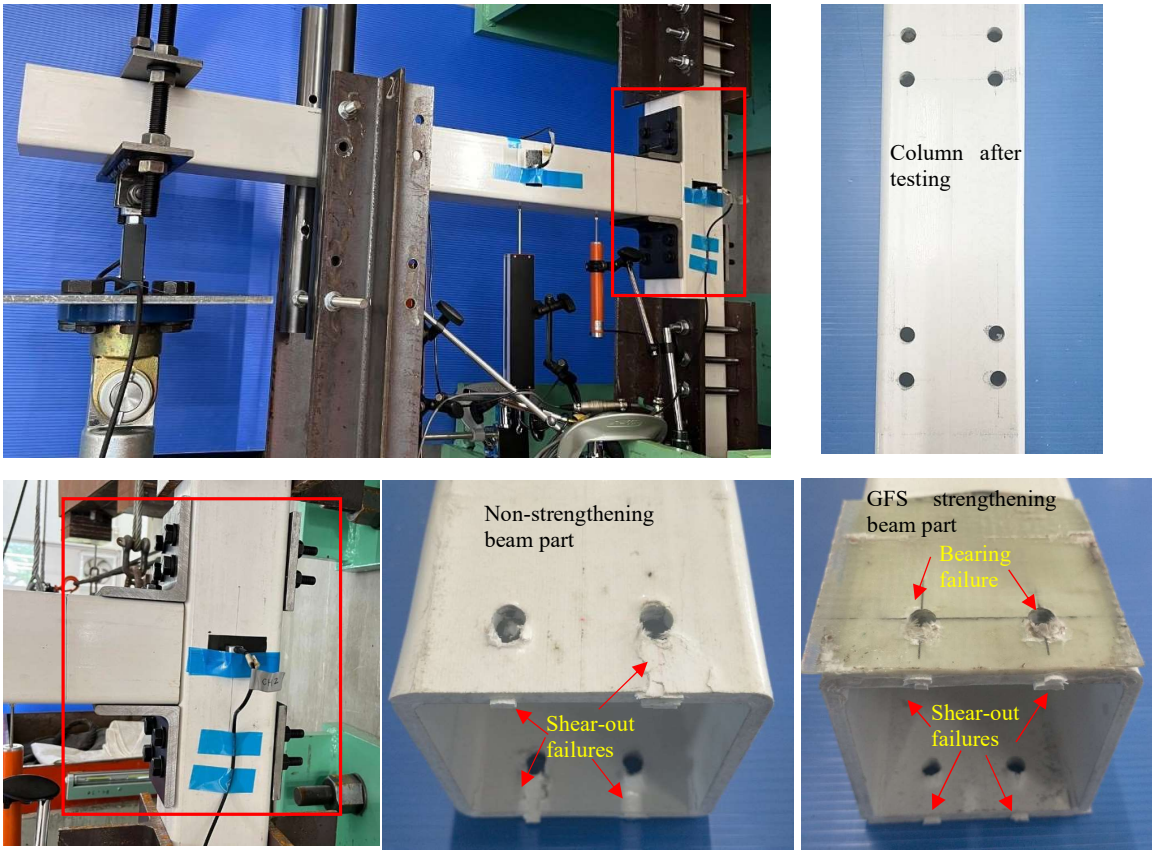

Figure 6.19 Test setup and failure part of specimens

6.2.6. Testing results in revision designate

After modifying the connection systems to utilize cleat-type connections with L-angle steel, the specimens showed failure in the beam profile with shear-out in CD layers or all sections while the maximum bending moment value kept similar (2.1 kN.m). Onsite testing progress and failures were recorded and depicted in Figure 6.19, while Figure 6.20 presented the capacity of the non-strengthening specimens under cyclic testing. Notably, failure was not observed in the column profile, highlighting the effectiveness of the revised designations.

The strengthening of a connection in a GFS specimen resulted in a noteworthy 50% increase (up to 3.01KNm) in the ultimate load, as indicated in Figure 6.20. Remarkably, no deformation was observed in the column during the loading process, like the non-strengthened specimen. SP500, SP300 and SP150 in Figure 6.20 presented for displacement transducer allocated at the corresponding distance: 500, 300, 150 from the connection point.

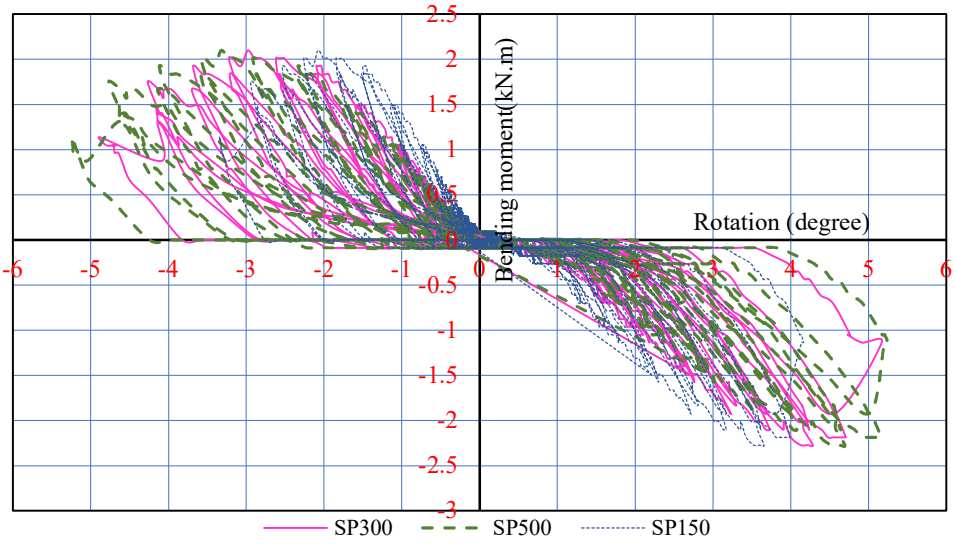

Figure 6.20 Bending moment and relative rotation curve of non-strengthening specimens after revised design on cyclic test

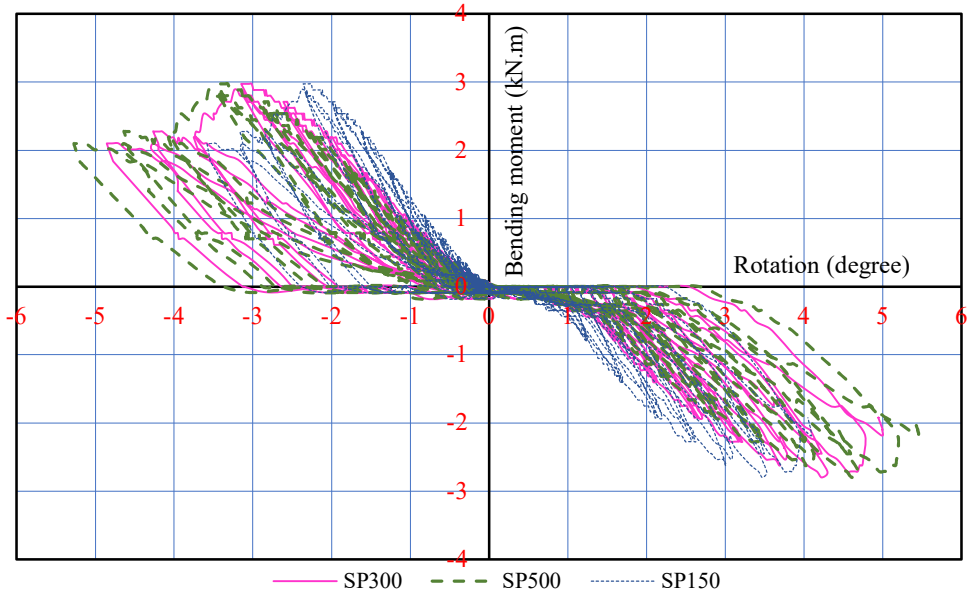

Figure 6.21 Bending moment and relative rotation curve of GFS strengthening specimens after revised design on cyclic test

When comparing the use of box-shaped connection parts with the newly presented cleat connection type, the bending moment-rotation curve was observed to have changed. Specifically, the rotation decreased rapidly as the absolute bending moment decreased, due to the influence of two steel cleats that tended to revert to the original position. Moreover, in both

instances, the gravitational force of the loading frames caused a reduced absolute value of bending moment on the downward beam (left side of the chart) compared to the downward beam's (right side of the chart).

The shear-out failure was observed in whole cross sections of both sides of the flanges of the beam in the non-strengthening specimen. The bearing failure was recorded in GFS layers while shear-out occurred in the PGFRP layer in strengthening specimens.

6.2.7. Discussion

(a) Influence of connection stiffness

Using top and bottom flange cleats, the connections' maximum bending moment could be increased compared to the steel box in the original design.

Table 6.8 Beam deflection for different connection types

Connection part	**Cleat**		**Box shape**	
	NS	GFS	NS	GFS (Column)
Applied load (KN)	0.99925	0.99925	0.99925	0.99925
Deflection (mm)	4.7	4.98	8.94	8.84

Table 6.8 also demonstrates that the stiffness of cleat connection specimens with a box shape is approximately two times higher than others. The applied load was taken around 1 kN and deflection was recorded in the middle transducer on the beam with 300 mm distance from the connection.

(b) Estimates of failure load

According to the failure that occurred in the revision connection design using the cleat, the maximum connection load depended on the shear-out strength (τ_{SO}) and the bearing strength (σ_{brL}). Those above values of the material were estimated using Eq. (6.1) and (6.2), respectively, in accordance with the recent prospect of a European Guidance for the Design of FRP Structures [36] as follows:

$$\tau_{SO}=\frac{F_u}{(2e-d)\,t} \tag{6.1}$$

$$\sigma_{brL}=\frac{F_u}{d\times t} \tag{6.2}$$

Where F_u is the failure load, d is the bolt diameter (8 mm) and t (5.5 mm) is the plate thickness. Eq. (6.1) was applied to the results of Series 1 (failure by shear-out), while Eq. (6.2)

was applied to the results of Series 2 (bearing failure).

Table 6.9 presents the results of the analytical estimation of failure loads and modes, along with a comparison to experimental data. The predicted failure mode (shear-out or bearing) corresponded to the lowest expected failure load. To determine the resistant bending moment for each connection, the governing failure load was multiplied by the lever arm associated with the distance between the top and bottom flanges of the beam. This calculation considered the fact that the rotation axis of the beam was located at the intersection of its bottom edge with the column, at 100mm. To be compared with the experimental results, the estimated ultimate load was calculated by dividing the bending moment by the distance between the load application point and the relevant bolt row (875 mm).

Table 6.9 Analytically estimated failure loads (F_{an}) and relative difference(Δ) to experimental (F_u)

Specimens	F_u **(kN)**	F_{an} **(kN)**	**Δ**
Non-strengthening	2.39	1.64	31%
GFS Strengthening	3.40	2.52	26%

The substantial relative differences, with an average of 26%, suggest that the failure mechanisms are significantly more intricate than what has been accounted for in this simple analytical method. Moreover, the result analytical method was estimated under monotonic moment condition, that ignores the dissipated energy in cyclic moment. It is necessary to investigate how dissipated energy by monotonic testing is to complete examination behavior in beam-to-column connections.

6.3. Conclusion

The present chapter presented a novel connection system for pultruded GFRP tubular profiles using internal steel parts and bolts, developed to be used in modular constructions.

The first experimental results did not align with the expected outcomes due to the unpredictable conditions in the design of the auxiliary steel parts in the beam. Despite the effectiveness of the GFS strengthening in improving the reinforcement of the column, it still suffered damage before the initial failure observed in the beam profile. Therefore, a revision was proposed, which entails changing the cleats connection.

The result of the revised experiment showed a reasonable proposed changing design in the connection part. The ultimate bending moment and failure modes of specimens demonstrated the effectiveness of the strengthening method by using GFS in beam-to-column

PGFRP multi-bolted connection. The failure load changed from shear-out in non-strengthening to bearing failure in GFS strengthening specimens. This failure behavior is safer for connection structures.

For a comprehensive evaluation of the behavior in beam-to-column connections, it is imperative to investigate the dissipated energy under monotonic loading in the future. In addition, a series with 4 bolts and 2 bolts (long end distance) in the beam should be conducted to compare the effectiveness of the GFS strengthening method in various connection parameters.

CHAPTER 7
SUMMARY AND CONCLUSION

7.1. Summary and conclusion

This study explored a novel method utilizing Glass Fiber Sheets (GFSs) to enhance the strength of multi-bolted PGFRP connections. To determine the maximum failure loads and failure modes of these connections, a total of 72 specimens were tested, and various geometric parameters were investigated, such as the number of bolts and the ratios of end-distance to bolt diameter (e/d). GFSs were applied to reinforce the PGFRP connections, which were created using the vacuum-assisted resin transfer molding (VaRTM) method. Three types of GFSs (0°/90°, ±45° glass-woven roving and chopped strand mat (CSM)) were employed to reinforce the PGFRP connections. Additionally, design equations were proposed to estimate the maximum failure loads (ultimate loads) of multi-bolted PGFRP connections that were reinforced by GFSs, considering various connection failure modes. In the study's second phase, experiments were conducted to investigate the effectiveness of GFS-strengthened PGFRP beam-to-column connections. Furthermore, factors that could influence the behavior of the connection, such as the bond strength in the GFM and CD layers in the PGFRP sheet, and the applied bolt-tightening force in multi-bolted connections, were evaluated.

Based on experiments, and analytical analysis, the following conclusions can be highlighted:

- The findings of this study indicate that applying glass fiber sheets to the connection area of the bolted connection in PGFRP significantly enhances its mechanical properties, as verified by the experimental results. The ultimate loads of GFS-strengthened connections increased from 1.61 to 2.77 times compared with non-strengthened specimens.
- Bond strength, which is a property in PGFRP manufacturing progress, was also a factor that affected the capacity of connection in the strengthened specimens. Bond strength can be measured by material testing. After that, the result was taken into estimating the connection strength. Depending on the failure mode of specimens, the effective area of bonding strength was separately measured.
- Diffident failure modes were found in different types of specimens. Five basic failure modes were found in the experimental analysis. The failure mode depends on the GFS

material and the geometries of the specimens.

- Failure modes and the ultimate load of the connection can be predicted. The proposed equations to calculate the connection strength for the strengthened PGFRP specimens showed good matching with the testing results. It is necessary to conduct a particular experiment to determine the C value more accurately for all types of GFS specimens.
- To prevent instantaneous failure, the end distance in the GFS sheet can be extended in the loaded end to prevent the debonding load. Meanwhile, net-tension failure can be prevented by increasing the width or thickness of the GFS sheet. Further investigation of this issue is required in future studies.
- The strengthening method by GFS remains effective under various conditions of bolted PGFRP connection, such as under tightening force applied to bolts. Even though the maximum load increased in all types of specimens compared to the case without applied tightening, the effectiveness before (NS) and after strengthening with GFSs (P_{st}/P_{NS}) slightly decreased. The failure modes can be explained by measuring the strength of the individual elements and then calculating to find the lowest combined strength. However, due to the complexity of the tightening force's effect, equations for the prediction ultimate load of connection could not be proposed.
- A new connection system for modular constructions, using internal steel parts and bolts in pultruded GFRP tubular profiles, was developed. However, the initial experimental results did not match the anticipated outcomes due to conditions in the design of the auxiliary steel parts in the beam. Therefore, a revision was proposed, which involved changing by the cleat's connection. The revised experiment yielded reasonable results, demonstrating the effectiveness of the strengthening method using GFS in beam-to-column PGFRP multi-bolted connections. The ultimate bending moment and failure modes of the specimens showed that the use of GFSs changed the failure load from shear-out in non-strengthened specimens to bearing failure in GFS-strengthened specimens. This failure behavior is safer for connection structures.

7.2. Recommendation for future research

The following are recommended research topics for future investigation to understand better FRP materials' applications for rehabilitating civil engineering structures.

1. To comprehensively assessment effective of the strengthening method, the finite

element method is recommended to be performed to compare with the result of the testing and the proposed predict strength formula. Consequently, it is important to carry out additional testing to determine the properties of materials sufficiently.

2. The strengthening effects of GFSs on the performance of PGFRP multi-bolted in beam-to-beam connection under monotonic and on additional parameters should be carried out in the next research to find out. It is imperative to investigate the dissipated energy under monotonic loading in the future. In addition, a series with 4 bolts and 2 bolts (long end distance) in the beam should be conducted to compare GFS strengthening method's effectiveness in various connection parameters.
3. Investigation into other connection types such as beam-to-beam connection, and column-to-beam connection should be implemented to comprehensively evaluate the effectiveness of the GFS strengthening method and develop the design guidelines and codes of practice.

REFERENCES

[1] Gand, A. K., Chan, T. M., & Mottram, J.T. Civil and structural engineering applications, recent trends, research and developments on pultruded fiber reinforced polymer closed sections: a review. Frontiers of Structural and Civil Engineering, 7, 227-244. (2013) https://link.springer.com/article/10.1007/s11709-013-0216-8

[2] Balsamo, A.; Coppola, L.; Zaffaroni, P. FRP in Construction: Applications, Advantages, Barriers and Perspectives. Compos. Constr 58–64. (2001) https://ascelibrary.org/doi/abs/10.1061/40596%28264%297

[3] Davalos, J. F., Salim, H. A., Qiao, P., Lopez-Anido, R., & Barbero, E. J. Analysis and design of pultruded FRP shapes under bending. *Composites Part B: Engineering*, *27*(3-4), 295-305. (1996)

Analysis and design of pultruded FRP shapes under bending - ScienceDirect

[4] Bank, LAWRENCE C. "Properties of Pultruded Fiber." *Transp. Res. Rec* 1223 H7 (1989) https://trid.trb.org/view/308507

[5] Saleem, Muhammad Azhar, et al. "Recent developments in the prefabricated bridge deck systems." Case Studies in Construction Materials 15: e00750 (2021) https://www.sciencedirect.com/science/article/pii/S2214509521002655

[6] Green, A.; Bisarnsin, T.; Love, E.A. Pultruded Reinforced Plastics for Civil Engineering Structural Applications. J. Reinf. Plast. Compos. 13, 942–951 (1994) https://journals.sagepub.com/doi/abs/10.1177/073168449401301008

[7] Kim, Y.J. State of the practice of FRP composites in highway bridges. Eng. Struct., 179, 1–8 (2019) https://www.sciencedirect.com/science/article/abs/pii/S0141029618311520?via%3Dihub

[8] Siddika, A.; Al Mamun, M.A.; Ferdous, W.; Rayed, A. Performances, challenges and opportunities in strengthening reinforced concrete structures by using FRPs–A state-of-the-art review. Eng. Fail. Anal., 111, 104480 (2020) https://www.sciencedirect.com/science/article/abs/pii/S1350630719311884

[9] El Damatty, A. A., M. Abushagur, and M. A. Youssef. "Rehabilitation of composite steel bridges using GFRP plates." Applied Composite Materials 12.5: 309-325 (2005)

https://link.springer.com/article/10.1007/s10443-005-2730-x

[10] Shin, Y.H.; Yoong, Y.Y.; Hejazi, F.; Saifulnaz, M.R.R. Review on pultruded FRP structural design for building construction. IOP Conf. Ser. Earth Environ. Sci., 357, 012006 (2019) https://iopscience.iop.org/article/10.1088/1755-1315/357/1/012006

[11] Correia, João R., et al. "Mechanical behaviour of pultruded glass fibre reinforced polymer composites at elevated temperature: Experiments and model assessment." Composite Structures 98: 303-313. (2013) https://www.sciencedirect.com/science/article/pii/S0263822312005521

[12] Mazzuca, Pietro, et al. "Influence of elevated temperatures on the mechanical properties of glass fibre reinforced polymer laminates produced by vacuum infusion." Construction and Building Materials 345: 128340 (2022) https://doi.org/10.1016/j.conbuildmat.2022.128340

[13] Bank, L.C.; Mosallam, A.S.; McCoy, G.T. Design and Performance of Connections for Pultruded Frame Structures. J. Reinf. Plast. Compos., 13, 199–212 (1994) https://journals.sagepub.com/doi/10.1177/073168449401300302

[14] Hassan, Nahla K., Mohamed A. Mohamedien, and Sami H. Rizkalla. "Multibolted joints for GFRP structural members." Journal of Composites for Construction 1.1: pp.3-9, (1997) https://ascelibrary.org/doi/abs/10.1061/(ASCE)1090-0268(1997)1:1(3)

[15] Turvey, G.J. Bolted connections in PFRP structures. Prog. Struct. Eng. Mater., 2, 146–156. (2000)https://onlinelibrary.wiley.com/doi/abs/10.1002/1528-2716(200004/06)2:2%3C146::AID-PSE18%3E3.0.CO;2-0

[16] Li, Y. F., Jobe, O., Yu, C. C., & Chiu, Y. T. Experiment and analysis of bolted GFRP beam–beam connections. Composite Structures, 127, 480-493. (2015) https://www.sciencedirect.com/science/article/pii/S0263822315001713

[17] Hai, N. D., Mutsuyoshi, H., Shiroki, K., & Ishihama, T. Development of an effective joining method for a pultruded hybrid CFRP/GFRP laminate. In Advances in FRP Composites in Civil Engineering: Proceedings of the 5th International Conference on FRP Composites in Civil Engineering (CICE 2010), Sep 27–29, 2010, Beijing, China (pp. 103-106). Springer Berlin Heidelberg. (2011) https://link.springer.com/chapter/10.1007/978-3-642-17487-2_20

[18] Coelho, Ana M. Girão, and J. Toby Mottram. "A review of the behaviour and analysis of bolted connections and joints in pultruded fibre reinforced polymers." *Materials & Design* 74 pp.86-107 (2015) https://www.sciencedirect.com/science/article/abs/pii/S0261306915000576

[19] Li, B., Gong, Y., Xiao, H., Gao, Y., & Liang, E. A two-dimensional model for pin-load distribution and failure analysis of composite bolted joints. Materials, 14(13), 3646. (2021) https://www.mdpi.com/1996-1944/14/13/3646

[20] Balc, R., Chira, A., & Chira, N. Finite element analysis of beam to column end plate bolted connection. Acta Technica Napocensis: Civil Engineering & Architecture, 55(1), 24-29. (2012) Google Scholar

[21] Feo, L., Marra, G., & Mosallam, A. S. Stress analysis of multi-bolted joints for FRP pultruded composite structures. Composite Structures, 94(12), 3769-3780. (2012) https://www.sciencedirect.com/science/article/pii/S0263822312003030

[22] Russo, S. On failure modes and design of multi-bolted FRP plate in structural joints. *Composite Structures*, *218*, 27-38. (2019)

https://www.sciencedirect.com/science/article/abs/pii/S0263822318347305?via%3Dihub

[23] Horn, W. J., & Schmitt, R. R. Influence of clamp-up force on the strength of bolted composite joints. *AIAA journal*, *32*(3), 665-667. (1994)

https://arc.aiaa.org/doi/10.2514/3.60001

[24] Yan, Y., Wen, W. D., Chang, F. K., & Shyprykevich, P. (1999). Experimental study on clamping effects on the tensile strength of composite plates with a bolt-filled hole. *Composites Part A: Applied science and manufacturing*, *30*(10), 1215-1229.

https://www.sciencedirect.com/science/article/pii/S1359835X99000020

[25] Chakherlou, T. N., Abazadeh, B., & Vogwell, J. The effect of bolt clamping force on the fracture strength and the stress intensity factor of a plate containing a fastener hole with edge cracks. *Engineering Failure Analysis*, *16*(1), 242-253. (2009)

https://www.sciencedirect.com/science/article/pii/S1350630708000800

[26] Crews, J. H. *Bolt-bearing fatigue of a graphite/epoxy laminate* (pp. 131-144). West

Conshohocken, PA: ASTM International. (1981)

https://scholar.google.co.jp/scholar?hl=en&as_sdt=0%2C5&q=BOLT-BEARING+FATIGUE+OF+A+GRAPHITE%2FEPOXY+LAMINATE.&btnG=

[27] Khashaba, U. A., Sallam, H. E. M., Al-Shorbagy, A. E., & Seif, M. A. Effect of washer size and tightening torque on the performance of bolted joints in composite structures. *Composite Structures*, *73*(3), 310-317. (2006)

https://www.sciencedirect.com/science/article/pii/S0263822305000449

[28] Sen, F., Pakdil, M., Sayman, O., & Benli, S. Experimental failure analysis of mechanically fastened joints with clearance in composite laminates under preload. *Materials & Design*, *29*(6), 1159-1169. (2008)

https://www.sciencedirect.com/science/article/pii/S0261306907001495

[29] Ramkumar, R. L., & Tossavainen, E. W. *Strength and lifetime of bolted laminates* (pp. 251-273). ASTM International. (1986)

https://scholar.google.com/scholar?hl=en&as_sdt=0%2C5&q=STRENGTH+AND+LIFETIME+OF+BOLTED+LAMINATES&btnG=

[30] Poon, C., & Gould, R. *Behaviour of mechanically fastened joints in advanced composites*. NATIONAL AERONAUTICAL ESTABLISHMENT OTTAWA (ONTARIO) STRUCTURES AND MATERIALS SECTION. (1988)

https://scholar.google.com/scholar?hl=en&as_sdt=0%2C5&q=Poon+C%2C+Gould+R.+Behaviour+of+mechanically+fastened+joints+in+advanced+composites.+In%3A+AGARD+proceedings.+Madrid%2C+April%2C+1988%3B427.+p.21-22&btnG=#d=gs_cit&t=1683019446902&u=%2Fscholar%3Fq%3Dinfo%3A3TrQyNH25r8J%3Ascholar.google.com%2F%26output%3Dcite%26scirp%3D0%26hl%3Den

[31] Ascione, F.; Feo, L.; Maceri, F. On the pin-bearing failure load of GFRP bolted laminates: An experimental analysis on the influence of bolt diameter. Compos. Part B Eng., 41, 482–490 (2010) https://www.sciencedirect.com/science/article/abs/pii/S1359836810000612?via%3Dihub

[32] Cooper, C.; Turvey, G. Effects of joint geometry and bolt torque on the structural

performance of single bolt tension joints in pultruded GRP sheet material. Compos. Struct. 32, 217–226. (1995) https://www.sciencedirect.com/science/article/abs/pii/0263822395000712?via%3Dihub

[33] Wang, Y. Bearing Behavior of Joints in Pultruded Composites. J. Compos. Mater., 36, 2199–2216 (2002) https://journals.sagepub.com/doi/10.1177/0021998302036018535

[34] Hassan, N.K.; Mohamedien, M.A.; Rizkalla, S.H. Multibolted Joints for GFRP Structural Members. J. Compos. Constr., 1, 3–9 (1997) https://ascelibrary.org/doi/10.1061/%28ASCE%291090-0268%281997%291%3A1%283%29

[35] American Composites Manufactures Association. "Pre-standard for load & resistance factor design (LRFD) of pultruded fiber reinforced polymer (FRP) structures." *Arlington, VA: ACMA* 14 (2012)

[36] Ascione, L., Caron, J. F., Godonou, P., van IJselmuijden, K., Knippers, J., Mottram, T., & Tromp, L. Prospect for new guidance in the design of FRP: Support to the implementation, harmonization and further development of the Eurocodes. Publications Office of the European Union. (2016)

[37] Kumar, T. V., Shankar, G. S., & Shankar, B. L. Experimental study on effect of stacking sequence, clearance and clamping torque on strength of FRP composite bolted joints. *Materials Today: Proceedings*, *4*(10), 10746-10750. (2017)

https://www.sciencedirect.com/science/article/pii/S2214785317316504

[38] Machado, J. J. M., Marques, E. A. S., & da Silva, L. F. Adhesives and adhesive joints under impact loadings: An overview. *The Journal of adhesion*, *94*(6), 421-452. (2018)

https://www.tandfonline.com/doi/abs/10.1080/00218464.2017.1282349

[39] Nerilli, F., & Vairo, G. Progressive damage in composite bolted joints via a computational micromechanical approach. *Composites Part B: Engineering*, *111*, 357-371. (2017)

https://www.sciencedirect.com/science/article/pii/S1359836816324982

[40] Agubra, Victor A., Peter S. Owuor, and Mahesh V. Hosur. Influence of nanoclay dispersion methods on the mechanical behavior of E-glass/epoxy

nanocomposites. Nanomaterials 3.3, pp.550-563. (2013)

https://www.mdpi.com/2079-4991/3/3/550

[41] Qiu, Jingjing, et al. Carbon nanotube integrated multifunctional multiscale composites. Nanotechnology 18.27: 275708. (2007)

https://iopscience.iop.org/article/10.1088/0957-4484/18/27/275708/meta

[42] Mara, Valbona, Reza Haghani, and Mohammad Al-Emrani. Improving the performance of bolted joints in composite structures using metal inserts. Journal of composite materials 50.21, pp.3001-3018. (2016)

https://journals.sagepub.com/doi/abs/10.1177/0021998315615204?journalCode=jcma

[43] Uddin, Nasim, et al. Cost-effective bridge girder strengthening using vacuum-assisted resin transfer molding (VARTM). Advanced Composite Materials 13.3-4, pp.255-281. (2004)

https://www.tandfonline.com/doi/abs/10.1163/1568551042580163

[44] Phan Viet Nhut, Yoresta, F. S., Kitane, Y., Hashimoto, K., & Matsumoto, Y. "On the strengthening of pultruded GFRP connections using glass fiber sheets: A study on the influence of bolt diameter." *Applied Composite Materials* 29.2: pp.651-681 (2022) https://link.springer.com/article/10.1007/s10443-021-09972-1

[45] Nhut Phan Viet., Yoresta, F. S., Kitane, Y., Hashimoto, K., & Matsumoto, Y. "Improving the shear strength of bolted connections in pultruded GFRP using glass fiber sheets." *Composite Structures* 255: 112896 (2021) https://www.sciencedirect.com/science/article/abs/pii/S0263822320328221

[46] Phan Viet Nhut, Quang Duc Tran, and Matsumoto Yukihiro. "Pin-bearing connection strength of single-bolted pultruded glass fiber-reinforced polymer profiles strengthened by glass fiber sheet." *Polymer Composites* (2022) https://onlinelibrary.wiley.com/doi/abs/10.1002/pc.26774

[47] Martins, D., Gonilha, J., Correia, J. R., & Silvestre, N. Exterior beam-to-column bolted connections between GFRP I-shaped pultruded profiles using stainless steel cleats. Part 1: Experimental study. *Thin-Walled Structures*, *163*, 107719. (2021) https://www.sciencedirect.com/science/article/pii/S0263823121001889

[48] Bank, L. C., Mosallam, A. S., & Gonsior, H. E. Beam-to-column connections for pultruded FRP structures. In Serviceability and Durability of Construction Materials (pp. 804-813). ASCE. (1990)

https://cedb.asce.org/CEDBsearch/record.jsp?dockey=0067680

[49] Gonilha, J. A., Correia, J. R., & Branco, F. A. Creep response of GFRP–concrete hybrid structures: Application to a footbridge prototype. Composites Part B: Engineering, 53, 193-206. (2013)
https://www.sciencedirect.com/science/article/abs/pii/S1359836813002023

[50] Turvey, G. J., & Zhang, Y. S. Flexural moduli and end connection stiffnesses of symmetrically loaded GFRP beams for limit state serviceability design analysis. Composite Structures, 202, 1164-1175. (2018)

https://www.sciencedirect.com/science/article/abs/pii/S0263822317342824

[51] Qureshi, J., & Mottram, J. T. Moment-rotation response of nominally pinned beam-to-column joints for frames of pultruded fibre reinforced polymer. *Construction and Building Materials*, *77*, 396-403. (2015)

https://www.sciencedirect.com/science/article/pii/S0950061814013592

[52] Mosallam, A. S. Design for FRP composite connections, ASCE manuals and reports on engineering practice MOP# 102. (2011)

[53] Turvey, G. J., & Cooper, C. Review of tests on bolted joints between pultruded GRP profiles. Proceedings of the Institution of Civil Engineers-Structures and Buildings, 157(3), 211-233. (2004)
https://www.icevirtuallibrary.com/doi/abs/10.1680/stbu.2004.157.3.211

[54] Mottram, J. T., & Zheng, Y. Further tests of beam-to-column connections for pultruded frames: flange-cleated. *Journal of Composites for Construction*, *3*(3), 108-116. (1999)
https://ascelibrary.org/doi/abs/10.1061/(ASCE)1090-0268(1999)3:3(108)

[55] Mottram, J. T., & Zheng, Y. Further tests on beam-to-column connections for pultruded frames: web-cleated. *Journal of Composites for Construction*, *3*(1), 3-11. (1999)
https://ascelibrary.org/doi/abs/10.1061/(ASCE)1090-0268(1999)3:1(3)
https://cedb.asce.org/CEDBsearch/record.jsp?dockey=0067680

[56] Bass, A. J., & Mottram, J. T. Behaviour of connections in frames of fibre-reinforced-

polymer section. *Struct. Eng.*, *72*(17), 280-284. (1994)

[57] Turvey, G. J., & Cooper, C. Semi-rigid pultruded GRP frame connections: tests to determine static moment-rotation characteristics. In *ECCM-7: Seventh European Conference on Composite Materials. Realising Their Commercial Potential.* (Vol. 2, pp. 295-300). (1996)

[58] Bank, L. C., Mosallam, A. S., & McCoy, G. T. Design and performance of connections for pultruded frame structures. *Journal of reinforced plastics and composites*, *13*(3), 199-212. (1994) https://journals.sagepub.com/doi/abs/10.1177/073168449401300302?journalCode=jrpa

[59] Smith, S. J., Parsons, I. D., & Hjelmstad, K. D. Finite-element and simplified models of GFRP connections. *Journal of structural engineering*, *125*(7), 749-756. (1999)

https://ascelibrary.org/doi/abs/10.1061/(ASCE)0733-9445(1999)125:7(749)

[60] Bank, L. C., Yin, J., Moore, L., Evans, D. J., & Allison, R. W. Experimental and numerical evaluation of beam-to-column connections for pultruded structures. Journal of reinforced plastics and composites, 15(10), 1052-1067. (1996)

[61] Qureshi, J., & Mottram, J. T. Behaviour of pultruded beam-to-column joints using steel web cleats. *Thin-Walled Structures*, *73*, 48-56. (2013)

https://www.sciencedirect.com/science/article/pii/S0263823113001651

[62] Martins, D., Gonilha, J., Correia, J. R., & Silvestre, N. Exterior beam-to-column bolted connections between GFRP I-shaped pultruded profiles using stainless steel cleats, Part 2: Prediction of initial stiffness and strength. *Thin-Walled Structures*, *164*, 107762. (2021)

https://www.sciencedirect.com/science/article/pii/S0263823121002135

[63] Smith, S. J., Parsons, I. D., & Hjelmstad, K. D. Experimental comparisons of connections for GFRP pultruded frames. *Journal of Composites for Construction*, *3*(1), 20-26. (1999) https://ascelibrary.org/doi/abs/10.1061/(ASCE)1090-0268(1999)3:1(20)

[64] Martins, D., Proença, M., Correia, J. R., Gonilha, J., Arruda, M., & Silvestre, N. Development of a novel beam-to-column connection system for pultruded GFRP tubular profiles. *Composite Structures*, *171*, 263-276. (2017)

https://www.sciencedirect.com/science/article/pii/S0263822317304993

[65] Mosallam, A. S. Design considerations for pultruded composite beam-to-column connections subjected to cyclic and sustained loading conditions. *Marketing technical regulatory sessions of the composites institutes international composites expo*, 14-B. (1997)

[66] Zhang, Z., Bai, Y., He, X., Jin, L., & Zhu, L. Cyclic performance of bonded sleeve beam-column connections for FRP tubular sections. *Composites Part B: Engineering*, *142*,171-182. (2018) https://www.sciencedirect.com/science/article/pii/S1359836817339458

[67] AISC (American Institute of Steel Construction). (2010). Seismic provisions for structural steel buildings. Supersedes the Seismic Provisions for Structural Steel Buildings dated June 22, 2010 and all previous versions (2016), Chicago: AISC.

[68] Manual, E. C. C. S. Recommended testing procedures for assessing the behaviour of structural steel elements under cyclic loads. In *European Convention for Constructional Steelwork: Brussels, Belgium*. (1986)

[69] Martins, D., Sa, M. F., Gonilha, J. A., Correia, J. R., Silvestre, N., & Ferreira, J. G. Experimental and numerical analysis of GFRP frame structures. Part 2: Monotonic and cyclic sway behaviour of plane frames. *Composite Structures*, *220*, 194-208. (2019)

[70] Dastin, Sam. "Repairing advanced composite materials." Machine Design 58.4: pp.86-90 (1986)

[71] Rosner, Charles N. Single-bolted connections for orthotropic fibre-reinforced composite structural members. MS thesis. (1992) https://mspace.lib.umanitoba.ca/bitstream/handle/1993/18684/Rosner_Single-bolted_connections.pdf?sequence=1

[72] Hart-Smith, L. J. "Design and analysis of bolted and riveted joints in fibrous composite structures." Recent advances in structural joints and repairs for composite materials. Springer, Dordrecht, pp.211-254 (2003) https://link.springer.com/chapter/10.1007/978-94-017-0329-1_7

[73] Hassan, N. K. Evaluation of multi-bolted connections for GFRP members. Diss. Ph. D. dissertation (1994) https://cedb.asce.org/CEDBsearch/record.jsp?dockey=0091032

RELATED PUBLICATIONS

List of papers

1. Tran Quang Duc, Nhut Phan Viet, Matsumoto Yukihiro, “Multi-Bolted Connection for Pultruded Glass Fiber Reinforced Polymer’s Structure: A Study on Strengthening by Multiaxial Glass Fiber Sheets”, Polymers, Volume 14, Issue 8, 1561, 2022.4.
2. Tran Quang Duc, Nhut Phan Viet, Matsumoto Yukihiro, "Strengthening of multi-bolted connections in pultruded GFRP by glass fiber sheets: an experimental study", Applied Composite Materials, Volume 30, issue 3, pp.833-856, 2023.3.

List of papers at International Conference with Referee’s review

1. Tran Quang Duc, Nhut Phan Viet, Matsumoto Yukihiro, “Multi-bolted connection pultruded GFRP strengthening by glass fiber sheets: influence of bond strength”, International Conference on Materials Design and Applications (ICMDA2023), Chiba University, Chiba, Japan, 2023.4